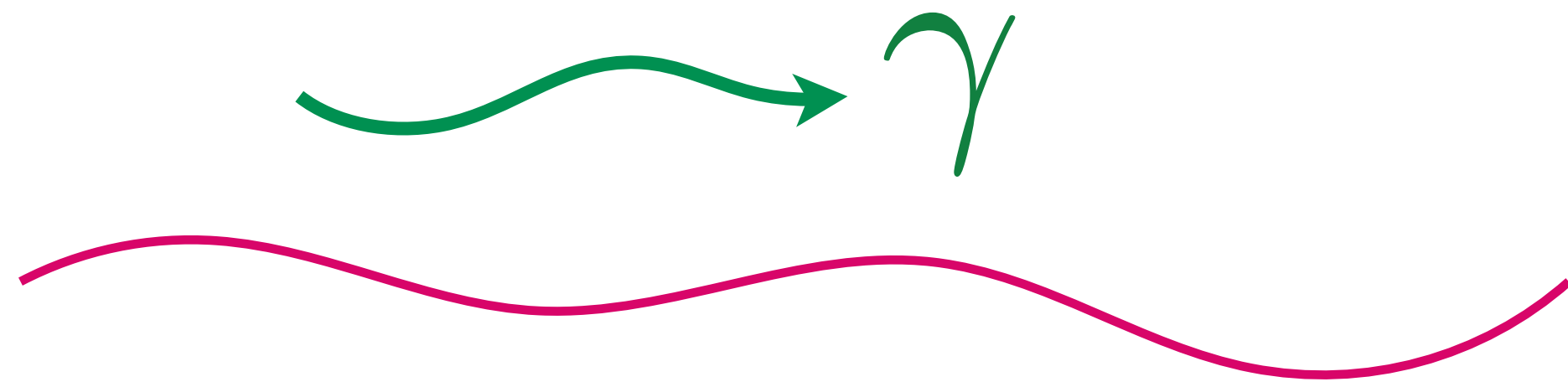

Electromagnetic Detection of Gravitational Waves

Sebastian A. R. Ellis

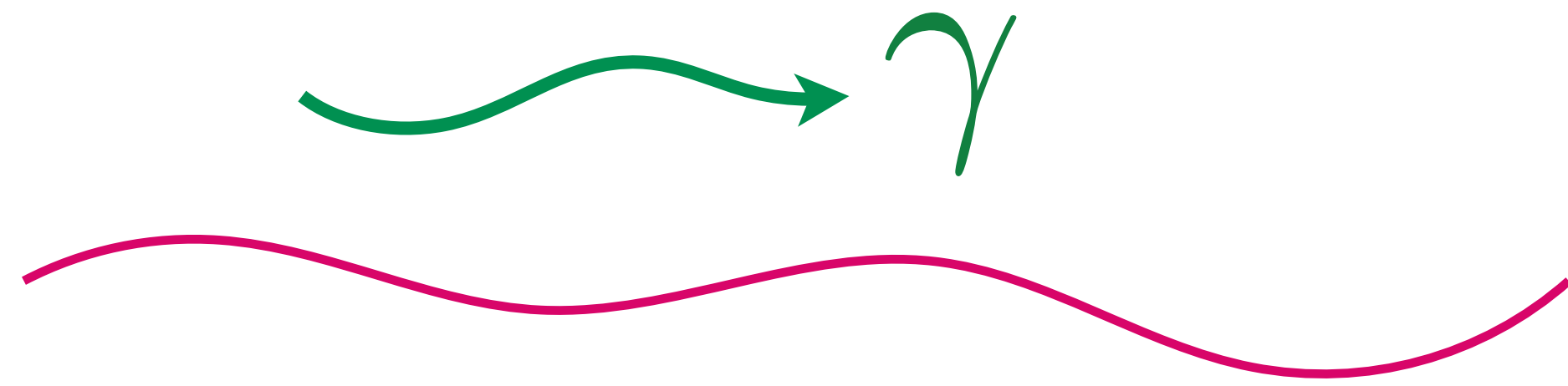
University of Geneva

Electromagnetism in Curved Space



$$S_{\text{EM}} = \int d^4x \sqrt{-g} \left(-\frac{1}{4} g^{\mu\alpha} g^{\nu\beta} F_{\mu\nu} F_{\alpha\beta} + g^{\mu\nu} J_{\mu} A_{\nu} \right)$$

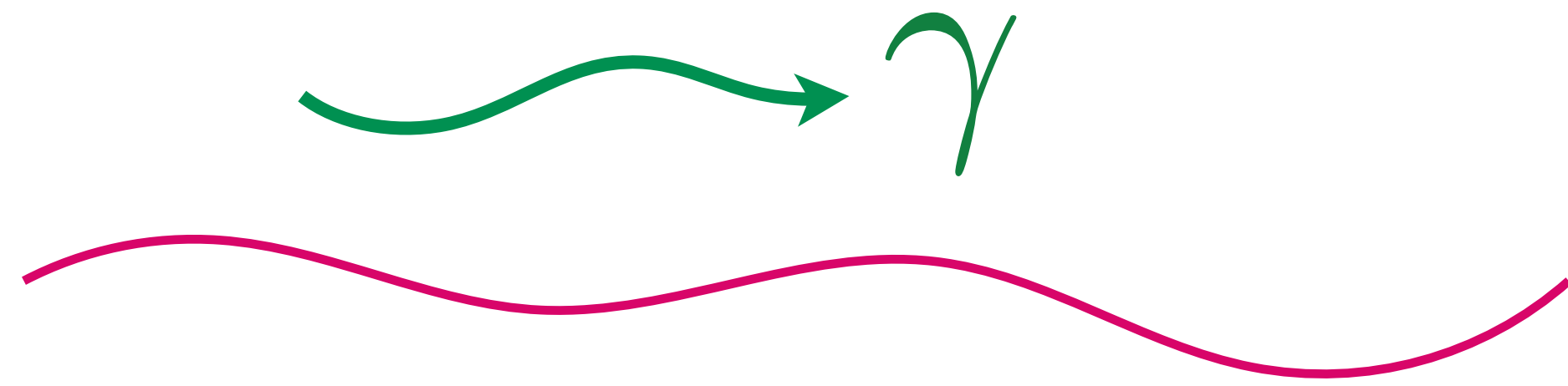
Electromagnetism in Curved Space



$$S_{\text{EM}} = \int d^4x \sqrt{-g} \left(-\frac{1}{4} g^{\mu\alpha} g^{\nu\beta} F_{\mu\nu} F_{\alpha\beta} + g^{\mu\nu} J_\mu A_\nu \right)$$

$$g_{\mu\nu} = \eta_{\mu\nu} + h_{\mu\nu}, \quad g^{\mu\nu} = \eta^{\mu\nu} - h^{\mu\nu} \quad \longrightarrow \quad \mathcal{L} \supset \mathcal{O}(hF^2)$$

Electromagnetism in Curved Space

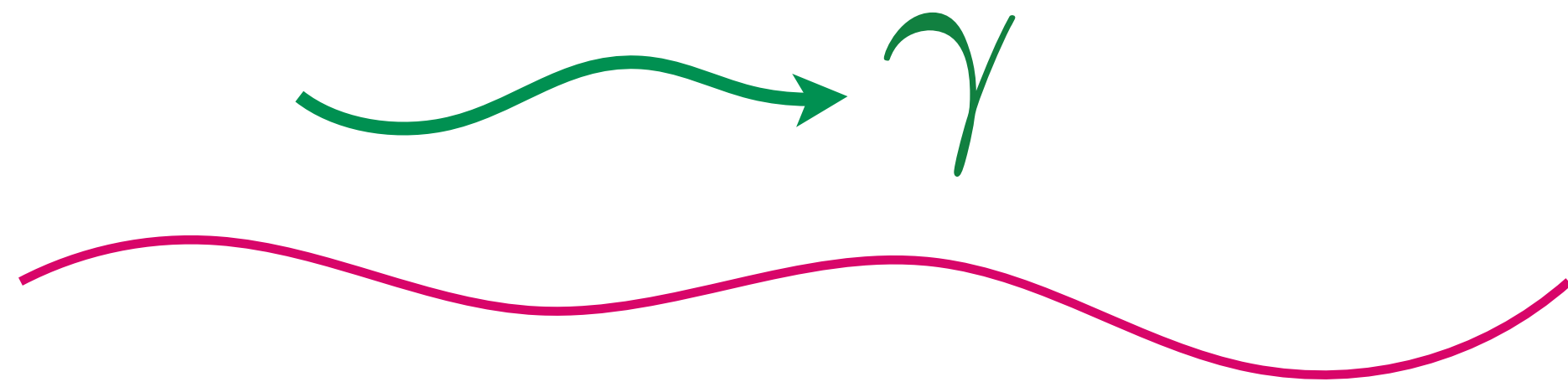


$$S_{\text{EM}} = \int d^4x \sqrt{-g} \left(-\frac{1}{4} g^{\mu\alpha} g^{\nu\beta} F_{\mu\nu} F_{\alpha\beta} + g^{\mu\nu} J_\mu A_\nu \right)$$

$$g_{\mu\nu} = \eta_{\mu\nu} + h_{\mu\nu}, \quad g^{\mu\nu} = \eta^{\mu\nu} - h^{\mu\nu} \quad \longrightarrow \quad \mathcal{L} \supset \mathcal{O}(hF^2)$$

Equation of motion: $\partial F \sim -\partial(hF)$

Electromagnetism in Curved Space



$$S_{\text{EM}} = \int d^4x \sqrt{-g} \left(-\frac{1}{4} g^{\mu\alpha} g^{\nu\beta} F_{\mu\nu} F_{\alpha\beta} + g^{\mu\nu} J_\mu A_\nu \right)$$

$$g_{\mu\nu} = \eta_{\mu\nu} + h_{\mu\nu}, \quad g^{\mu\nu} = \eta^{\mu\nu} - h^{\mu\nu} \quad \longrightarrow \quad \mathcal{L} \supset \mathcal{O}(hF^2)$$

Equation of motion: $\partial F \sim -\partial(hF)$

Effective current from spatial or temporal variations of h or F

$$j_{\text{eff}}^\mu \equiv \partial_\nu \left(\frac{1}{2} h F^{\mu\nu} + h^\nu_\alpha F^{\alpha\mu} - h^\mu_\alpha F^{\alpha\nu} \right)$$

Berlin, Blas, D'Agnolo, SARE, Harnik, Kahn, Schutte-Engel (PRD 2022)

GW/Axion similarities

Effective current from spatial or temporal variations of h or F

$$j_{\text{eff}}^{\mu} \equiv \partial_{\nu} \left(\frac{1}{2} h F^{\mu\nu} + h^{\nu}_{\alpha} F^{\alpha\mu} - h^{\mu}_{\alpha} F^{\alpha\nu} \right)$$

GW/Axion similarities

Effective current from spatial or temporal variations of h or F

$$j_{\text{eff}}^{\mu} \equiv \partial_{\nu} \left(\frac{1}{2} h F^{\mu\nu} + h^{\nu}_{\alpha} F^{\alpha\mu} - h^{\mu}_{\alpha} F^{\alpha\nu} \right)$$

Currents can excite cavity modes \mathbf{E}_{cav} as long as η non-zero:

$$\eta \propto \int_V \mathbf{E}_{\text{cav}}^* \cdot \mathbf{J}_{\text{eff}}$$

GW/Axion similarities

Effective current from spatial or temporal variations of h or F

$$j_{\text{eff}}^{\mu} \equiv \partial_{\nu} \left(\frac{1}{2} h F^{\mu\nu} + h^{\nu}_{\alpha} F^{\alpha\mu} - h^{\mu}_{\alpha} F^{\alpha\nu} \right)$$

Currents can excite cavity modes \mathbf{E}_{cav} as long as η non-zero:

$$\eta \propto \int_V \mathbf{E}_{\text{cav}}^* \cdot \mathbf{J}_{\text{eff}}$$

Should be reminiscent of axion physics...

GW/Axion similarities

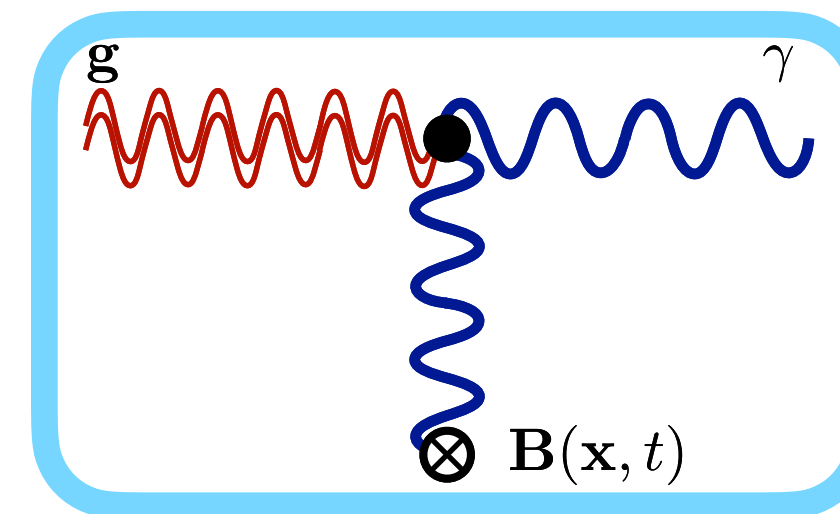
Effective current from spatial or temporal variations of h or F

$$j_{\text{eff}}^{\mu} \equiv \partial_{\nu} \left(\frac{1}{2} h F^{\mu\nu} + h^{\nu}_{\alpha} F^{\alpha\mu} - h^{\mu}_{\alpha} F^{\alpha\nu} \right)$$

Currents can excite cavity modes \mathbf{E}_{cav} as long as η non-zero:

$$\eta \propto \int_V \mathbf{E}_{\text{cav}}^* \cdot \mathbf{J}_{\text{eff}}$$

Should be reminiscent of axion physics...



Gertsenshtein effect (1962)

Also Zeldovich (1973)

$$j_g \sim \partial (h F)$$

GW/Axion similarities

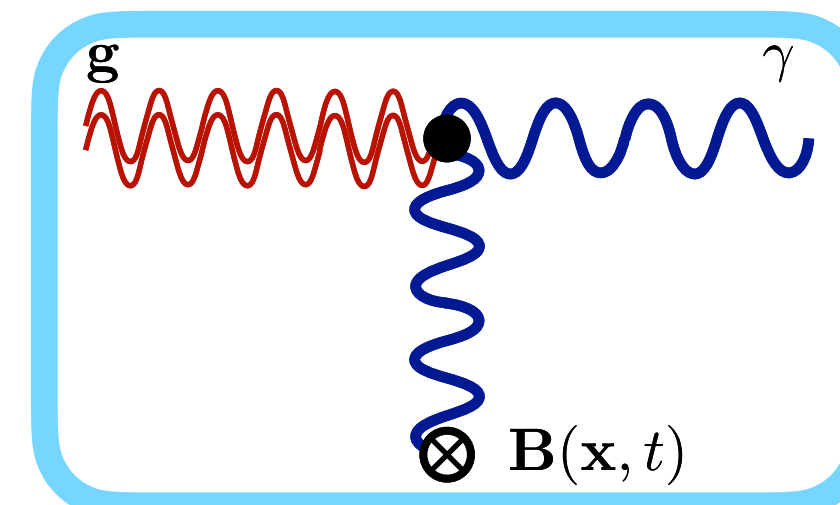
Effective current from spatial or temporal variations of h or F

$$j_{\text{eff}}^{\mu} \equiv \partial_{\nu} \left(\frac{1}{2} h F^{\mu\nu} + h^{\nu}_{\alpha} F^{\alpha\mu} - h^{\mu}_{\alpha} F^{\alpha\nu} \right)$$

Currents can excite cavity modes \mathbf{E}_{cav} as long as η non-zero:

$$\eta \propto \int_V \mathbf{E}_{\text{cav}}^* \cdot \mathbf{J}_{\text{eff}}$$

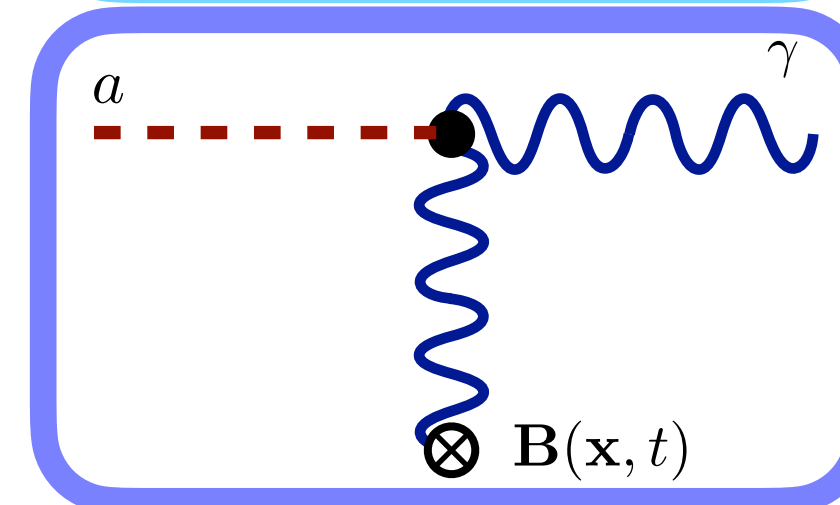
Should be reminiscent of axion physics...



Gertsenshtein effect (1962)

Also Zeldovich (1973)

$$j_g \sim \partial (h F)$$



$$j_a \sim g_{a\gamma\gamma} \partial (a F)$$

GW/Axion similarities

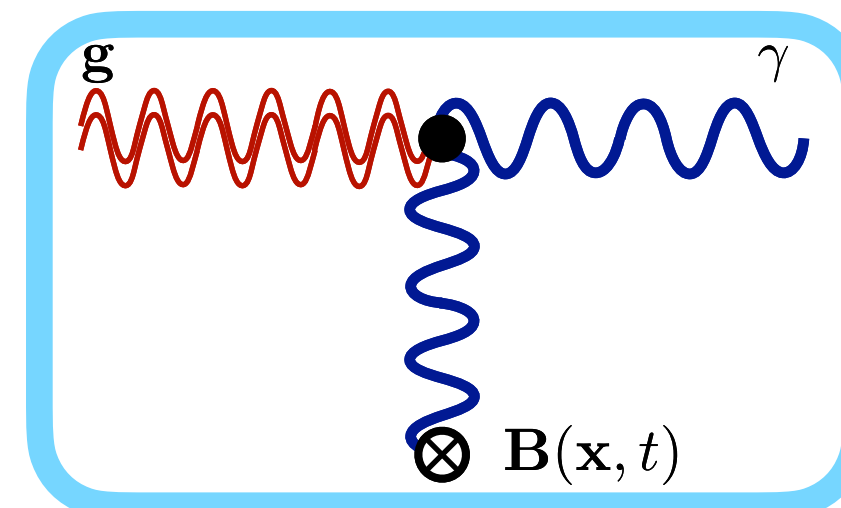
Effective current from spatial or temporal variations of h or F

$$j_{\text{eff}}^{\mu} \equiv \partial_{\nu} \left(\frac{1}{2} h F^{\mu\nu} + h^{\nu}_{\alpha} F^{\alpha\mu} - h^{\mu}_{\alpha} F^{\alpha\nu} \right)$$

Currents can excite cavity modes \mathbf{E}_{cav} as long as η non-zero:

$$\eta \propto \int_V \mathbf{E}_{\text{cav}}^* \cdot \mathbf{J}_{\text{eff}}$$

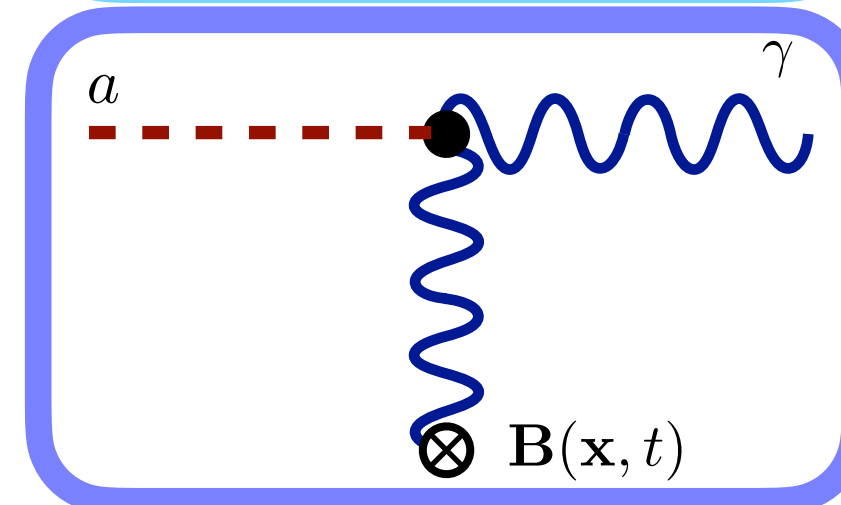
Should be reminiscent of axion physics...



Gertsenshtein effect (1962)

Also Zeldovich (1973)

$$j_g \sim \partial (h F)$$



$$j_a \sim g_{a\gamma\gamma} \partial (a F)$$

Raffelt & Stodolsky (1988)

Framing the Question

Detailed estimates require some GR

Framing the Question

Detailed estimates require some GR

GW in TT gauge: $\partial_\mu h^{\mu\nu} = 0$, $h_\mu{}^\mu = 0$, $h_{00} = h_{0i} = 0$

Framing the Question

Detailed estimates require some GR

GW in TT gauge: $\partial_\mu h^{\mu\nu} = 0$, $h_\mu{}^\mu = 0$, $h_{00} = h_{0i} = 0$

Riemann tensor invariant at $O(h)$:

$$R_{0i0j} = -\frac{1}{2}\partial_t^2 h_{ij}^{\text{TT}},$$

$$R_{0ijk} = \frac{1}{2}\partial_t (\partial_k h_{ij}^{\text{TT}} - \partial_j h_{ik}^{\text{TT}}),$$

$$R_{ikjl} = \frac{1}{2} (\partial_k \partial_j h_{il}^{\text{TT}} + \partial_i \partial_l h_{jk}^{\text{TT}} - \partial_i \partial_j h_{kl}^{\text{TT}} - \partial_k \partial_l h_{ij}^{\text{TT}})$$

Framing the Question

Crucial to work in appropriate reference frame!

Framing the Question

Crucial to work in appropriate reference frame!

Detector in Local Inertial Frame (LIF)

$$\hat{n} \times \mathbf{E} = 0$$

$$\hat{n} \cdot \mathbf{B} = 0$$

Maxwell (19th century)

Framing the Question

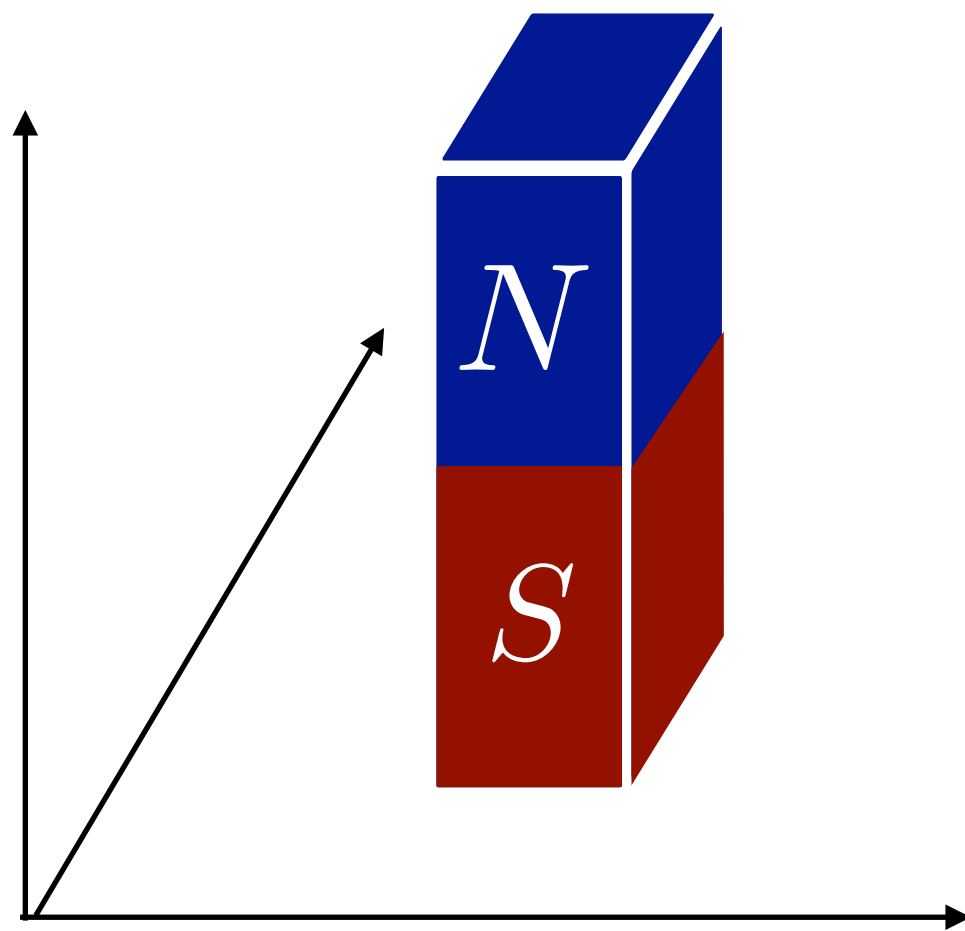
Crucial to work in appropriate reference frame!

Detector in Local Inertial Frame (LIF)

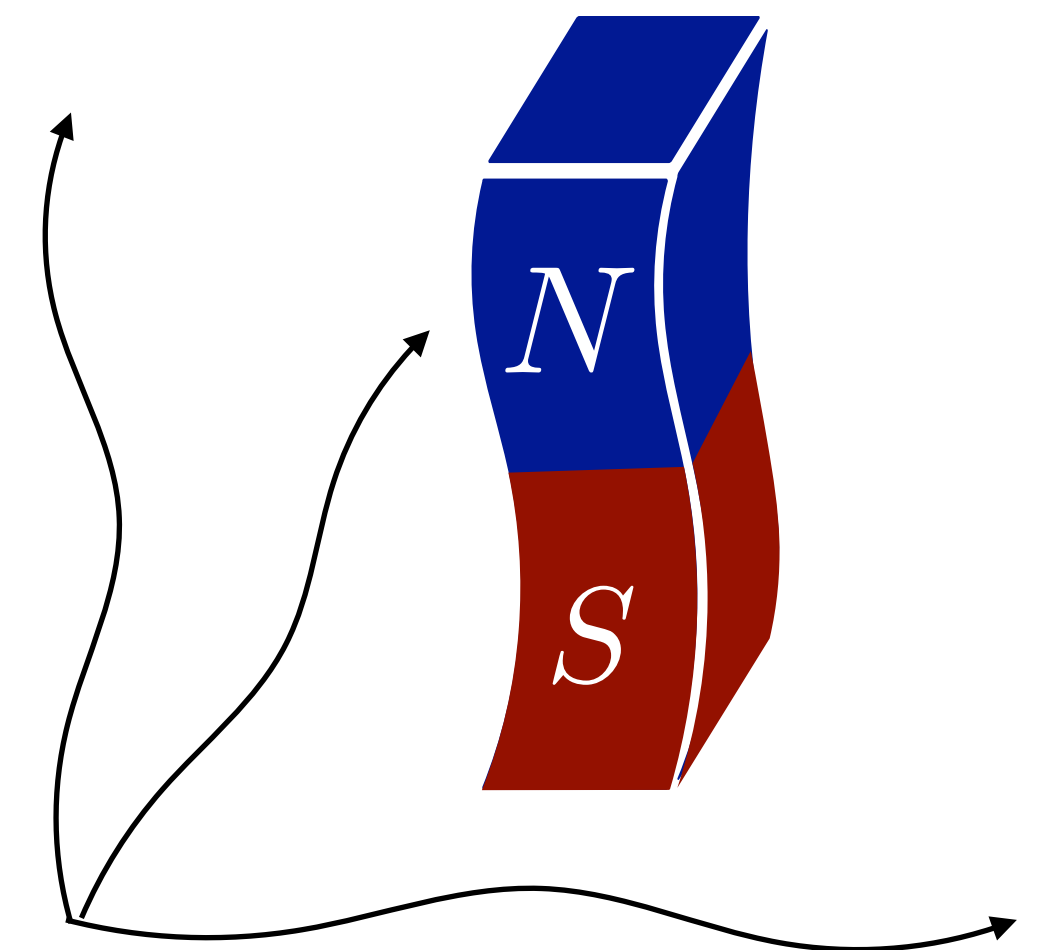
$$\hat{n} \times \mathbf{E} = 0$$

$$\hat{n} \cdot \mathbf{B} = 0$$

Maxwell (19th century)



B -field in LIF \neq B -field in TT



Framing the Question

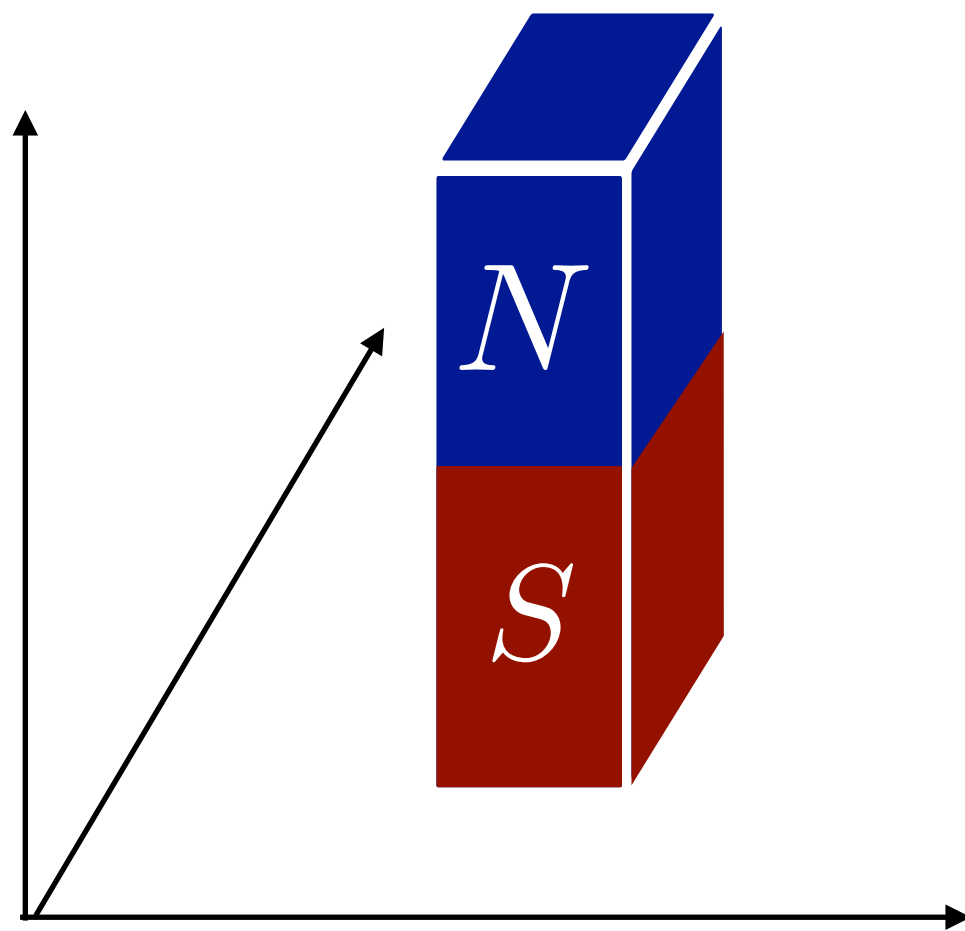
Crucial to work in appropriate reference frame!

Detector in Local Inertial Frame (LIF)

$$\hat{n} \times \mathbf{E} = 0$$

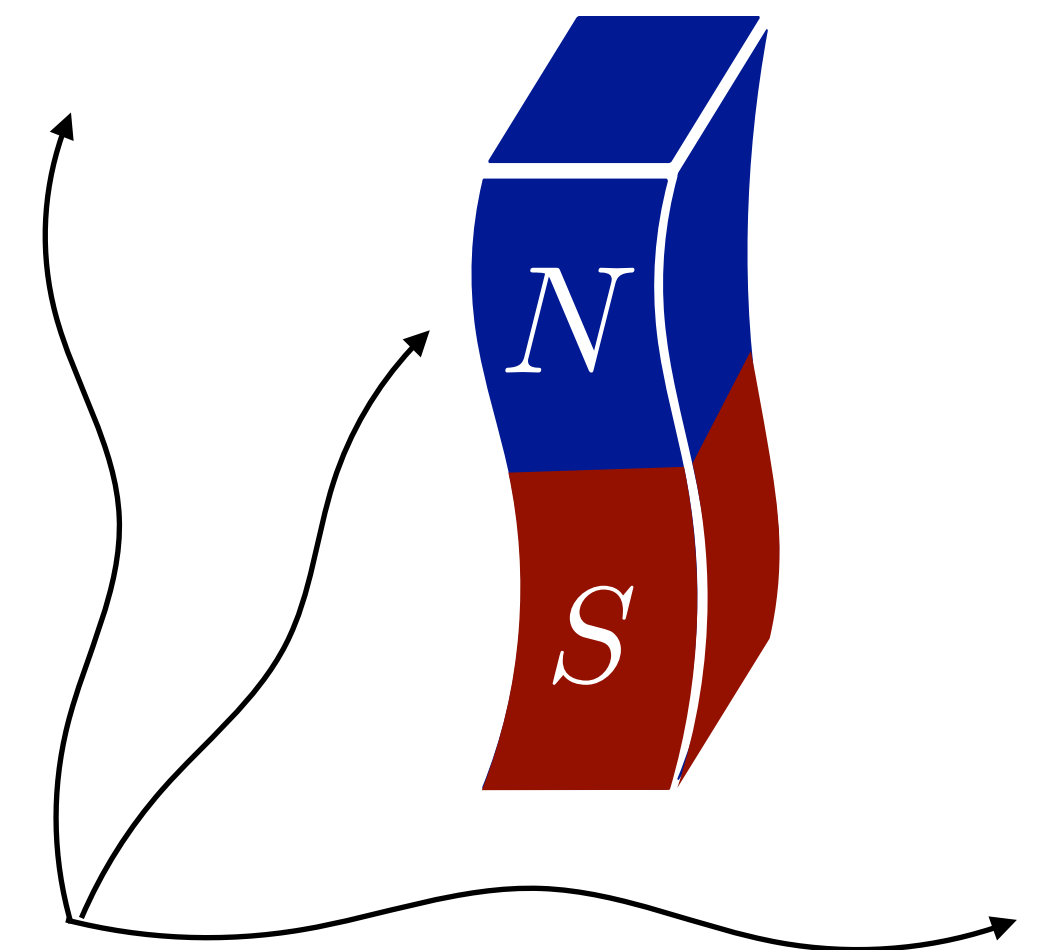
$$\hat{n} \cdot \mathbf{B} = 0$$

Maxwell (19th century)



B -field in LIF \neq B -field in TT

Which frame is the right one to use?



Framing the Question

Proper Detector Frame — complication

Framing the Question

Proper Detector Frame — complication

Textbooks give long-wavelength approximation $\omega_g R_{\text{cav}} \ll 1$

$$ds^2 \simeq -dt^2(1 + R_{0i0j}x^i x^j) - \frac{4}{3} dt dx^i (R_{0ijk}x^j x^k) + dx^i dx^j \left(\delta_{ij} - \frac{1}{3} R_{ikjl}x^k x^l \right) \text{ e.g. Maggiore (2007)}$$

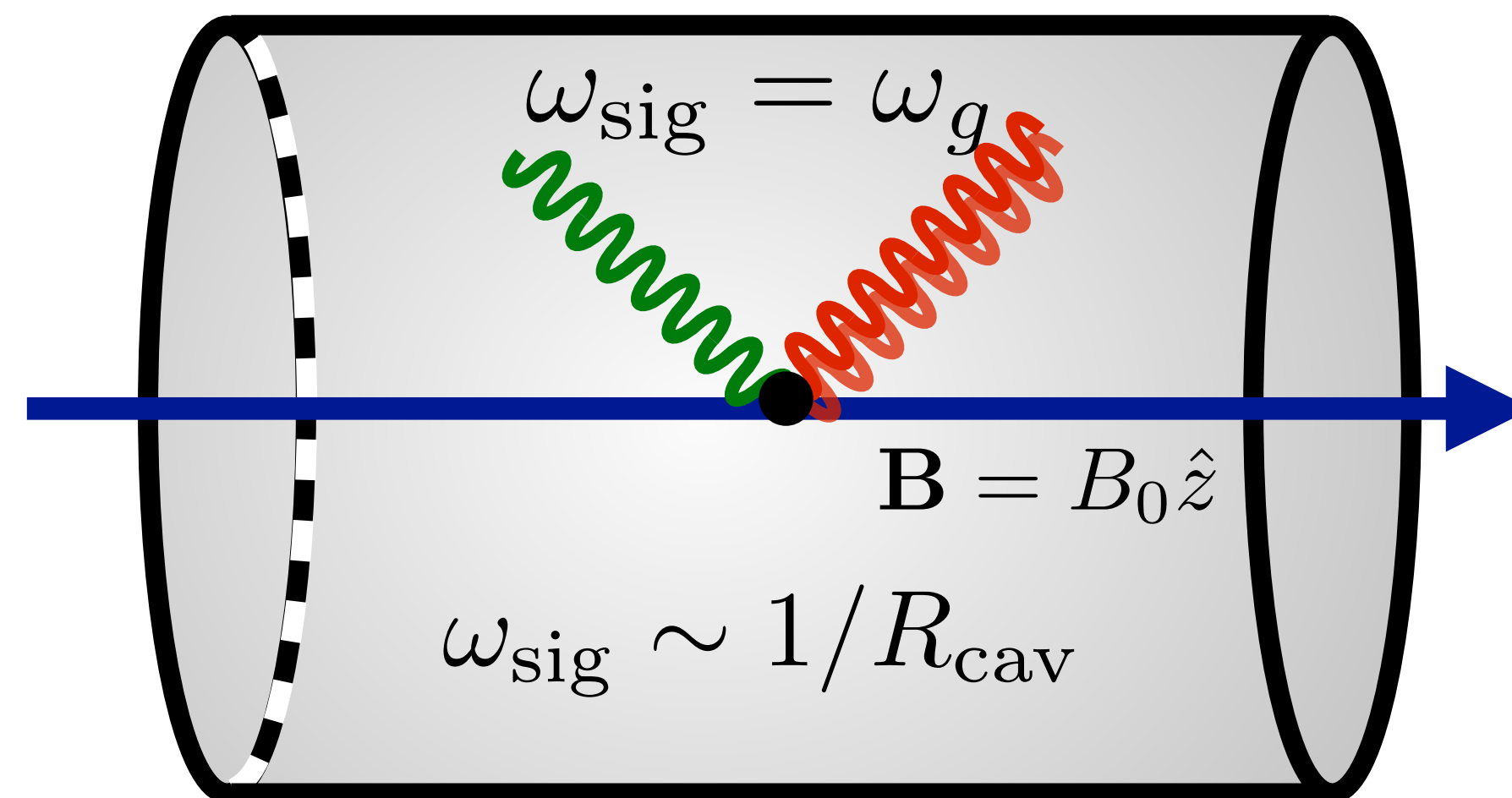
Framing the Question

Proper Detector Frame — complication

Textbooks give long-wavelength approximation $\omega_g R_{\text{cav}} \ll 1$

$$ds^2 \simeq -dt^2(1 + R_{0i0j}x^i x^j) - \frac{4}{3} dt dx^i (R_{0ijk}x^j x^k) + dx^i dx^j \left(\delta_{ij} - \frac{1}{3} R_{ikjl}x^k x^l \right) \text{ e.g. Maggiore (2007)}$$

Resonant Cavity:



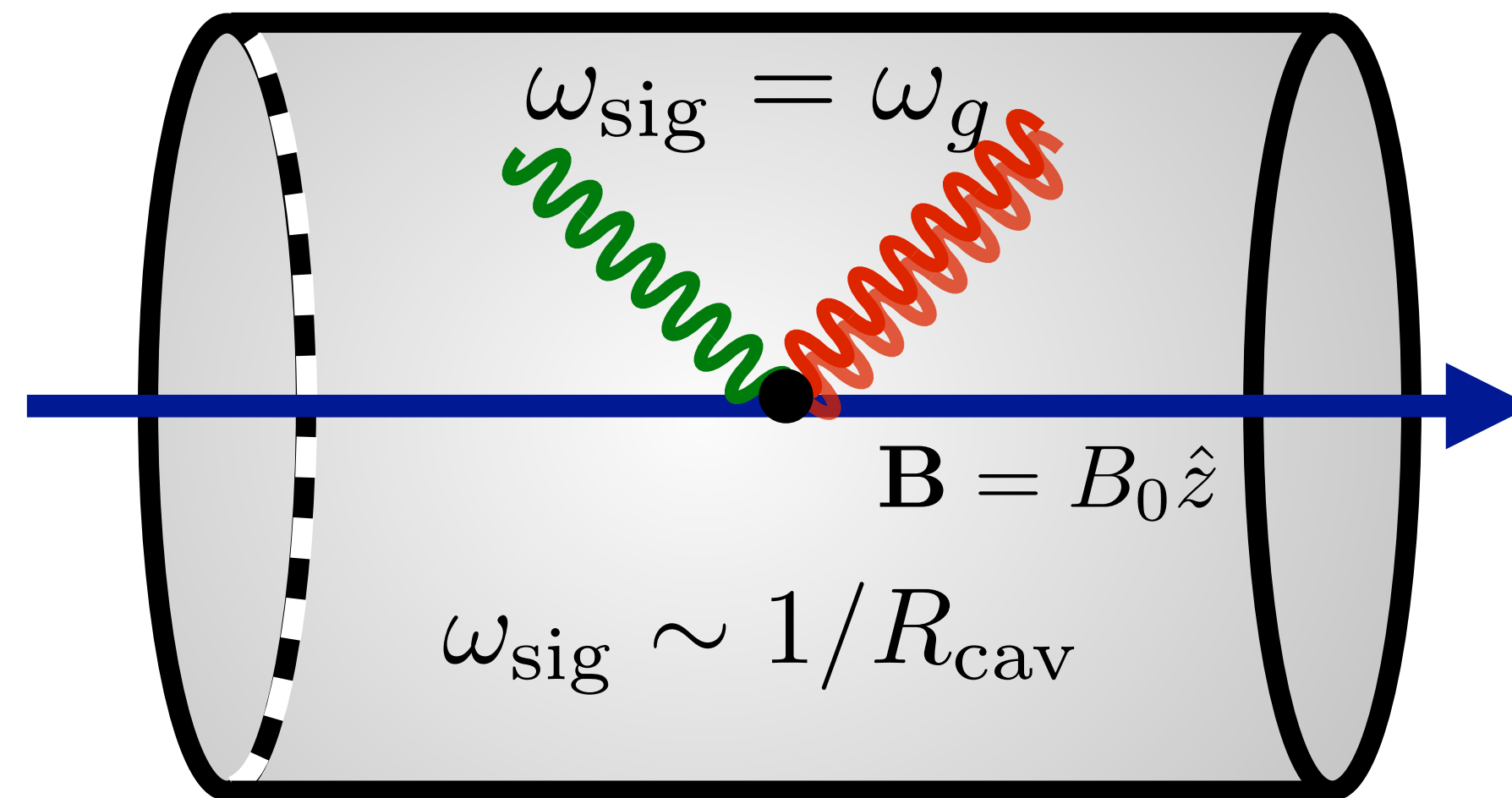
Framing the Question

Proper Detector Frame — complication

Textbooks give long-wavelength approximation $\omega_g R_{\text{cav}} \ll 1$

$$ds^2 \simeq -dt^2(1 + R_{0i0j}x^i x^j) - \frac{4}{3} dt dx^i (R_{0ijk}x^j x^k) + dx^i dx^j \left(\delta_{ij} - \frac{1}{3} R_{ikjl}x^k x^l \right) \text{ e.g. Maggiore (2007)}$$

Resonant Cavity:



Framing the Question

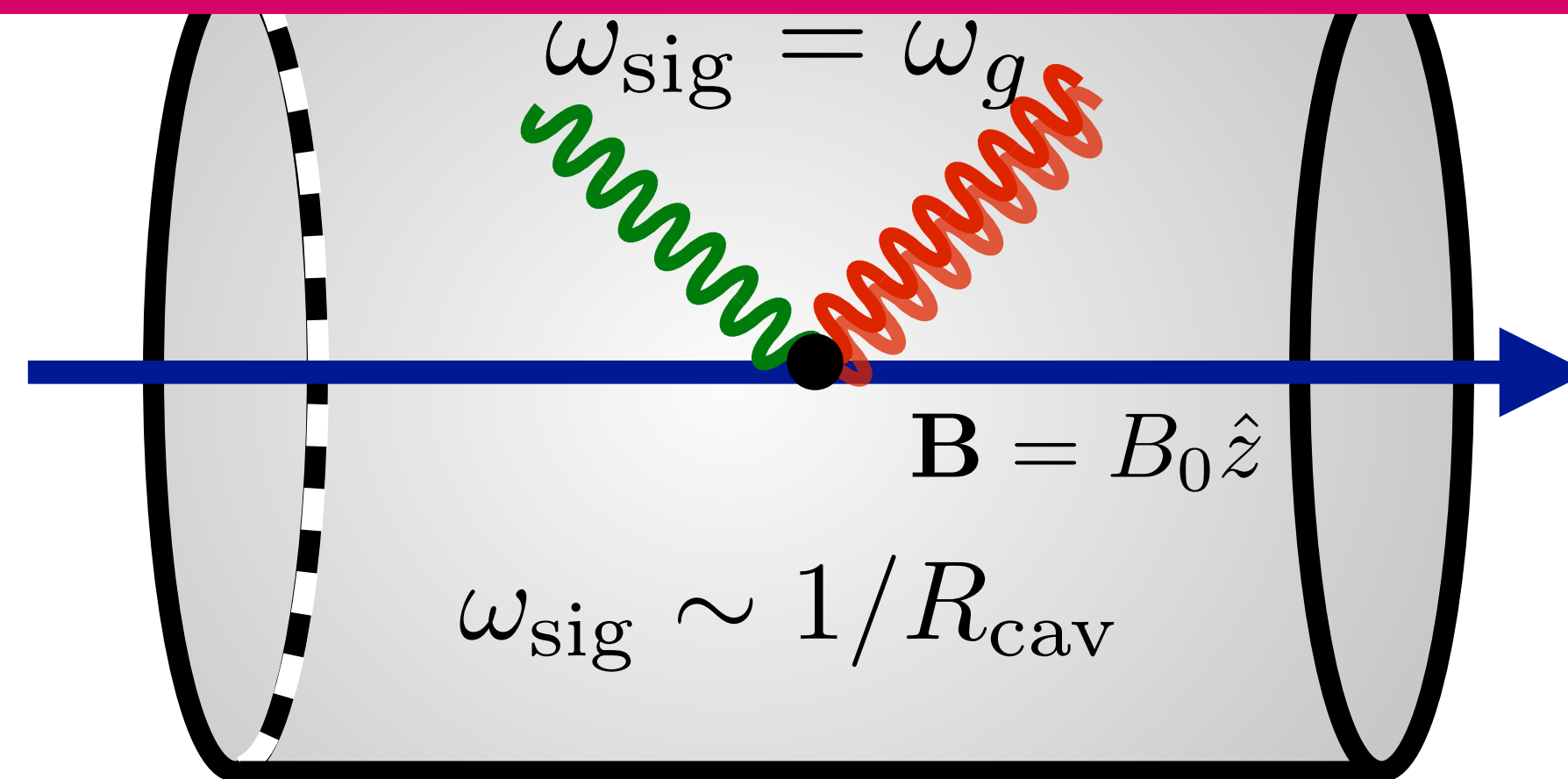
Proper Detector Frame — complication

Textbooks give long-wavelength approximation $\omega_g R_{\text{cav}} \ll 1$

$$ds^2 \simeq -dt^2(1 + R_{0i0j}x^i x^j) - \frac{4}{3} dt dx^i (R_{0ijk}x^j x^k) + dx^i dx^j \left(\delta_{ij} - \frac{1}{3} R_{ikjl}x^k x^l \right) \text{ e.g. Maggiore (2007)}$$

Long-wavelength limit invalid!

Resonant Cavity:



Framing the Question

Solution — GW as sum of plane waves

$$h \propto e^{i\omega_g(t-z)} \longrightarrow \partial_i h_{jk}^{\text{TT}} \sim -\delta_{iz} \partial_t h_{jk}^{\text{TT}}$$

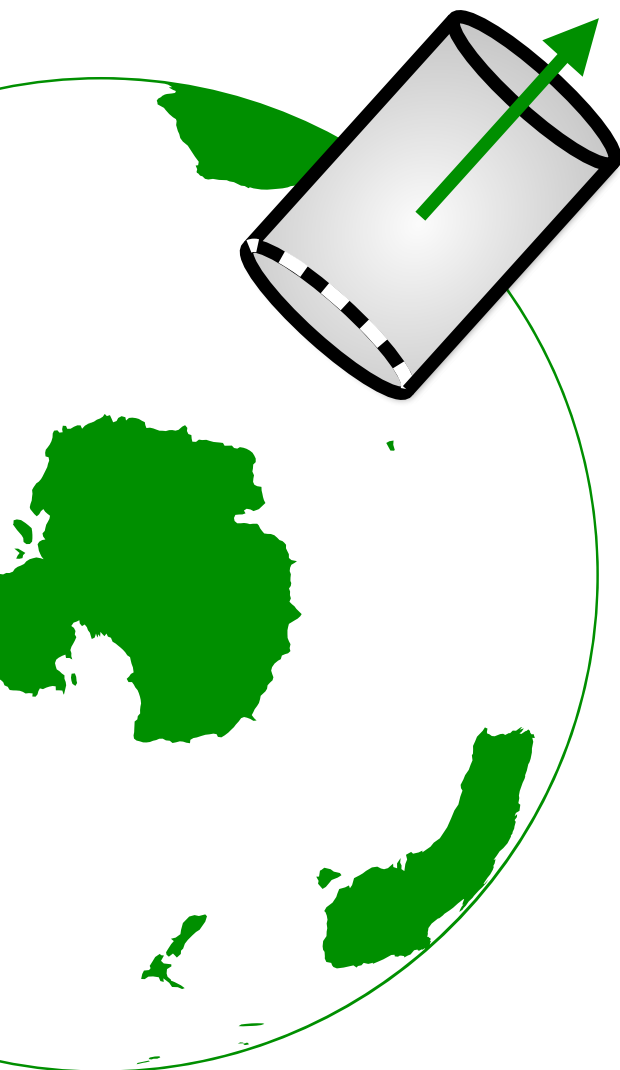
$$x^{k_1} \dots x^{k_r} R_{\mu\nu\rho\sigma, k_1 \dots k_r} = (-i\omega_g z)^r R_{\mu\nu\rho\sigma}$$

$$h_{00} = -2 \sum_{r=0}^{\infty} \frac{r+3}{(r+3)!} R_{0n0n, k_1, \dots, k_r} x^m x^n x^{k_1} \dots x^{k_r}$$

$$h_{0i} = -2 \sum_{r=0}^{\infty} \frac{r+2}{(r+3)!} R_{0nin, k_1, \dots, k_r} x^m x^n x^{k_1} \dots x^{k_r}$$

$$h_{ij} = -2 \sum_{r=0}^{\infty} \frac{r+1}{(r+3)!} R_{injn, k_1, \dots, k_r} x^m x^n x^{k_1} \dots x^{k_r}$$

Märzlin (1994)
Rakhmanov (2014)



Framing the Question

Solution — GW as sum of plane waves

$$h \propto e^{i\omega_g(t-z)} \longrightarrow \partial_i h_{jk}^{\text{TT}} \sim -\delta_{iz} \partial_t h_{jk}^{\text{TT}}$$

$$x^{k_1} \dots x^{k_r} R_{\mu\nu\rho\sigma, k_1 \dots k_r} = (-i\omega_g z)^r R_{\mu\nu\rho\sigma}$$

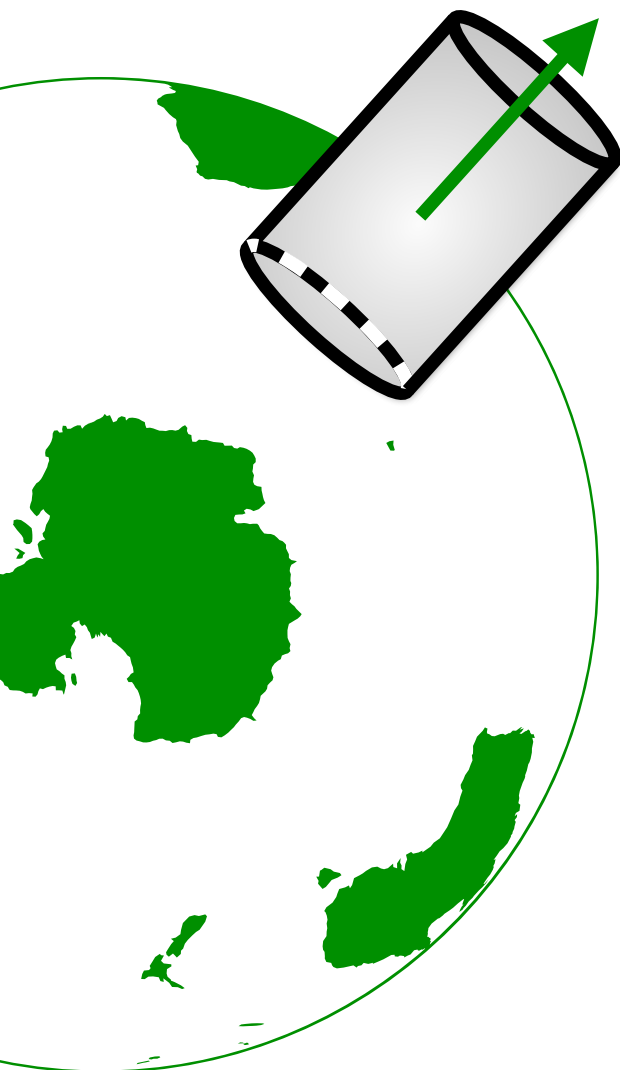
$$h_{00} = -2R_{0m0n} x^m x^n \left(-\frac{i}{\omega_g z} + \frac{1 + e^{-i\omega_g z}}{(\omega_g z)^2} \right)$$

$$h_{0i} = -2R_{0min} x^m x^n \left(-\frac{i}{2\omega_g z} - \frac{e^{-i\omega_g z}}{(\omega_g z)^2} - i \frac{1 - e^{-i\omega_g z}}{(\omega_g z)^3} \right)$$

$$h_{ij} = -2R_{imjn} x^m x^n \left(-\frac{1 + e^{-i\omega_g z}}{(\omega_g z)^2} - 2i \frac{1 - e^{-i\omega_g z}}{(\omega_g z)^3} \right)$$

Berlin, Blas, D'Agnolo, SARE, Harnik, Kahn, Schutte-Engel (PRD 2022)

Märzlin (1994)
Rakhmanov (2014)



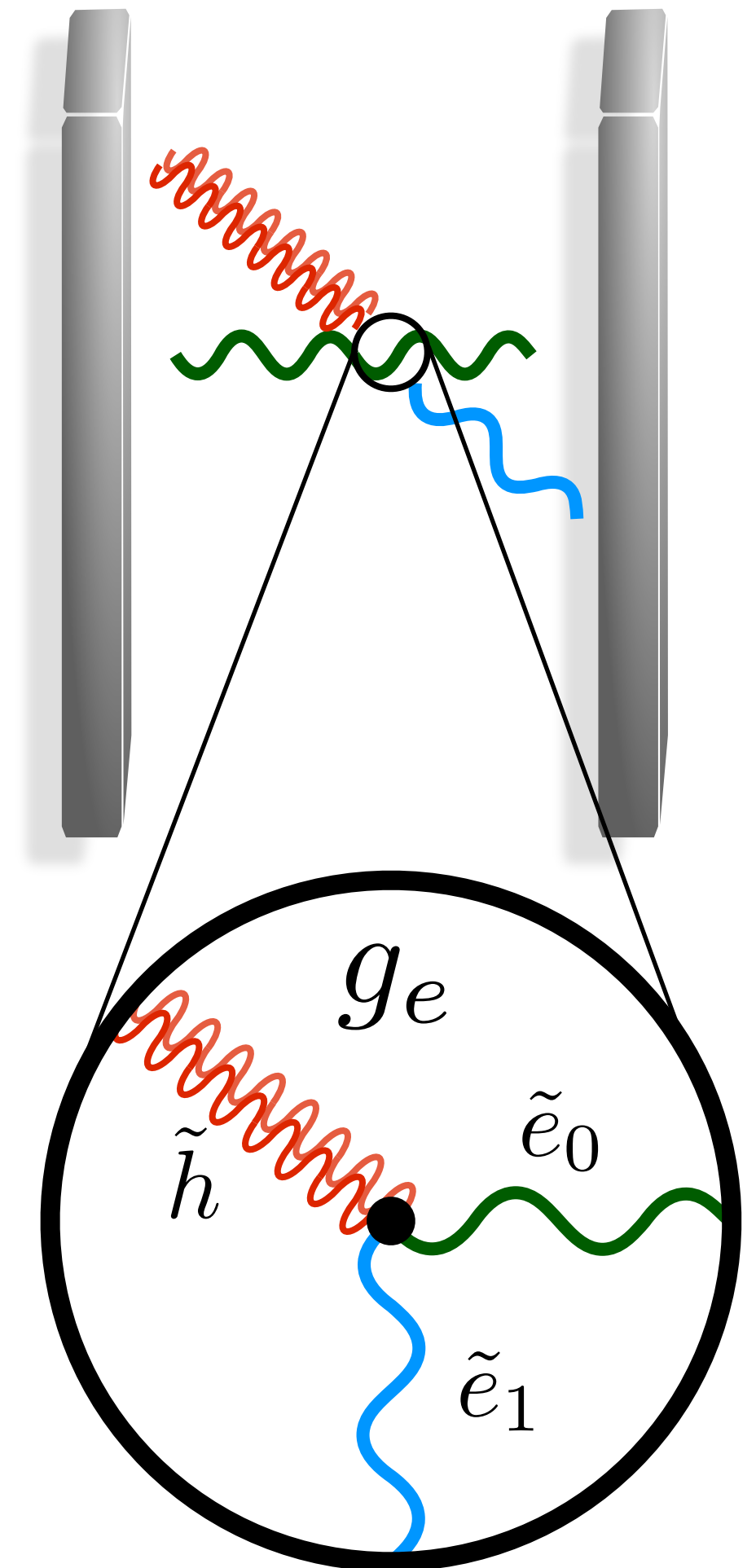
Transfer function for EM conversion

$$\left(\omega_1^2 - \omega^2 + i \frac{\omega \omega_1}{Q} \right) \tilde{e}_1(\omega) \simeq \int d\omega' \tilde{e}_0(\omega - \omega') g_e \omega \tilde{h}^{\text{TT}}(\omega')$$

$$g_e \equiv \omega_g (1 + \omega_g L + \omega_0 L) \min[1, \omega_g L]$$

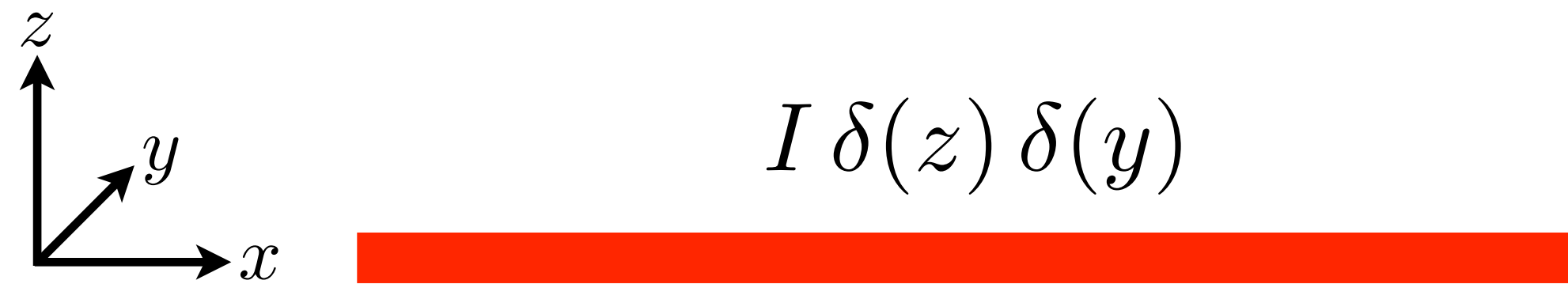
$$\mathcal{T}_{\text{EM}}^2(\omega) = \frac{\omega_g^2 \omega^2 (\omega_g L + \omega_0 L + 1)^2}{\left((\omega_1^2 - \omega^2)^2 + \frac{\omega^2 \omega_1^2}{Q^2} \right)} \min[1, \omega_g^2 L^2]$$

D'Agnolo, SARE (gr-qc/2412.17897)



Framing the Question

Further complications: What is an EM field?

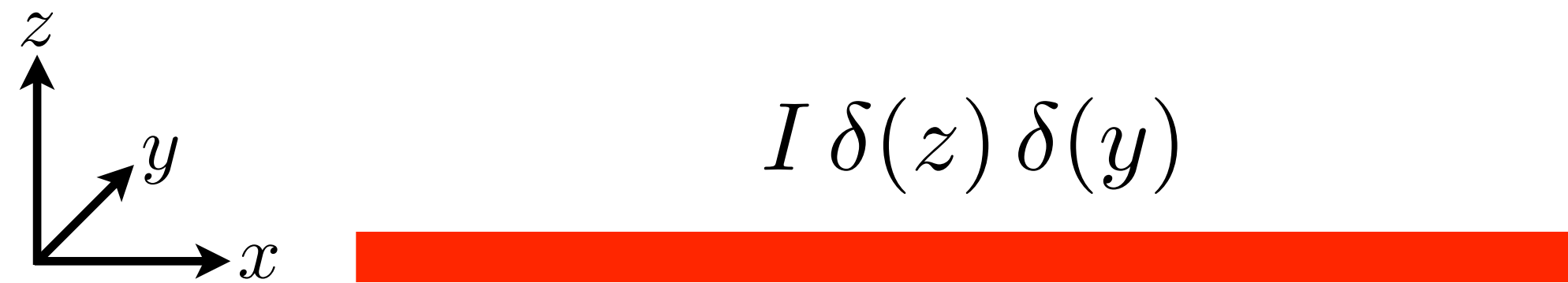


What does $I \delta(z) \delta(y)$ look like far from c.o.m.?

Framing the Question

Further complications: What is an EM field?

EM field generated by a charge/current distribution

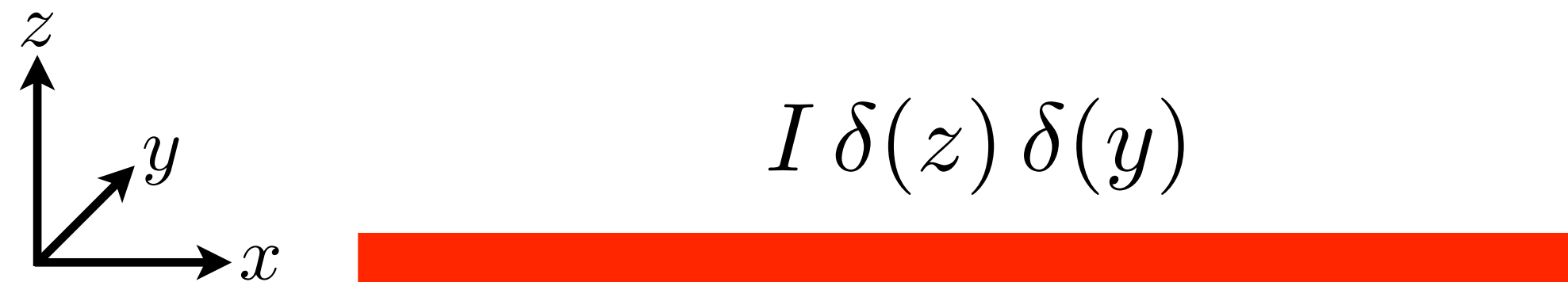


What does $I \delta(z) \delta(y)$ look like far from c.o.m.?

Framing the Question

Further complications: What is an EM field?

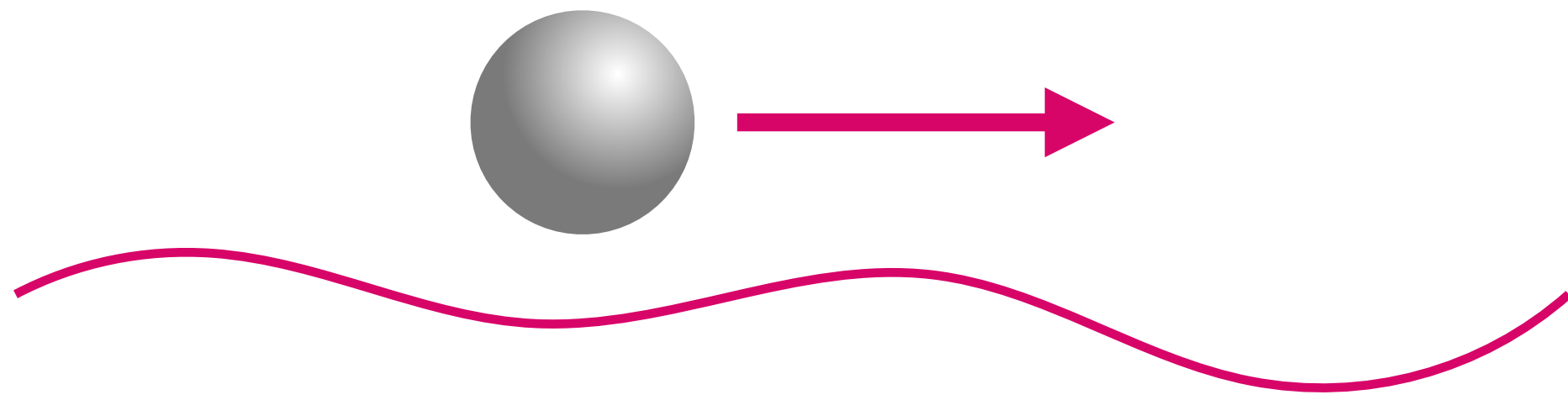
EM field generated by a charge/current distribution



Proper Detector Frame is expansion around c.o.m.

What does $I \delta(z) \delta(y)$ look like far from c.o.m.?

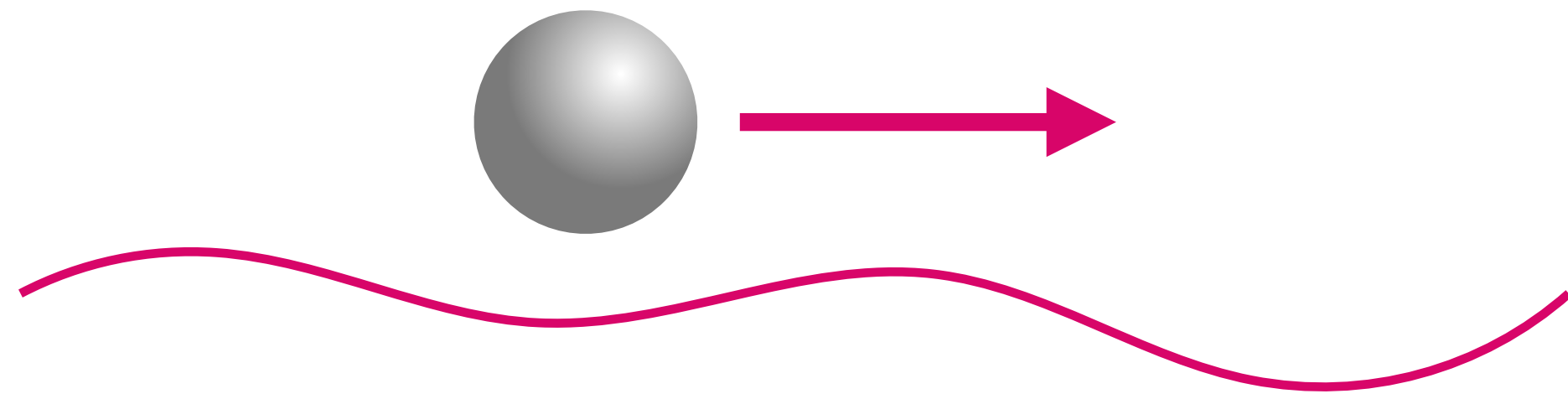
Interactions of Gravitational Waves *with masses*



$$S = - \int dt \, m \sqrt{-g_{\mu\nu} \frac{dx^\mu}{dt} \frac{dx^\nu}{dt}}$$

$$g_{\mu\nu} = \eta_{\mu\nu} + h_{\mu\nu}, \quad g^{\mu\nu} = \eta^{\mu\nu} - h^{\mu\nu}$$

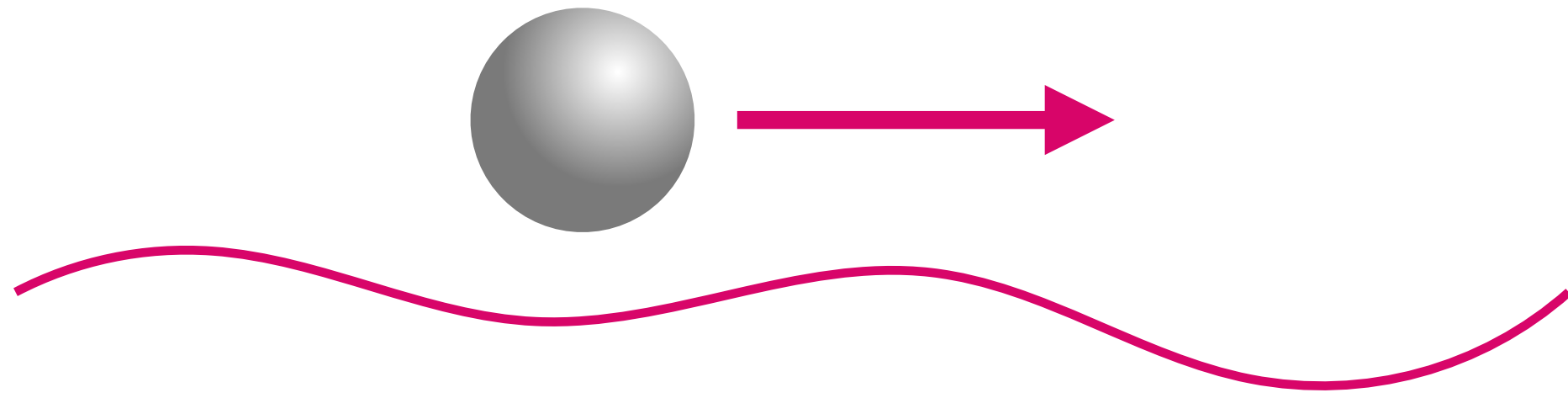
Interactions of Gravitational Waves *with masses*



$$S = - \int dt \, m \sqrt{-g_{\mu\nu} \frac{dx^\mu}{dt} \frac{dx^\nu}{dt}}$$

Equation of motion: $\frac{d^2 x^\mu}{d\tau^2} + \Gamma_{\nu\rho}^\mu(x) \frac{dx^\nu}{d\tau} \frac{dx^\rho}{d\tau} = 0$ $g_{\mu\nu} = \eta_{\mu\nu} + h_{\mu\nu}, \quad g^{\mu\nu} = \eta^{\mu\nu} - h^{\mu\nu}$

Interactions of Gravitational Waves *with masses*



$$S = - \int dt \, m \sqrt{-g_{\mu\nu} \frac{dx^\mu}{dt} \frac{dx^\nu}{dt}}$$

Equation of motion: $\frac{d^2 x^\mu}{d\tau^2} + \Gamma_{\nu\rho}^\mu(x) \frac{dx^\nu}{d\tau} \frac{dx^\rho}{d\tau} = 0$ $g_{\mu\nu} = \eta_{\mu\nu} + h_{\mu\nu}, \quad g^{\mu\nu} = \eta^{\mu\nu} - h^{\mu\nu}$

Effect of GW encoded in Christoffel symbol $\Gamma \propto \partial h$

Returning to Framing the Question

Consider Local Inertial Frame

e.g. Maggiore (2007)

Returning to Framing the Question

Consider Local Inertial Frame

Effect of GW in LIF is that of a Newtonian Force

e.g. Maggiore (2007)

Returning to Framing the Question

Consider Local Inertial Frame

Effect of GW in LIF is that of a Newtonian Force

$$\frac{d^2 \xi_i}{d\tau^2} \simeq -\frac{F_i}{m}$$

e.g. Maggiore (2007)

Returning to Framing the Question

Consider Local Inertial Frame

Effect of GW in LIF is that of a Newtonian Force

$$\frac{d^2 \xi_i}{d\tau^2} \simeq -\frac{F_i}{m}$$

$$\frac{d^2 \xi_i}{d\tau^2} \simeq -\partial_i \Gamma_{00}^j \xi^i$$

e.g. Maggiore (2007)

Returning to Framing the Question

Consider Local Inertial Frame

Effect of GW in LIF is that of a Newtonian Force

$$\frac{d^2 \xi_i}{d\tau^2} \simeq -\frac{F_i}{m}$$

$$\frac{d^2 \xi_i}{d\tau^2} \simeq -\partial_i \Gamma_{00}^j \xi^i$$

$$F_i \simeq \frac{m}{2} \ddot{h}_{ij}^{\text{TT}} x^i$$

e.g. Maggiore (2007)

Returning to Framing the Question

Consider Local Inertial Frame

Effect of GW in LIF is that of a Newtonian Force

$$\frac{d^2 \xi_i}{d\tau^2} \simeq -\frac{F_i}{m}$$

$$\frac{d^2 \xi_i}{d\tau^2} \simeq -\partial_i \Gamma_{00}^j \xi^i$$

$$F_i \simeq \frac{m}{2} \ddot{h}_{ij}^{\text{TT}} x^i$$

Long-wavelength approximation valid because materials have $c_s \ll 1$

e.g. Maggiore (2007)

Returning to Framing the Question

Consider Local Inertial Frame

Effect of GW in LIF is that of a Newtonian Force

$$\frac{d^2 \xi_i}{d\tau^2} \simeq -\frac{F_i}{m}$$

$$\frac{d^2 \xi_i}{d\tau^2} \simeq -\partial_i \Gamma_{00}^j \xi^i$$

$$F_i \simeq \frac{m}{2} \ddot{h}_{ij}^{\text{TT}} x^i$$

Long-wavelength approximation valid because materials have $c_s \ll 1$

$$ds^2 \simeq -dt^2 (1 + R_{0i0j} x^i x^j) - \frac{4}{3} dt dx^i (R_{0ijk} x^j x^k) + dx^i dx^j \left(\delta_{ij} - \frac{1}{3} R_{ikjl} x^k x^l \right) \text{ e.g. Maggiore (2007)}$$

Situation Report

Effective current from spatial or temporal variations of h or F

$$j_{\text{eff}}^{\mu} \equiv \partial_{\nu} \left(\frac{1}{2} h F^{\mu\nu} + h^{\nu}_{\alpha} F^{\alpha\mu} - h^{\mu}_{\alpha} F^{\alpha\nu} \right)$$

Situation Report

Effective current from spatial or temporal variations of h or F

$$j_{\text{eff}}^{\mu} \equiv \partial_{\nu} \left(\frac{1}{2} h F^{\mu\nu} + h^{\nu}_{\alpha} F^{\alpha\mu} - h^{\mu}_{\alpha} F^{\alpha\nu} \right)$$

Physical current itself also changing at $\mathcal{O}(h)$



Situation Report

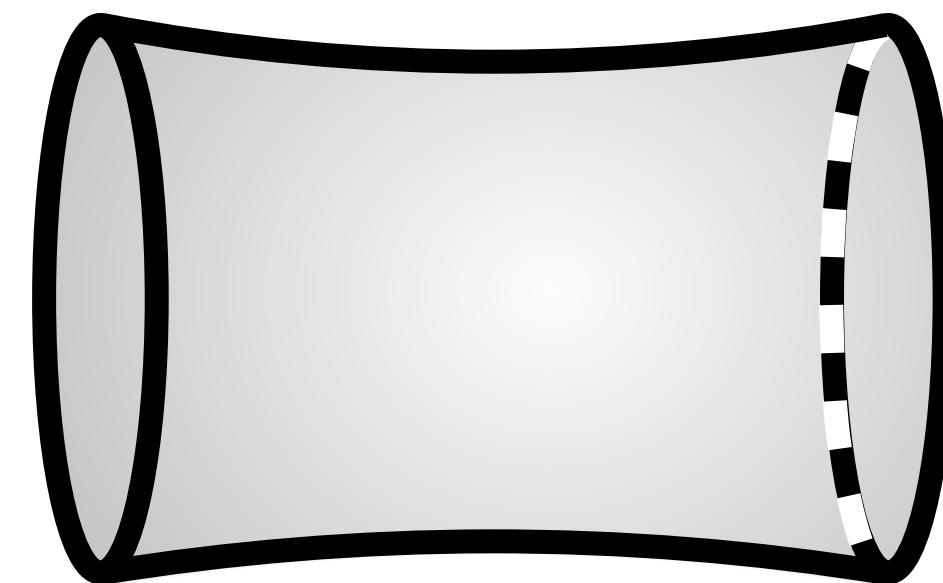
Effective current from spatial or temporal variations of h or F

$$j_{\text{eff}}^{\mu} \equiv \partial_{\nu} \left(\frac{1}{2} h F^{\mu\nu} + h^{\nu}_{\alpha} F^{\alpha\mu} - h^{\mu}_{\alpha} F^{\alpha\nu} \right)$$

Physical current itself also changing at $\mathcal{O}(h)$



Boundaries also changing at $\mathcal{O}(h)$



Situation Report

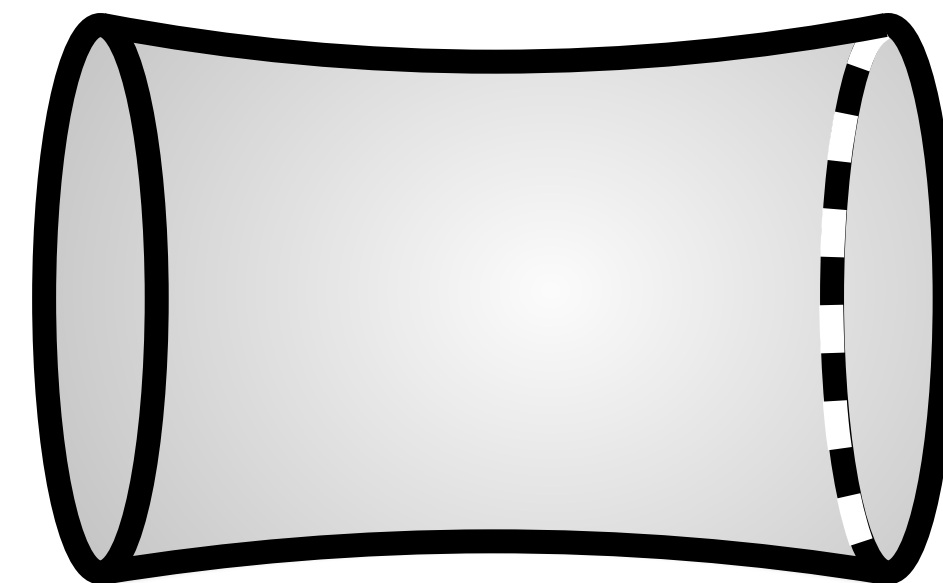
Effective current from spatial or temporal variations of h or F

$$j_{\text{eff}}^{\mu} \equiv \partial_{\nu} \left(\frac{1}{2} h F^{\mu\nu} + h^{\nu}_{\alpha} F^{\alpha\mu} - h^{\mu}_{\alpha} F^{\alpha\nu} \right)$$

Physical current itself also changing at $\mathcal{O}(h)$



Boundaries also changing at $\mathcal{O}(h)$



See, e.g., Ratzinger, Schenk, Schwaller (2024)

Cavity Regime

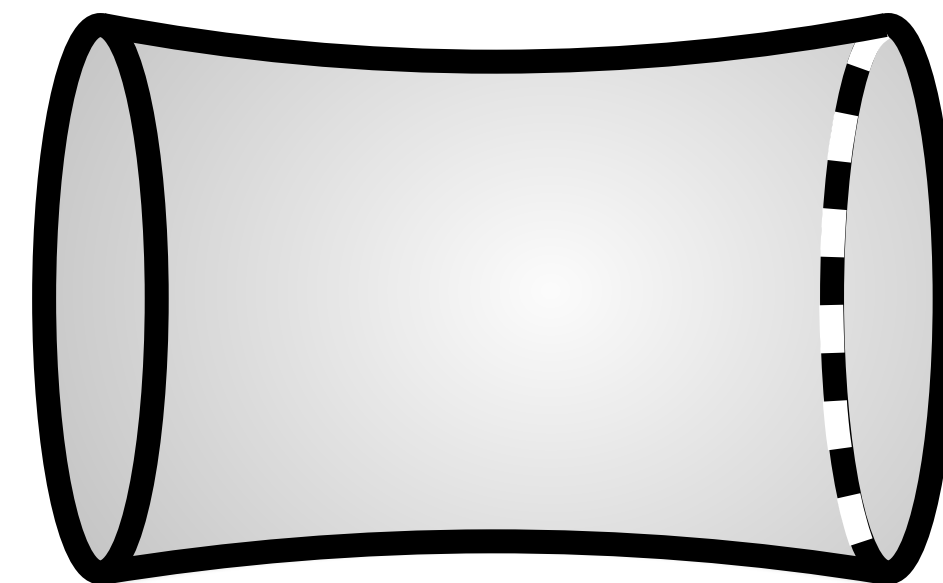
Effective current from spatial or temporal variations of h or F

$$j_{\text{eff}}^{\mu} \equiv \partial_{\nu} \left(\frac{1}{2} h F^{\mu\nu} + h^{\nu}_{\alpha} F^{\alpha\mu} - h^{\mu}_{\alpha} F^{\alpha\nu} \right)$$

Physical current itself also changing at $\mathcal{O}(h)$



Boundaries also changing at $\mathcal{O}(h)$



Cavity Regime

Effective current from spatial or temporal variations of h or F

$$j_{\text{eff}}^{\mu} \equiv \partial_{\nu} \left(\frac{1}{2} h F^{\mu\nu} + h^{\nu}_{\alpha} F^{\alpha\mu} - h^{\mu}_{\alpha} F^{\alpha\nu} \right)$$

Physical current itself also changing at $\mathcal{O}(h)$

Conductive Walls shield AC components of applied B-field

Boundaries also changing at $\mathcal{O}(h)$



Cavity Regime

Effective current from spatial or temporal variations of h or F

$$j_{\text{eff}}^{\mu} \equiv \partial_{\nu} \left(\frac{1}{2} h F^{\mu\nu} + h^{\nu}_{\alpha} F^{\alpha\mu} - h^{\mu}_{\alpha} F^{\alpha\nu} \right)$$

Physical current itself also changing at $\mathcal{O}(h)$



Conductive Walls shield AC components of applied B-field

Boundaries also changing at $\mathcal{O}(h)$



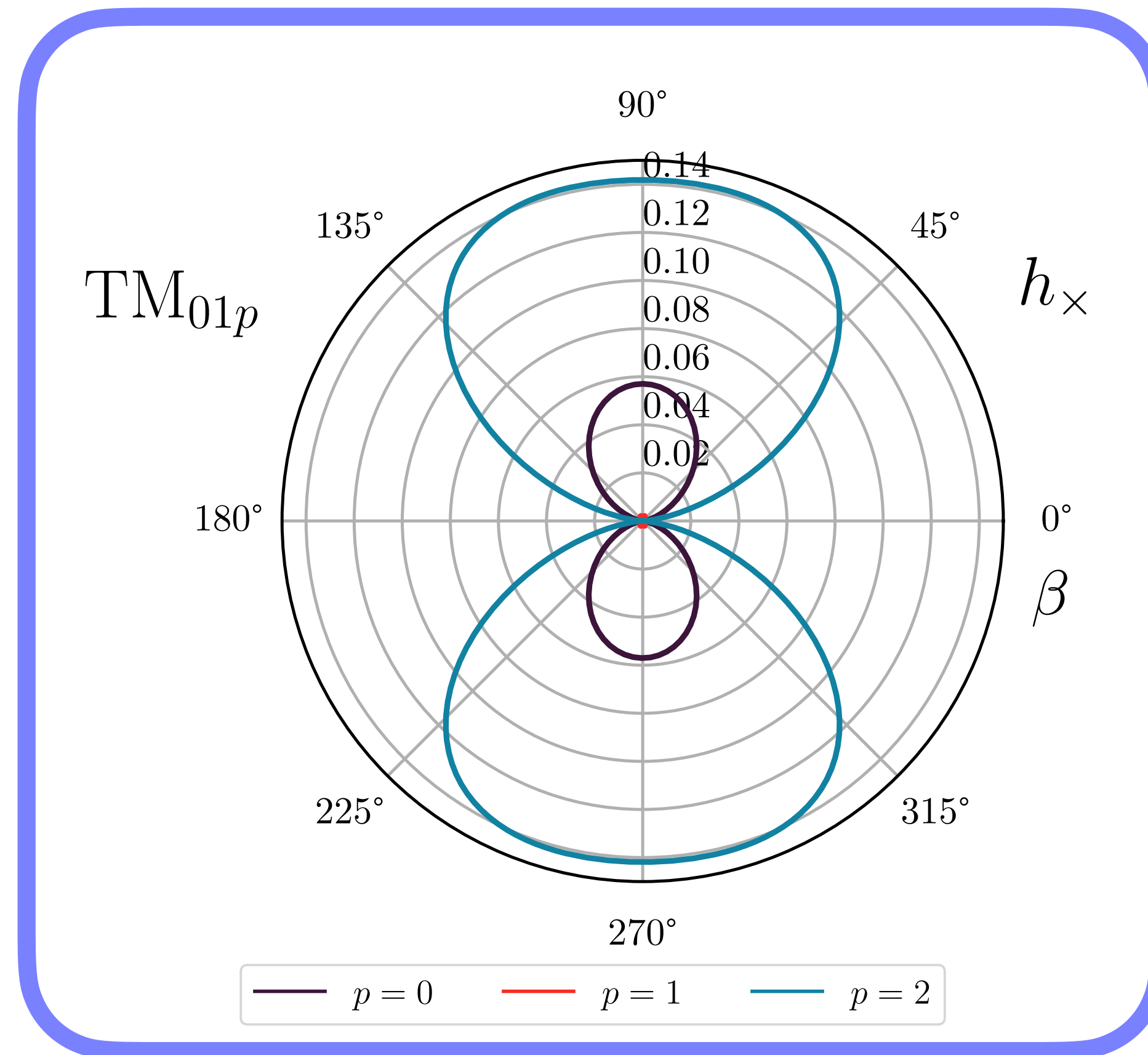
Change in boundary affects physical properties of modes

Axion Cavity Modes Couple to GWs

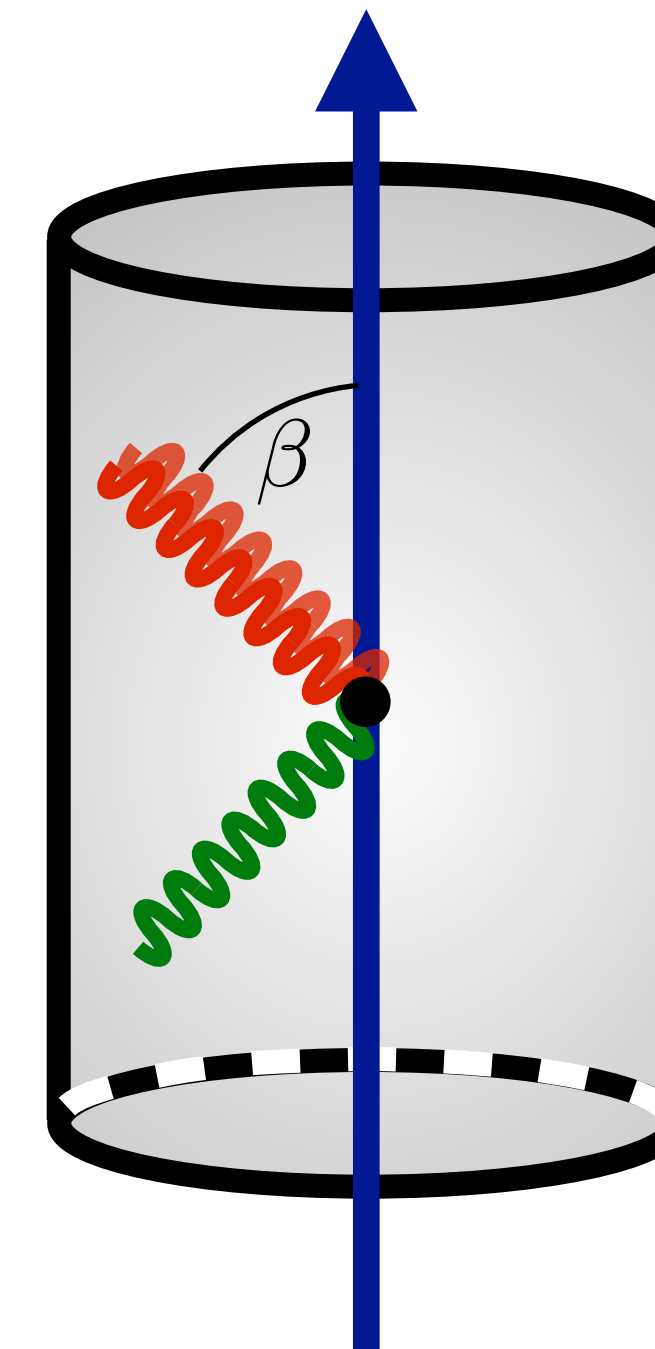
$$\eta \propto \int_V \mathbf{E}_{\text{cav}}^* \cdot \mathbf{J}_{\text{eff}}$$

Axion Cavity Modes Couple to GWs

$$\eta \propto \int_V \mathbf{E}_{\text{cav}}^* \cdot \mathbf{J}_{\text{eff}}$$

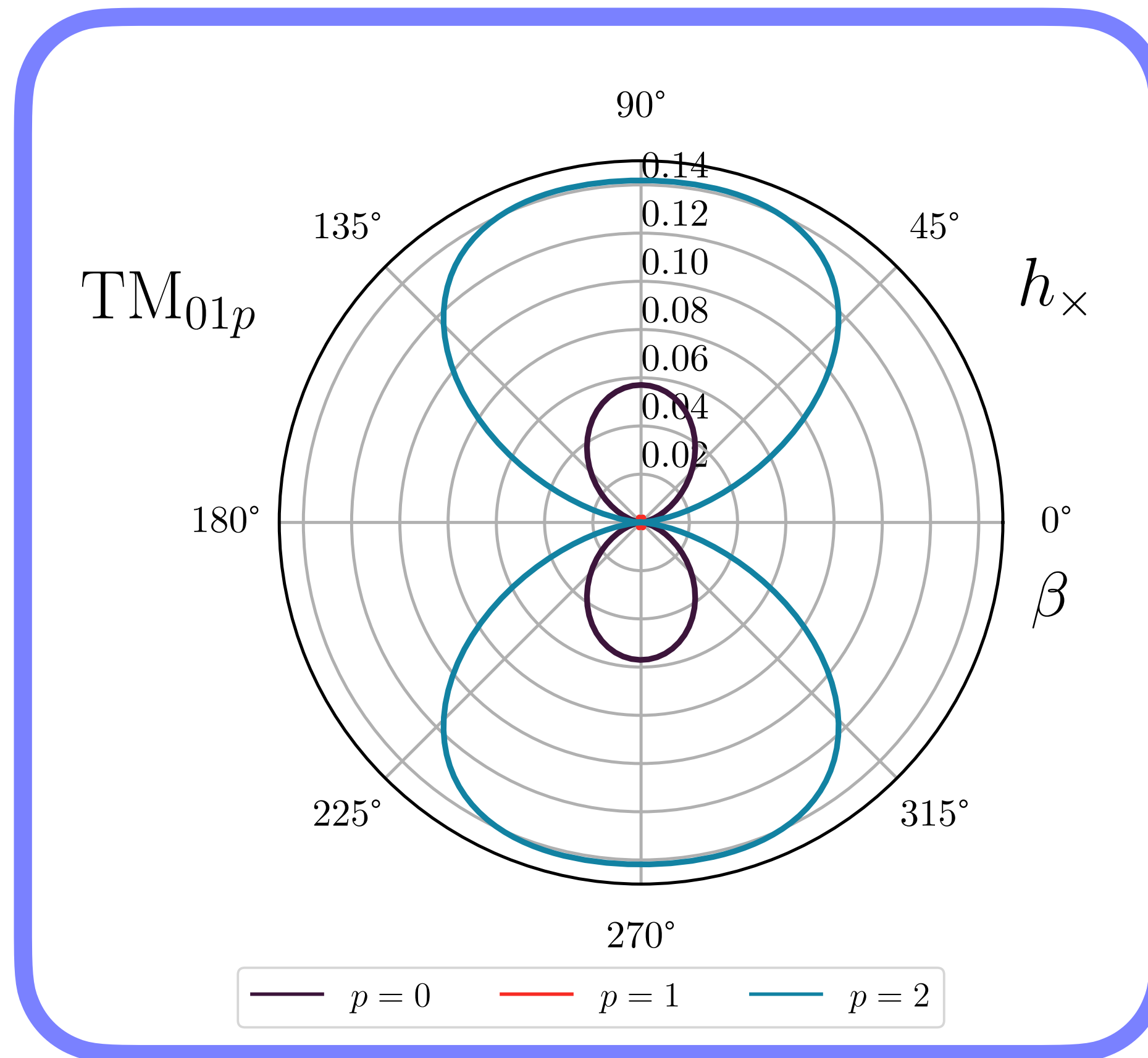


Berlin, Blas, D'Agnolo, SARE, Harnik, Kahn, Schutte-Engel (PRD 2022)



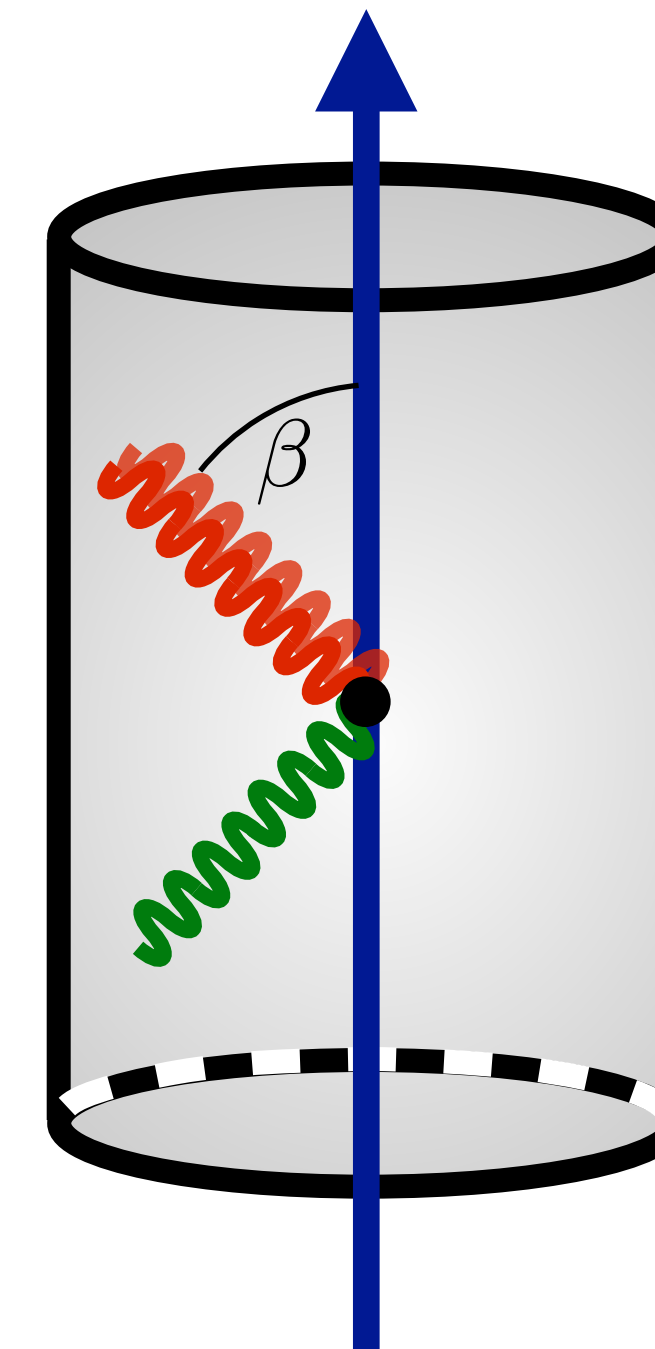
Axion Cavity Modes Couple to GWs

$$\eta \propto \int_V \mathbf{E}_{\text{cav}}^* \cdot \mathbf{J}_{\text{eff}}$$



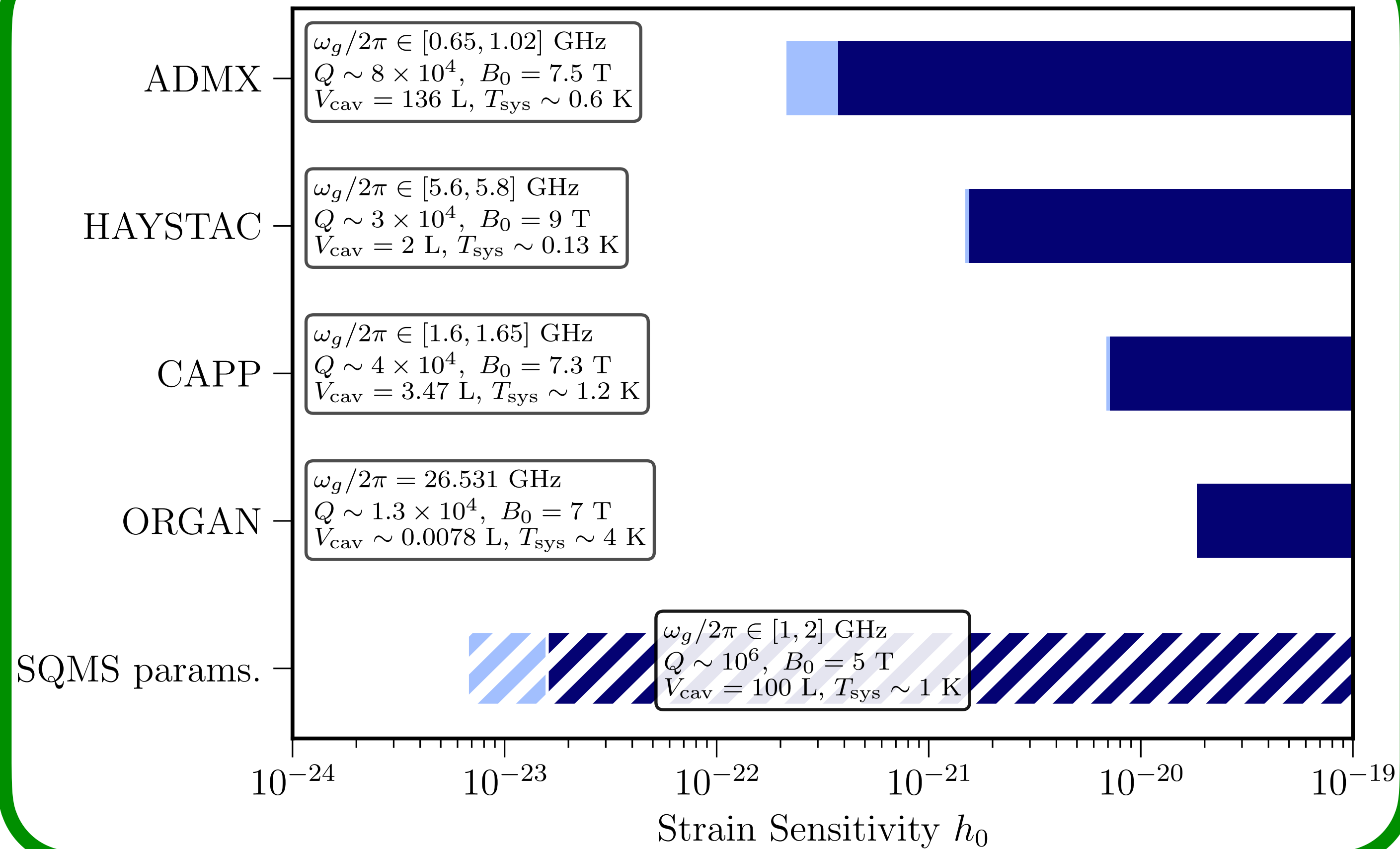
Berlin, Blas, D'Agnolo, SARE, Harnik, Kahn, Schutte-Engel (PRD 2022)

But TM modes not optimal...



Axion Cavity Sensitivity

Projected Sensitivities of Axion Experiments



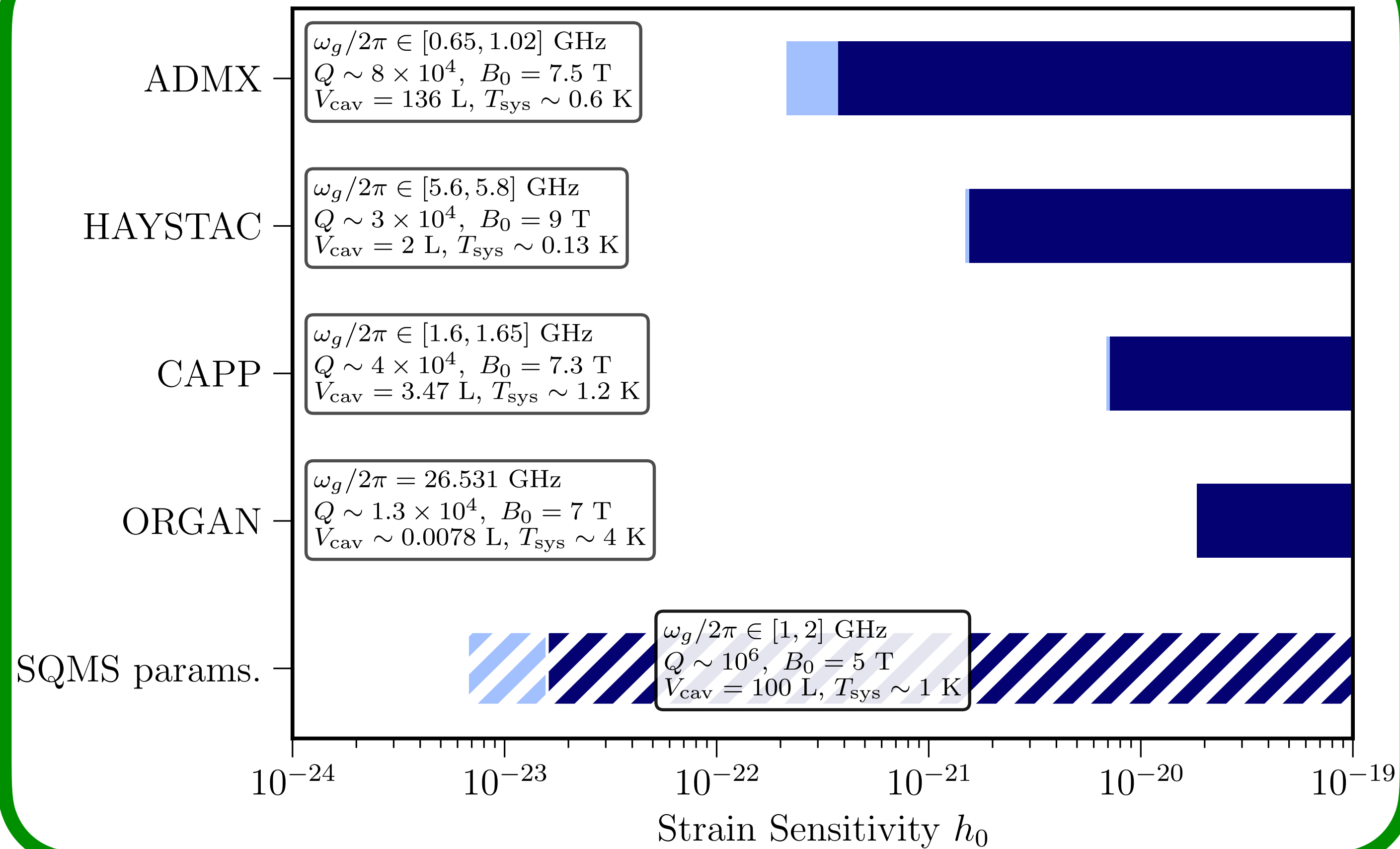
Berlin, Blas, D'Agnolo, SARE, Harnik, Kahn, Schutte-Engel (PRD 2022)

Coherent GW

$$P_{\text{sig}} = \frac{1}{2} Q \omega_g^3 V_{\text{cav}}^{5/3} (\eta_n h_0 B_0)^2$$

Axion Cavity Sensitivity

Projected Sensitivities of Axion Experiments



Berlin, Blas, D'Agnolo, SARE, Harnik, Kahn, Schutte-Engel (PRD 2022)

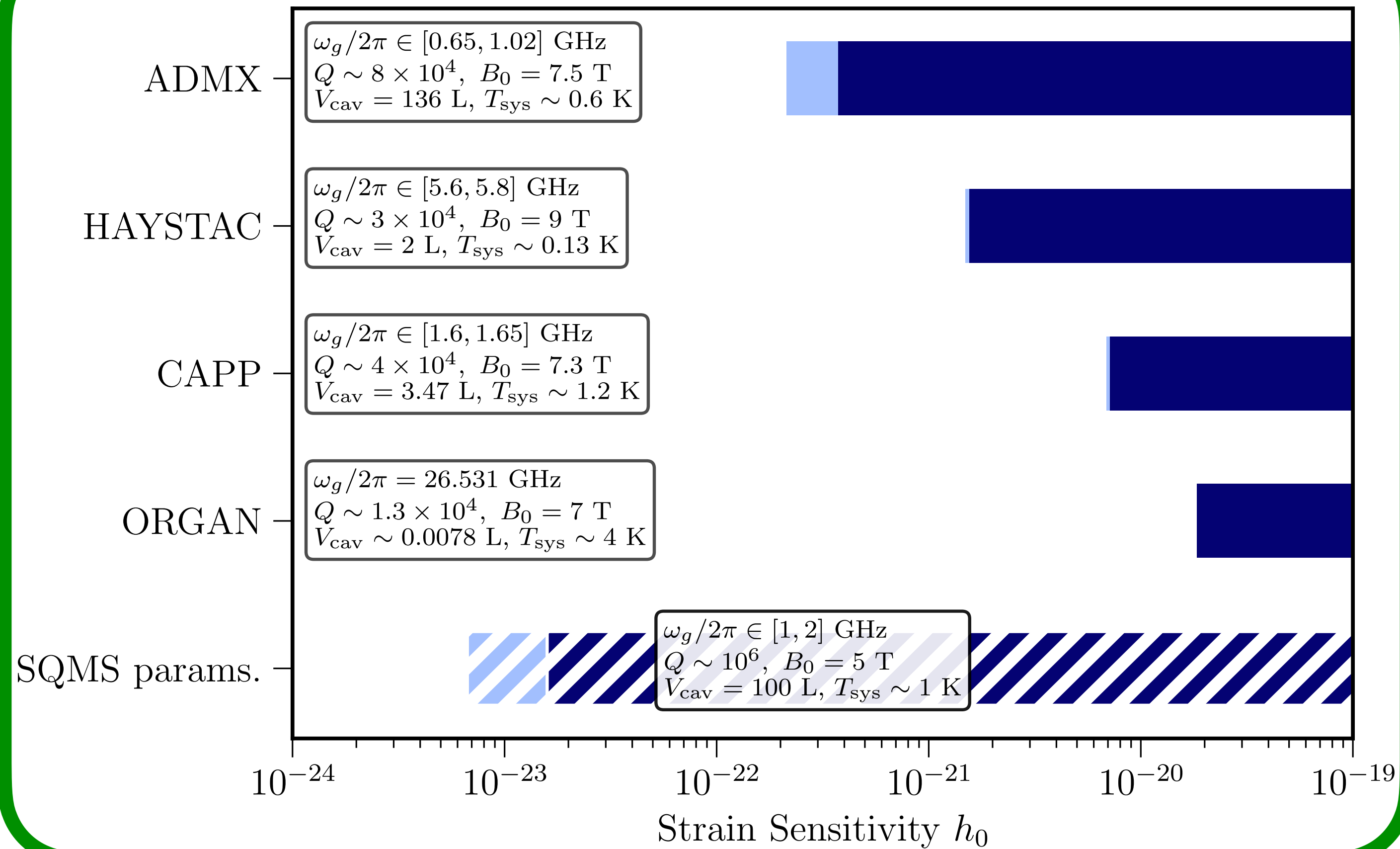
Coherent GW

$$P_{\text{sig}} = \frac{1}{2} Q \omega_g^3 V_{\text{cav}}^{5/3} (\eta_n h_0 B_0)^2$$

$$\mathcal{T} \sim Q \eta_0 (\omega_g V_{\text{cav}}^{1/3}) \sim 10^5$$

Axion Cavity Sensitivity

Projected Sensitivities of Axion Experiments



Berlin, Blas, D'Agnolo, SARE, Harnik, Kahn, Schutte-Engel (PRD 2022)

Coherent GW

$$P_{\text{sig}} = \frac{1}{2} Q \omega_g^3 V_{\text{cav}}^{5/3} (\eta_n h_0 B_0)^2$$

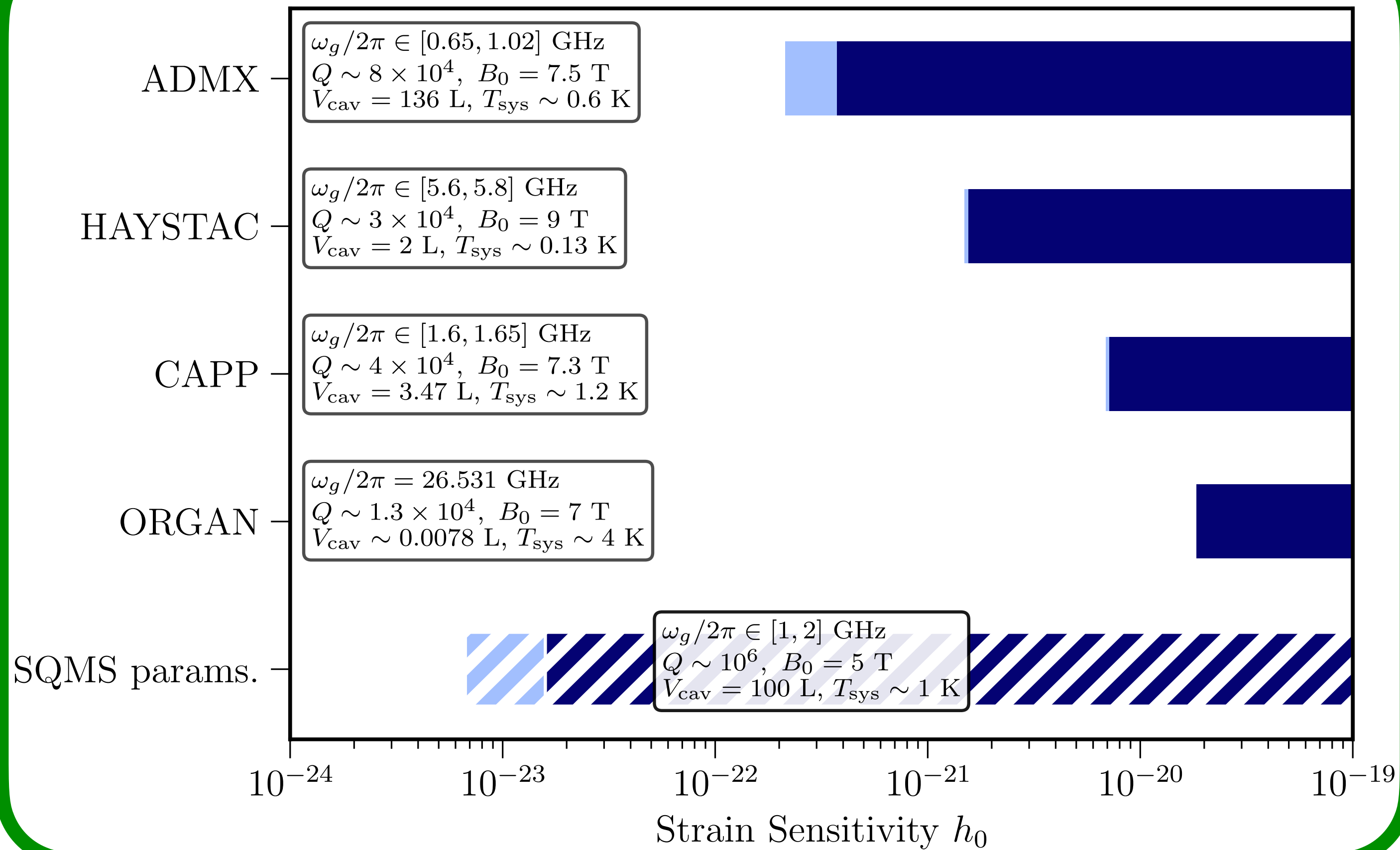
c.f. axion power:

$$P_{\text{sig}}^a \sim Q \omega V (\eta_a g_{a\gamma\gamma} a B_0)^2$$

$$\mathcal{T} \sim Q \eta_0 (\omega_g V_{\text{cav}}^{1/3}) \sim 10^5$$

Axion Cavity Sensitivity

Projected Sensitivities of Axion Experiments



Berlin, Blas, D'Agnolo, SARE, Harnik, Kahn, Schutte-Engel (PRD 2022)

Coherent GW

$$P_{\text{sig}} = \frac{1}{2} Q \omega_g^3 V_{\text{cav}}^{5/3} (\eta_n h_0 B_0)^2$$

c.f. axion power:

$$P_{\text{sig}}^a \sim Q \omega V (\eta_a g_{a\gamma\gamma} a B_0)^2$$

$$\mathcal{T} \sim Q \eta_0 (\omega_g V_{\text{cav}}^{1/3}) \sim 10^5$$

High-Frequency Regime

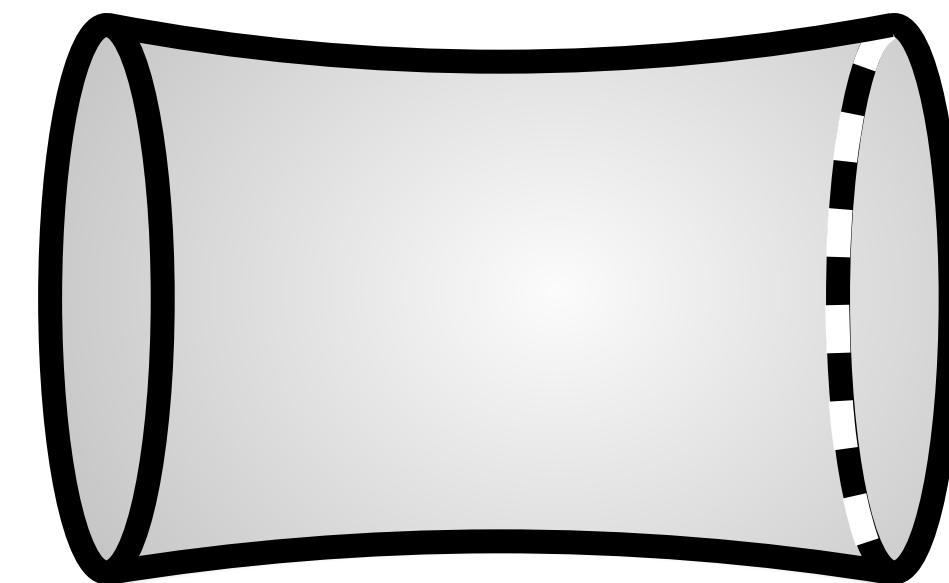
Effective current from spatial or temporal variations of h or F

$$j_{\text{eff}}^{\mu} \equiv \partial_{\nu} \left(\frac{1}{2} h F^{\mu\nu} + h^{\nu}_{\alpha} F^{\alpha\mu} - h^{\mu}_{\alpha} F^{\alpha\nu} \right)$$

Physical current itself also changing at $\mathcal{O}(h)$



Boundaries also changing at $\mathcal{O}(h)$



High-Frequency Regime

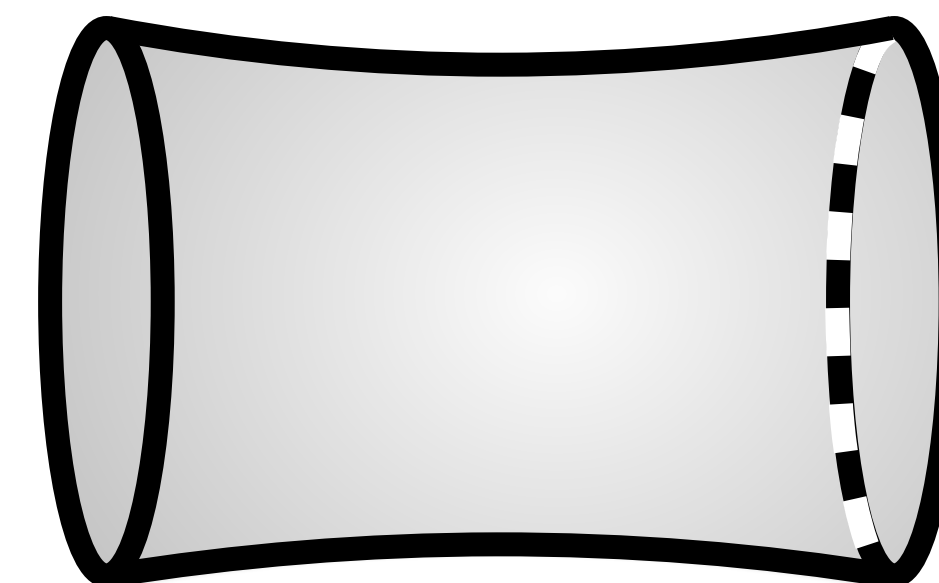
Effective current from spatial or temporal variations of h or F

$$j_{\text{eff}}^{\mu} \equiv \partial_{\nu} \left(\frac{1}{2} h F^{\mu\nu} + h^{\nu}_{\alpha} F^{\alpha\mu} - h^{\mu}_{\alpha} F^{\alpha\nu} \right)$$

Physical current itself also changing at $\mathcal{O}(h)$

— All detector components effectively free-falling: use TT frame

Boundaries also changing at $\mathcal{O}(h)$



High-Frequency Regime

Axion conversion in a b.g. magnetic field:

$$\mathbf{E}_a \sim -g_{a\gamma\gamma} a \mathbf{B}_0 e^{-i\omega t}$$

High-Frequency Regime

Axion conversion in a b.g. magnetic field:

$$\mathbf{E}_a \sim -g_{a\gamma\gamma} a \mathbf{B}_0 e^{-i\omega t}$$

GW conversion in a b.g. magnetic field (in TT gauge):

$$\mathbf{E}_v^p = -\frac{B_0}{2} \left[i\omega x (h_{\times} \hat{\mathbf{p}} + h_{+} \hat{\mathbf{s}}) + h_{\times} s_{\theta} \hat{\mathbf{k}} \right] e^{-i\omega(t - \hat{\mathbf{k}} \cdot \mathbf{x})}$$

Domcke, SARE, Kopp (2024)

High-Frequency Regime

Axion conversion in a b.g. magnetic field:

$$\mathbf{E}_a \sim -g_{a\gamma\gamma} a \mathbf{B}_0 e^{-i\omega t}$$

GW conversion in a b.g. magnetic field (in TT gauge):

$$\mathbf{E}_v^p = -\frac{B_0}{2} \left[i\omega x (h_{\times} \hat{\mathbf{p}} + h_{+} \hat{\mathbf{s}}) + h_{\times} s_{\theta} \hat{\mathbf{k}} \right] e^{-i\omega(t - \hat{\mathbf{k}} \cdot \mathbf{x})}$$

Domcke, SARE, Kopp (2024)

High-Frequency Regime

Axion conversion in a b.g. magnetic field:

$$\mathbf{E}_a \sim -g_{a\gamma\gamma} a \mathbf{B}_0 e^{-i\omega t}$$

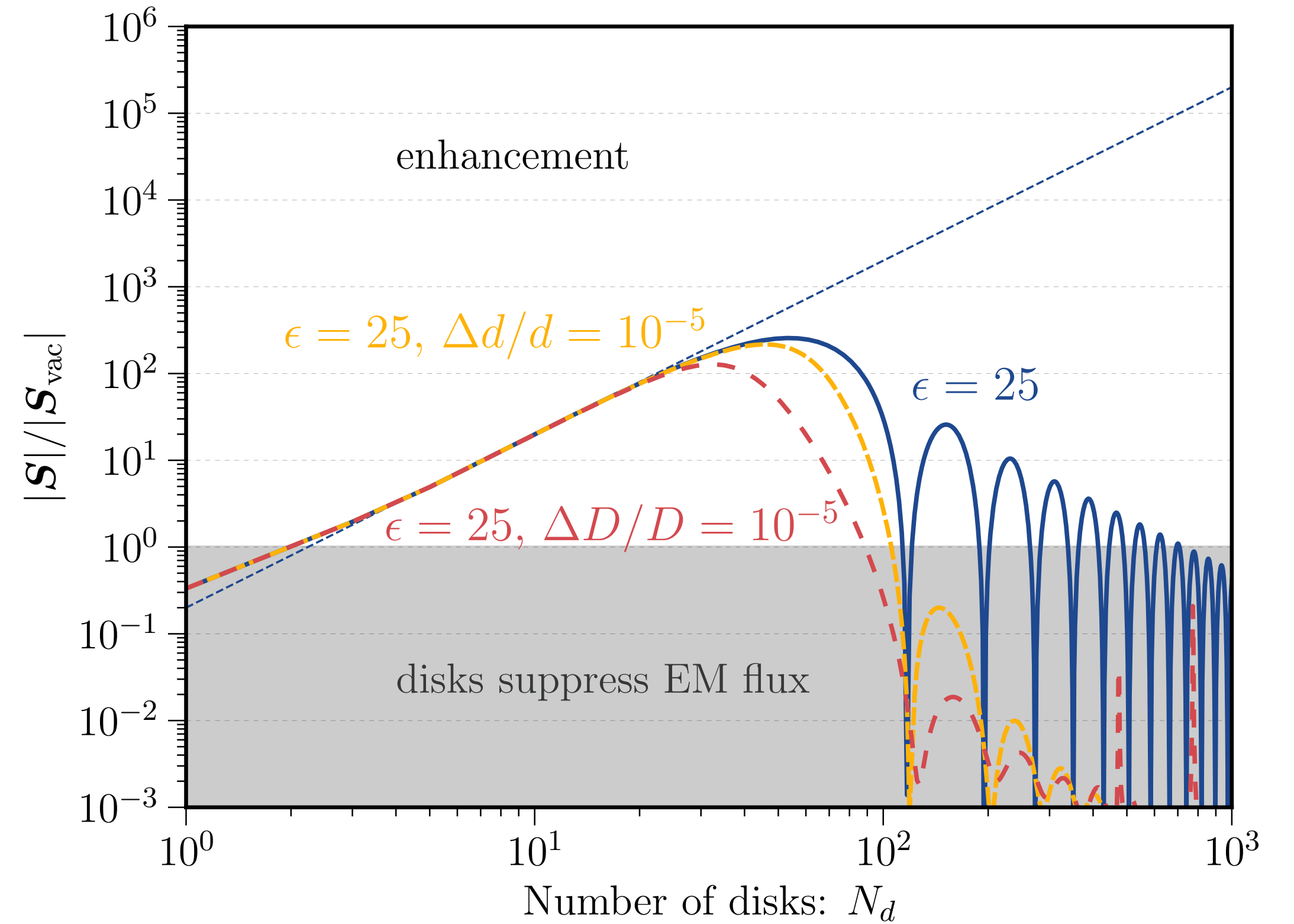
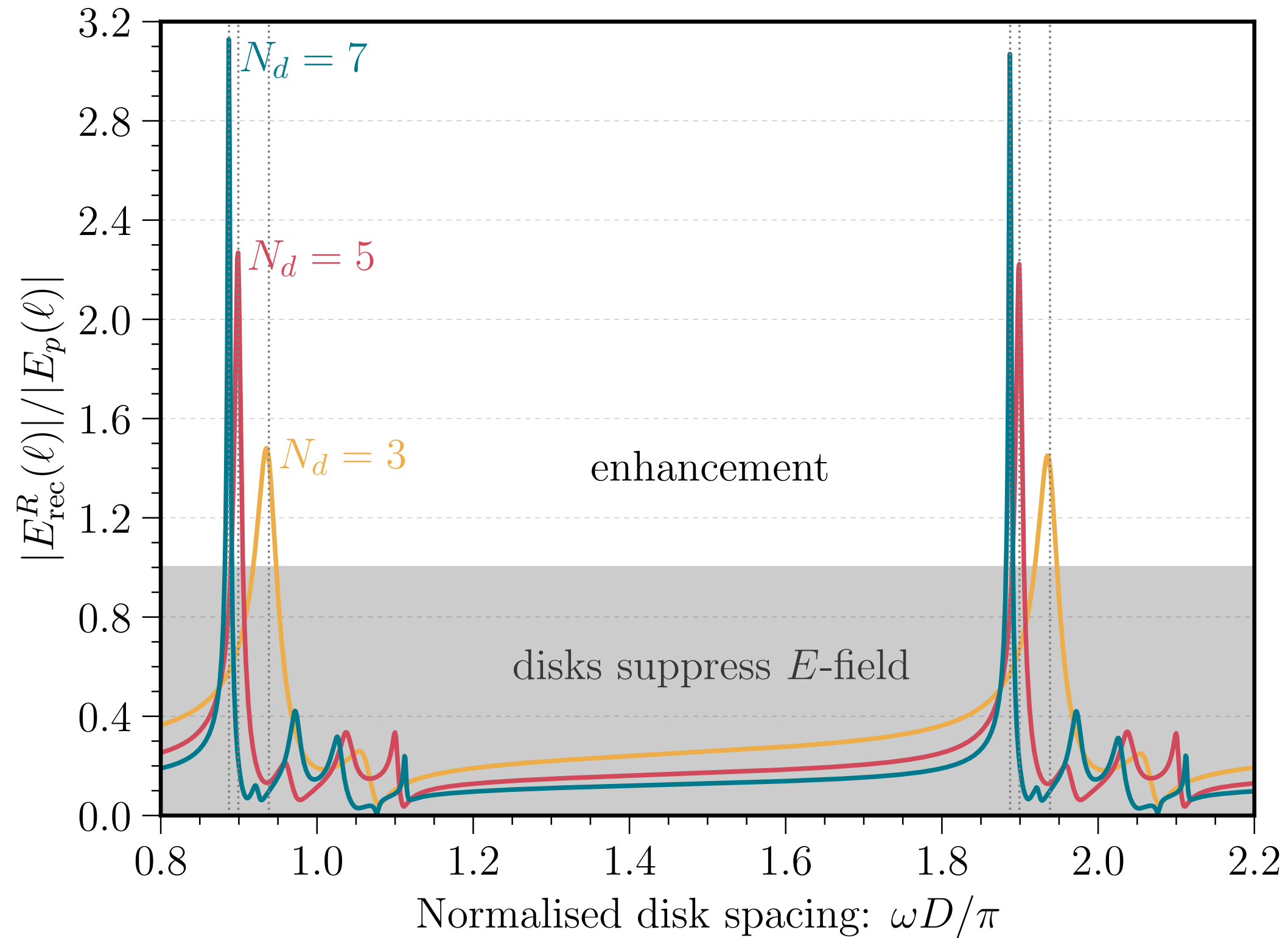
GW conversion in a b.g. magnetic field (in TT gauge):

$$\mathbf{E}_v^p = -\frac{B_0}{2} \left[i\omega x (h_{\times} \hat{\mathbf{p}} + h_{+} \hat{\mathbf{s}}) + h_{\times} s_{\theta} \hat{\mathbf{k}} \right] e^{-i\omega(t - \hat{\mathbf{k}} \cdot \mathbf{x})}$$

Domcke, SARE, Kopp (2024)

Consequence of mass degeneracy of photon and GW in vacuum

Dielectric Haloscopes

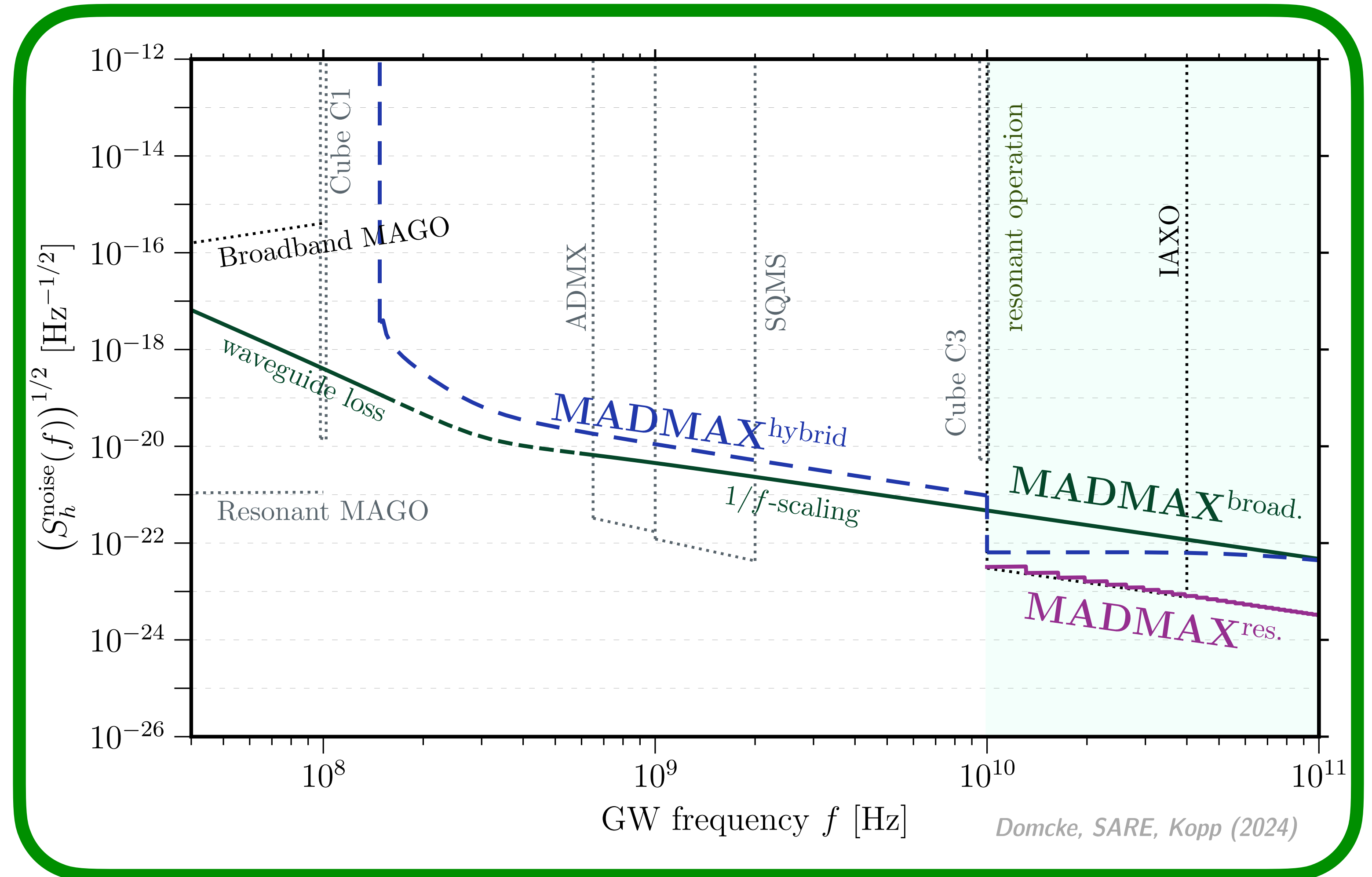


Disks giveth, but disks also taketh away

On resonance, flux density enhanced by ~ 200

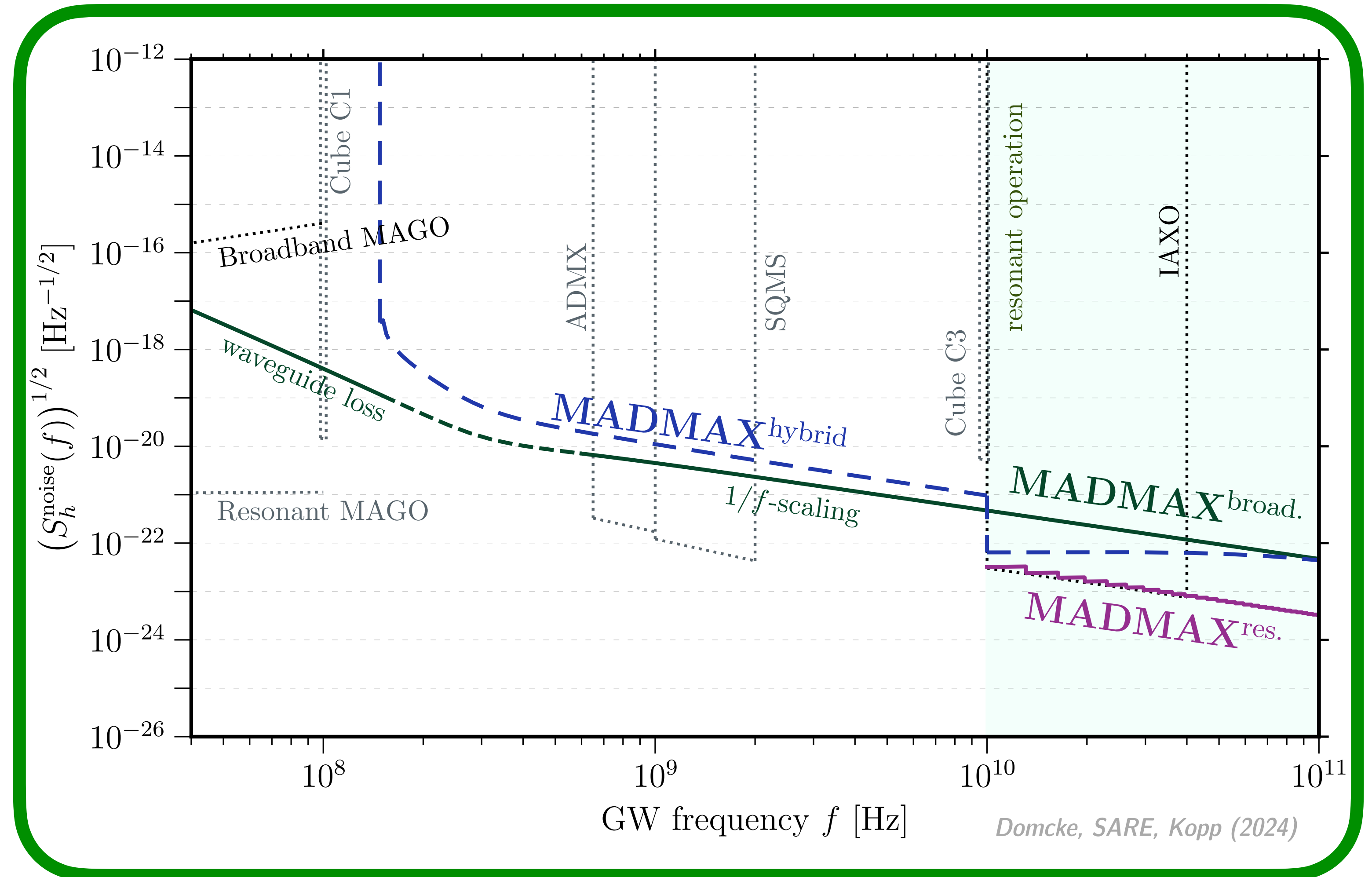
Domcke, SARE, Kopp (2024)

Dielectric* Haloscopes



Dielectric* Haloscopes

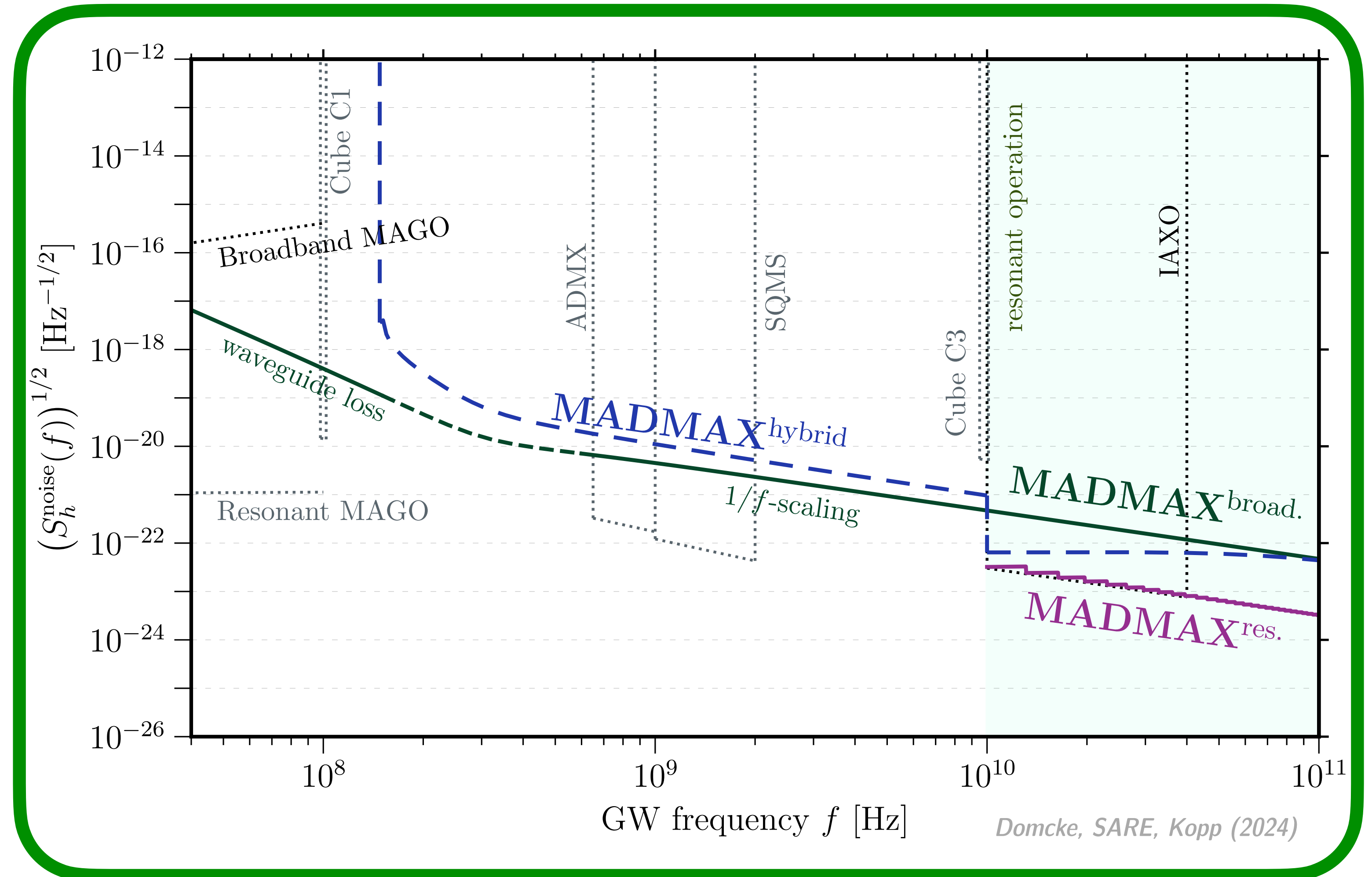
Fully resonant approach
requires scan, but improves
sensitivity by ~ 10



Dielectric* Haloscopes

Fully resonant approach
requires scan, but improves
sensitivity by ~ 10

Hybrid w/ half disks, half
vacuum

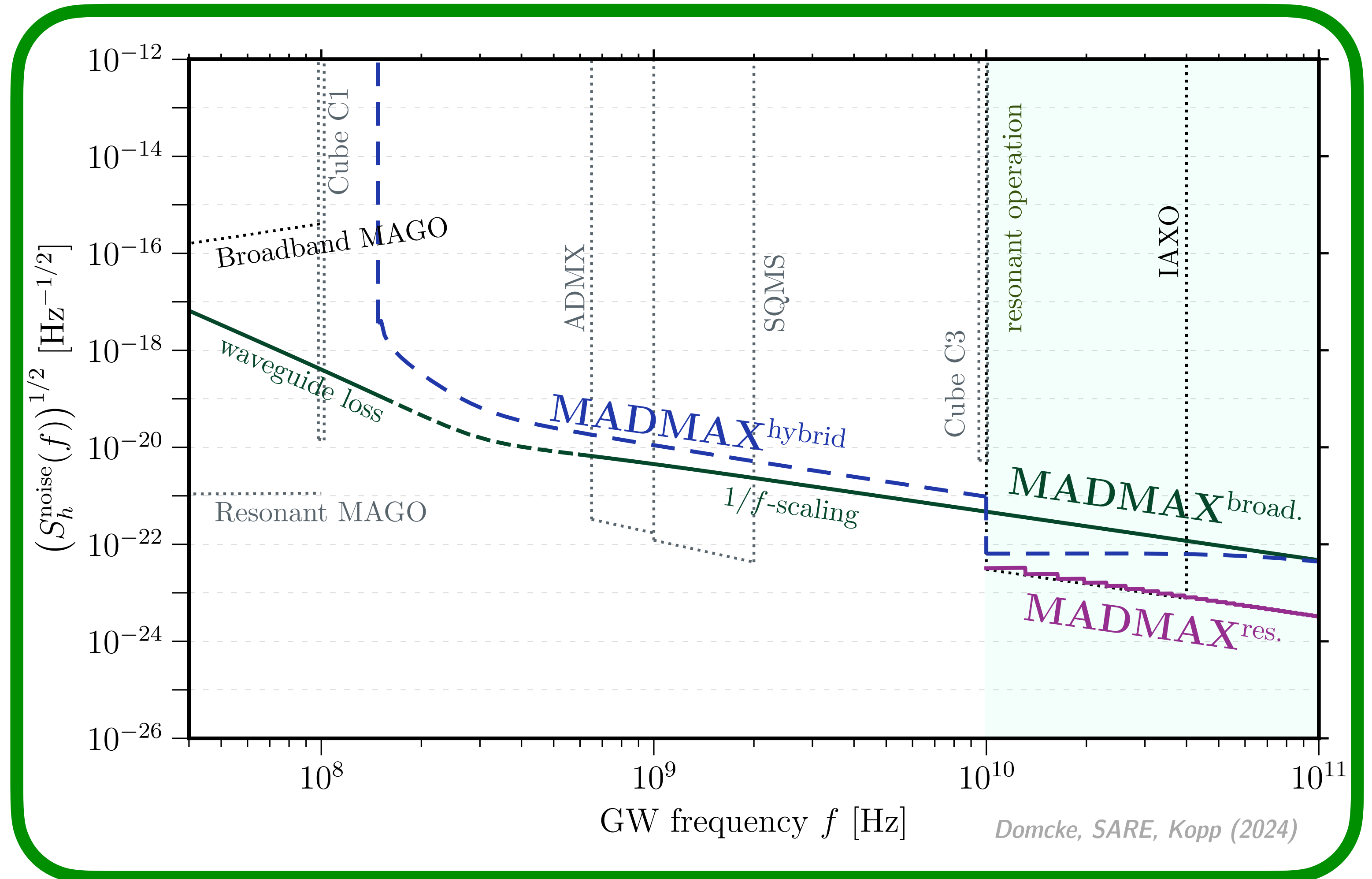


Dielectric* Haloscopes

Fully resonant approach
requires scan, but improves
sensitivity by ~ 10

Hybrid w/ half disks, half
vacuum

Take out disks, fully broadband



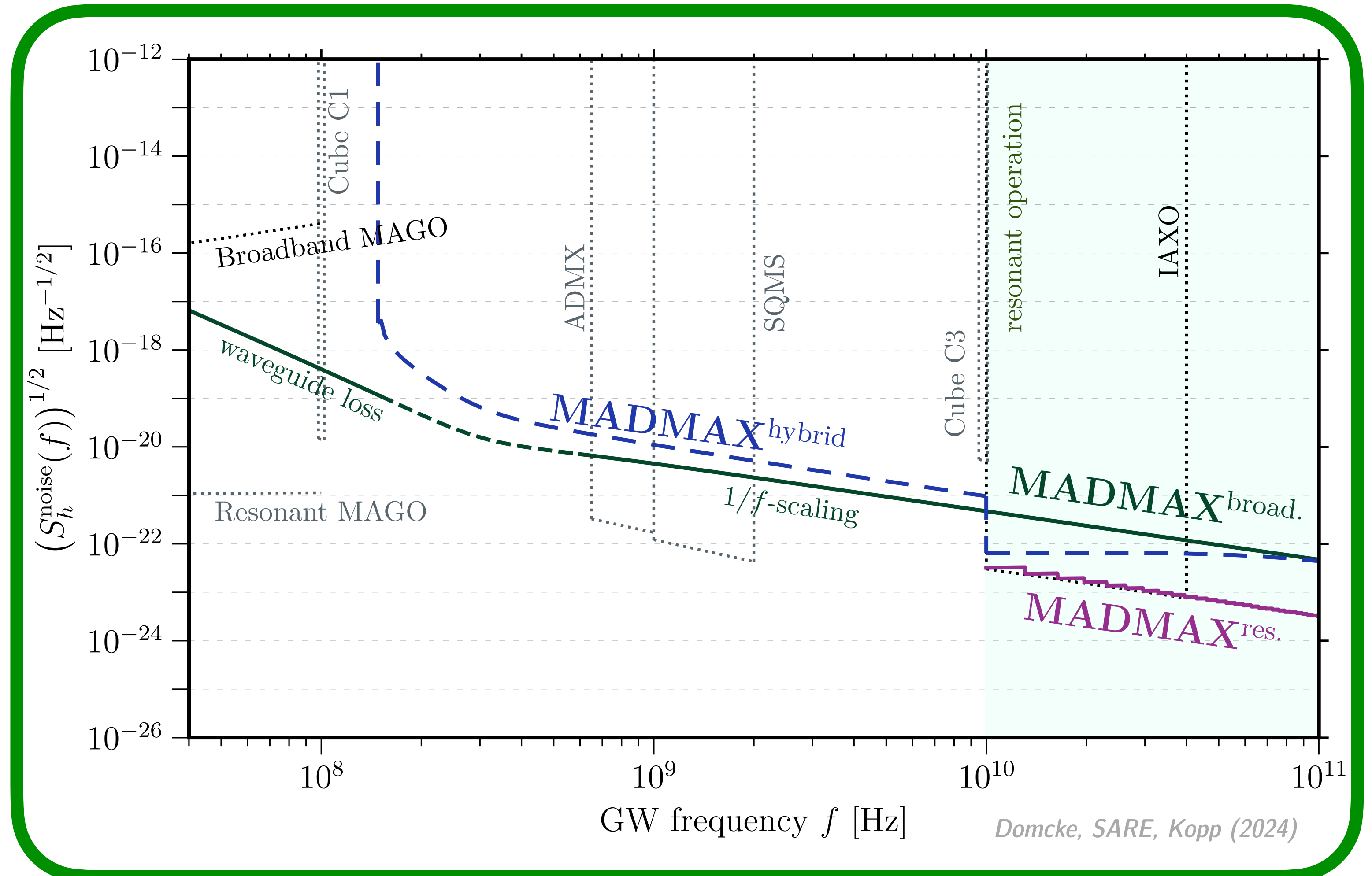
Dielectric* Haloscopes

Fully resonant approach
requires scan, but improves
sensitivity by ~ 10

Hybrid w/ half disks, half
vacuum

Take out disks, fully broadband

Note ωL enhancement from
vacuum conversion



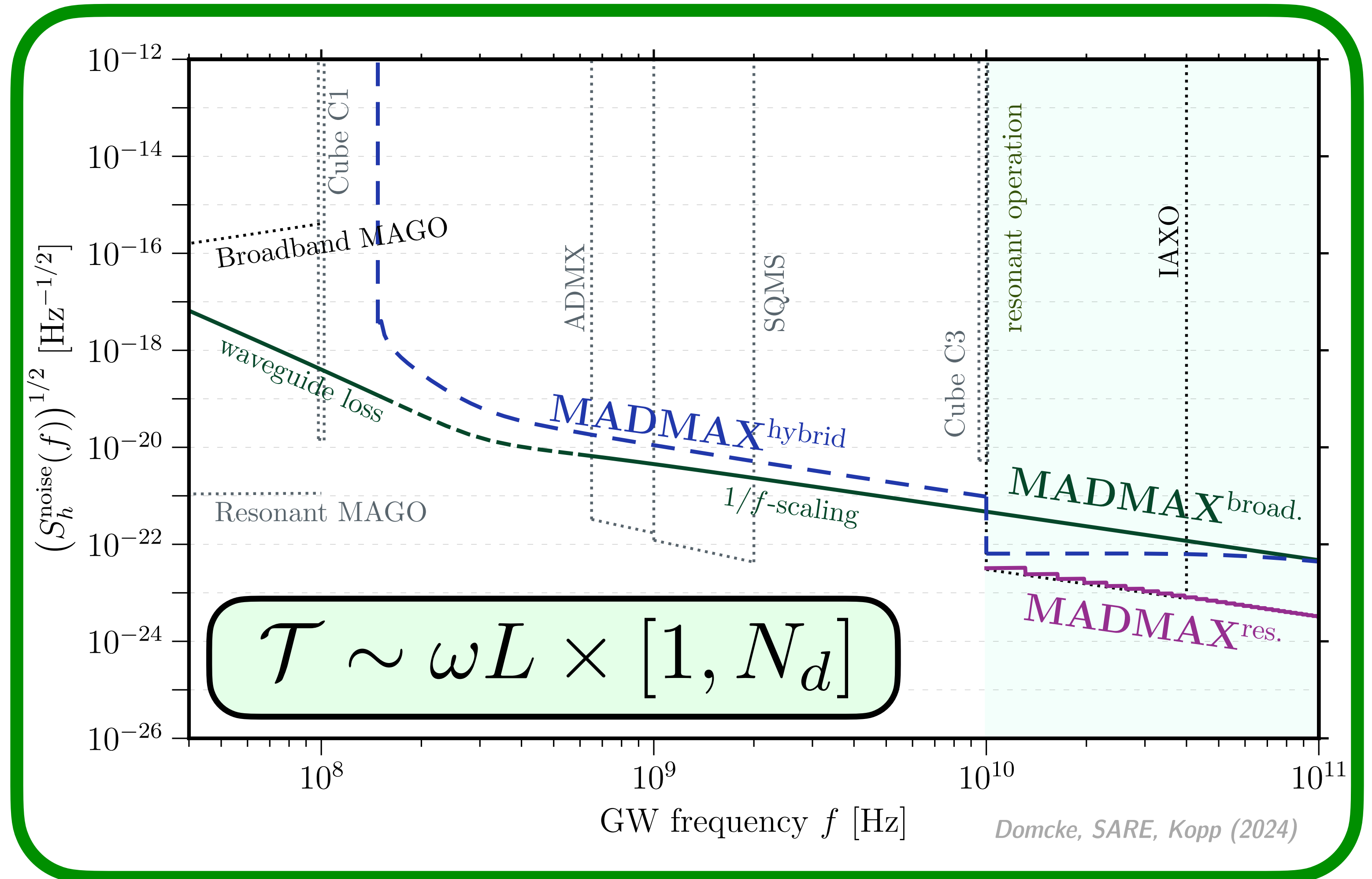
Dielectric* Haloscopes

Fully resonant approach
requires scan, but improves
sensitivity by ~ 10

Hybrid w/ half disks, half
vacuum

Take out disks, fully broadband

Note ωL enhancement from
vacuum conversion



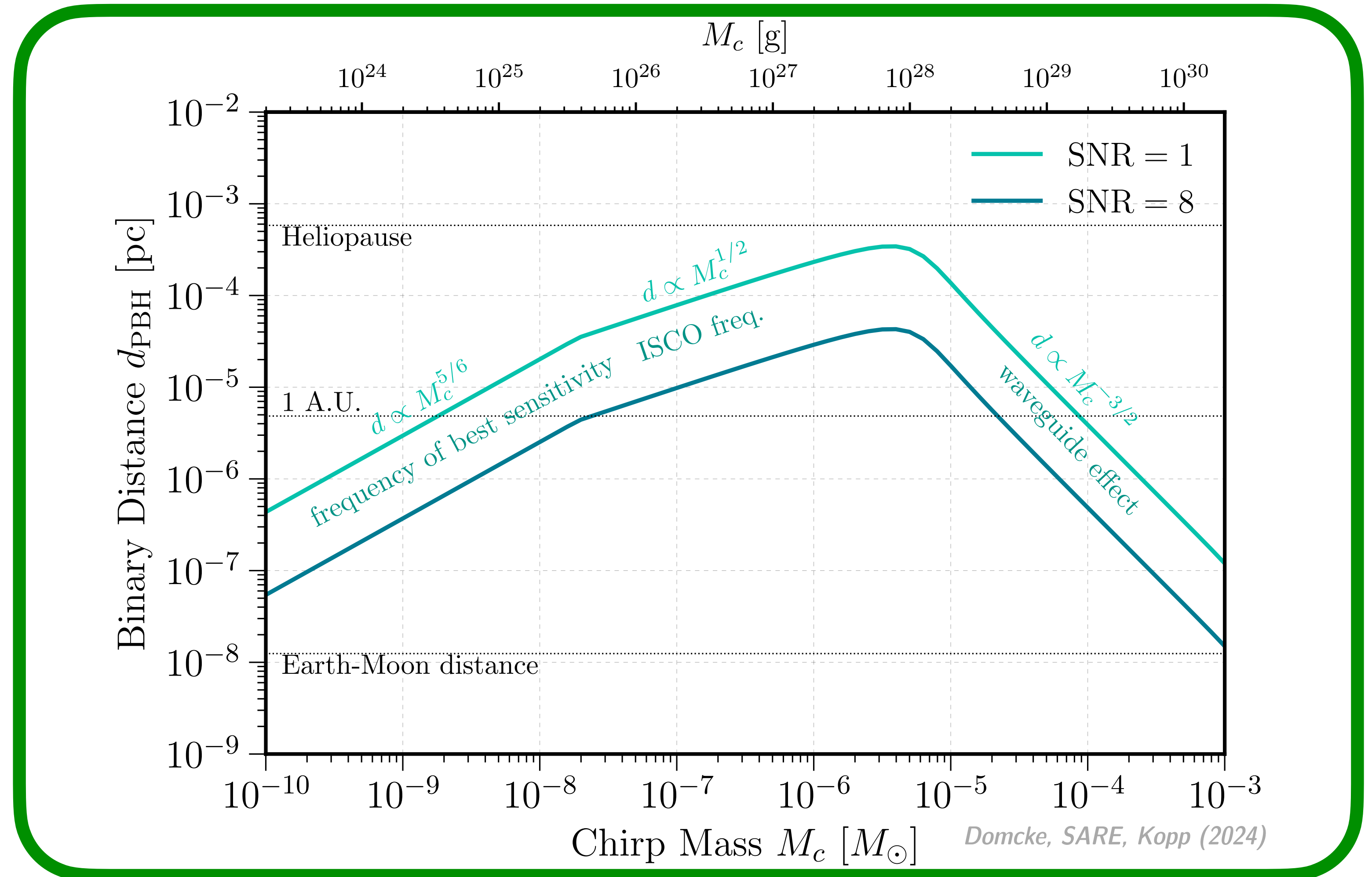
No-Disc MADMAX for PBHs

Take out disks, fully broadband

Typical distance to binary
 ~ 10 kpc

Franciolini, Maharana, Muia (2022)

Improves on resonant cavity



Low-Frequency Regime

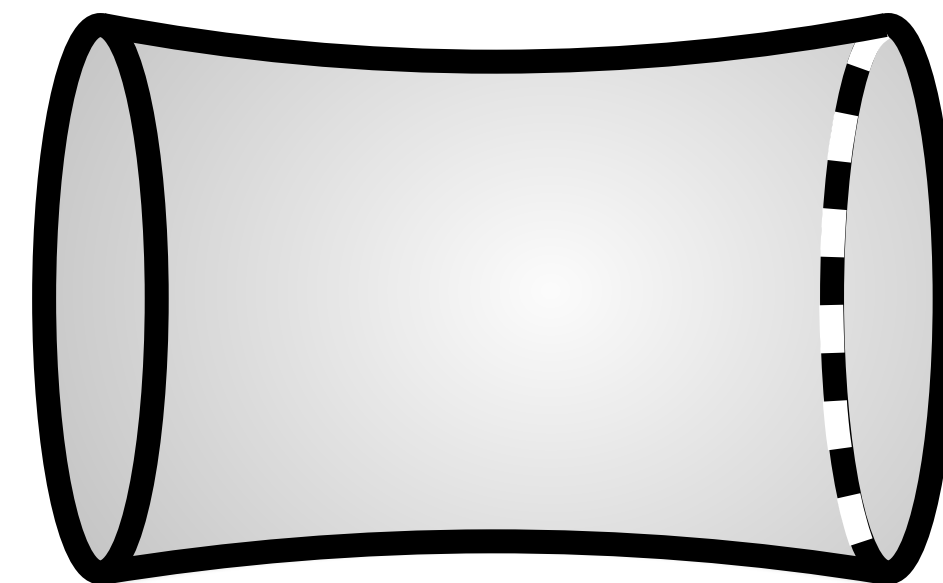
Effective current from spatial or temporal variations of h or F

$$j_{\text{eff}}^{\mu} \equiv \partial_{\nu} \left(\frac{1}{2} h F^{\mu\nu} + h^{\nu}_{\alpha} F^{\alpha\mu} - h^{\mu}_{\alpha} F^{\alpha\nu} \right)$$

Physical current itself also changing at $\mathcal{O}(h)$



Boundaries also changing at $\mathcal{O}(h)$



Low-Frequency Regime

Effective current from spatial or temporal variations of h or F

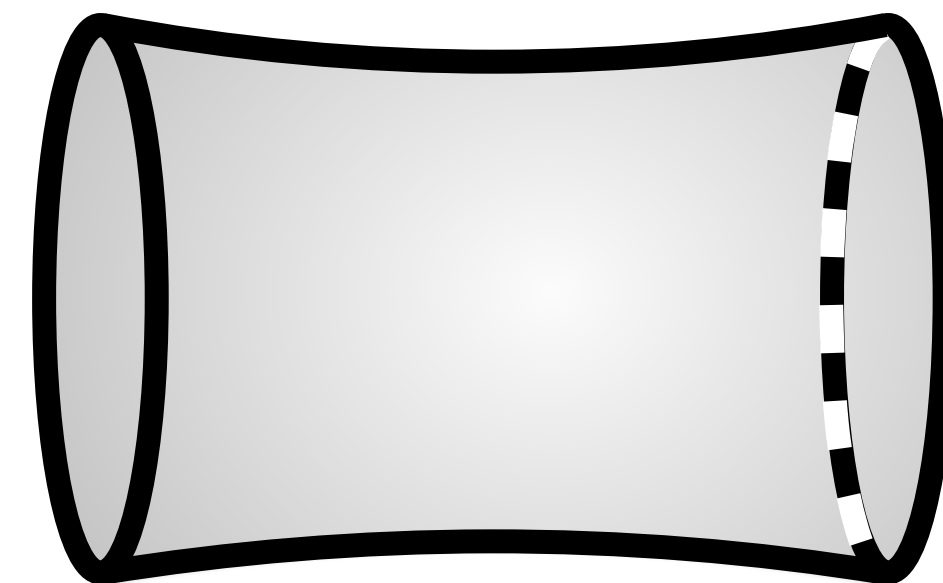
$$j_{\text{eff}}^{\mu} \equiv$$

Less relevant due to rigidity of photons, responding at c

Physical current itself also changing at $\mathcal{O}(h)$



Boundaries also changing at $\mathcal{O}(h)$



Low-Frequency Regime

Effective current from spatial or temporal variations of h or F

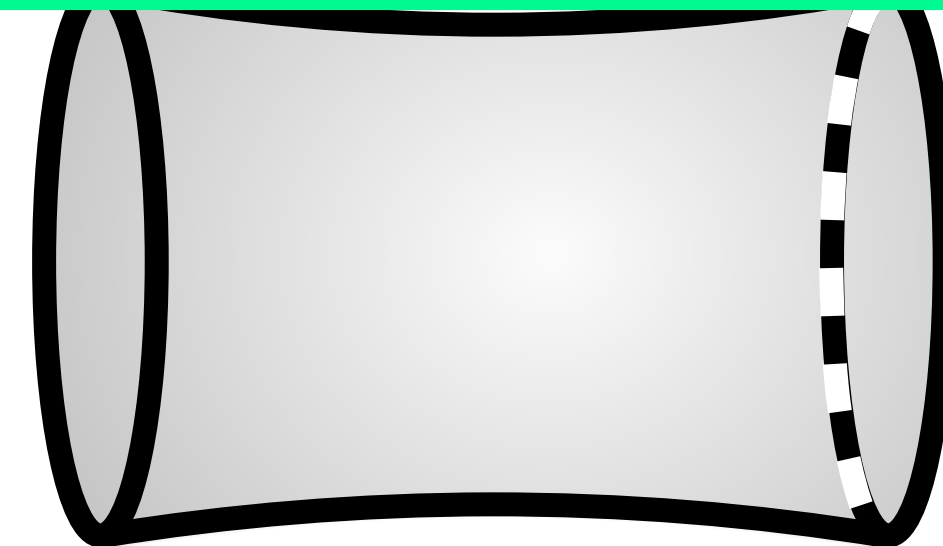
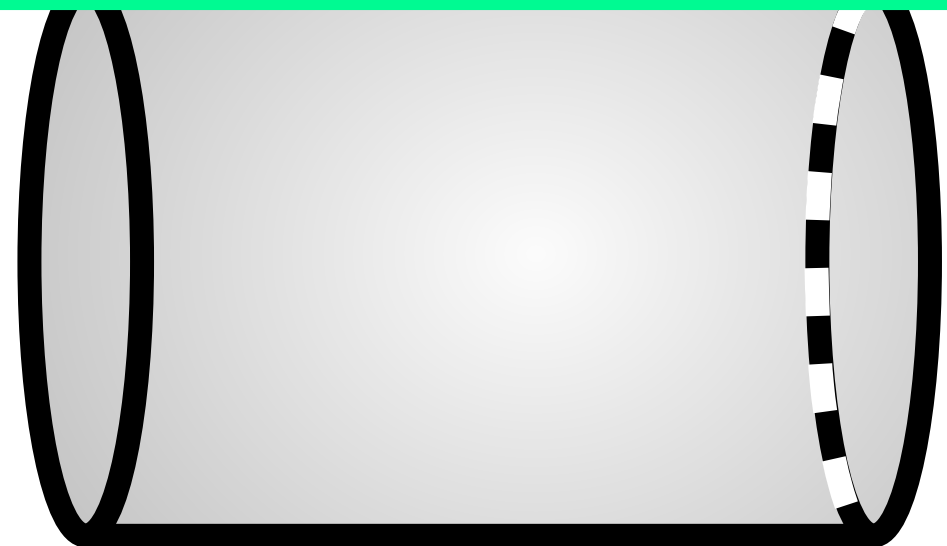
$$j_{\text{eff}}^{\mu} \equiv$$

Less relevant due to rigidity of photons, responding at c

Physical current itself also changing at $\mathcal{O}(h)$



Bou Some detector components moving: use PDF in long-wavelength regime



Transfer function for mechanical transduction

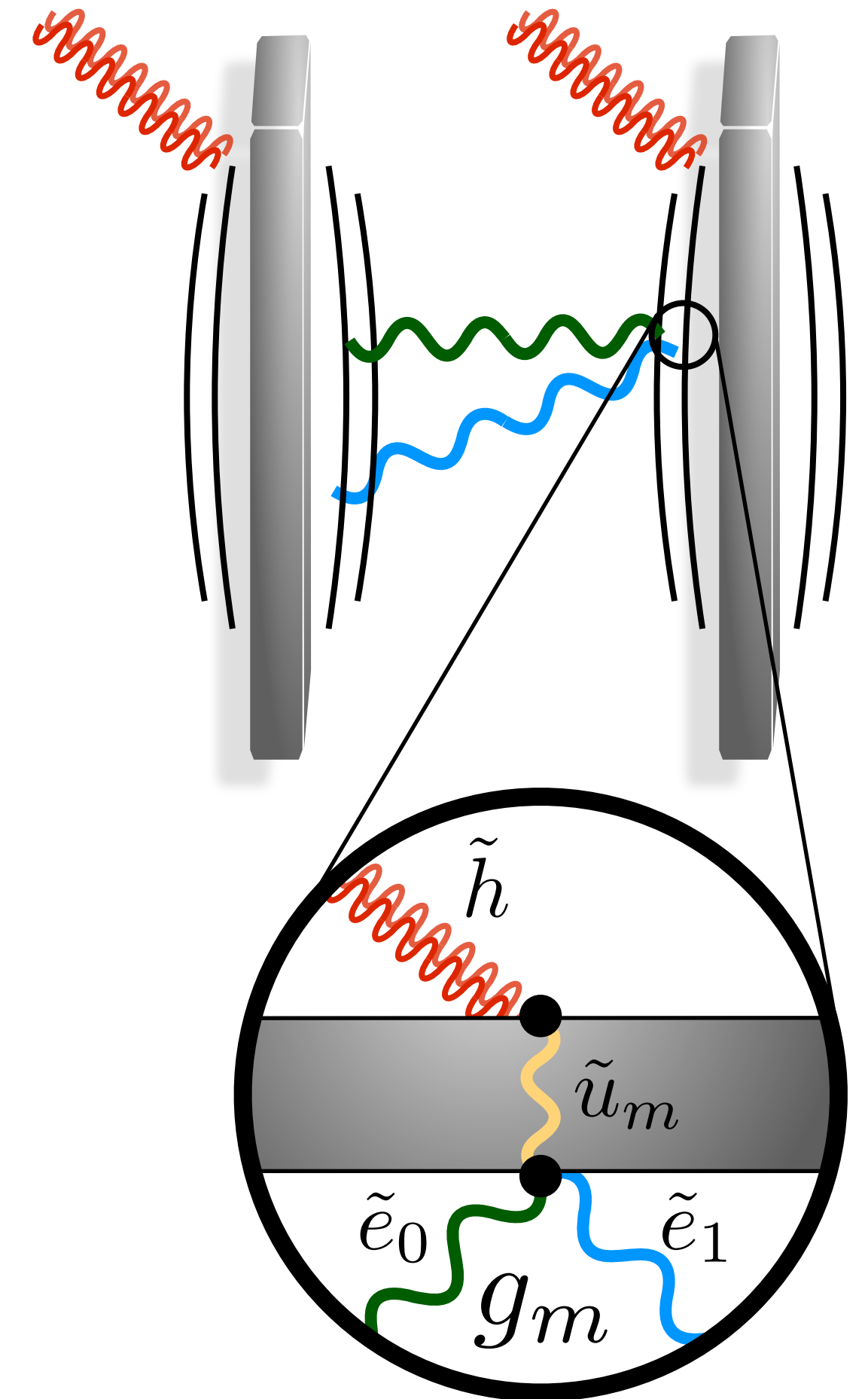
$$\left(\omega_m^2 - \omega^2 + i \frac{\omega \omega_m}{Q_m} \right) \tilde{u}_m(\omega) \simeq -\frac{\omega_g^2 L}{2} \tilde{h}^{\text{TT}}(\omega)$$

$$\left(\omega_1^2 - \omega^2 + i \frac{\omega \omega_1}{Q} \right) \tilde{e}_1(\omega) \simeq \int d\omega' \tilde{e}_0(\omega - \omega') g_m \tilde{u}_m(\omega')$$

$$g_m \equiv -\frac{2\omega_1^2}{L}$$

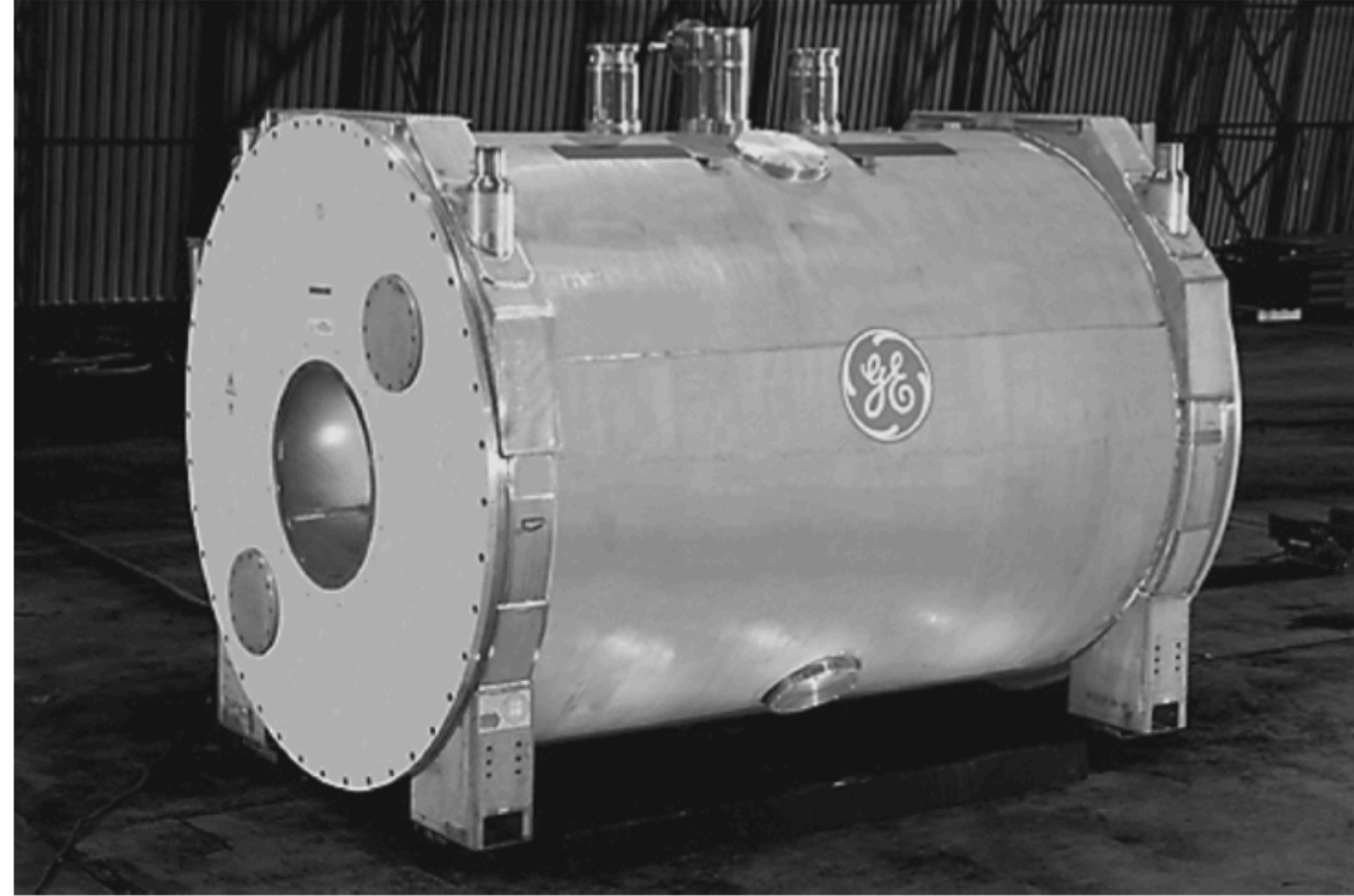
$$\mathcal{T}_{\text{mech}}^2(\omega) = \frac{\omega_g^4 \omega_1^4}{\left((\omega_1^2 - \omega^2)^2 + \frac{\omega^2 \omega_1^2}{Q^2} \right) \left((\omega_m^2 - \omega^2)^2 + \frac{\omega_g^2 \omega_m^2}{Q_m^2} \right)}$$

D'Agnolo, SARE (gr-qc/2412.17897)



Magnetic Weber Bar

Domcke, SARE, Rodd (2024)



140 MJ stored energy $\leftrightarrow S_h^{1/2} \sim 10^{-21} \text{ Hz}^{-1/2}$
(up to transfer function)

Fig. 10. GE 9.4 T MRI magnet before shipment.

TABLE II
PARAMETERS OF GE 9.4 T MRI MAGNET

Central Field B_0 (T)	9.4
B_{peak}/B_0	1.024
Uniformity at 40cm DSV, peak-to-peak	5 ppm
Stored energy (MJ)	140
Conductor length (km)	540
Conductor weight (ton)	30
Magnet weight (ton)	45
Magnet length (m)	3.1
Room shielding weight (ton)	520

Magnetic Weber Bar

Domcke, SARE, Rodd (2024)

140 MJ stored energy $\leftrightarrow S_h^{1/2} \sim 10^{-21} \text{ Hz}^{-1/2}$
(up to transfer function)

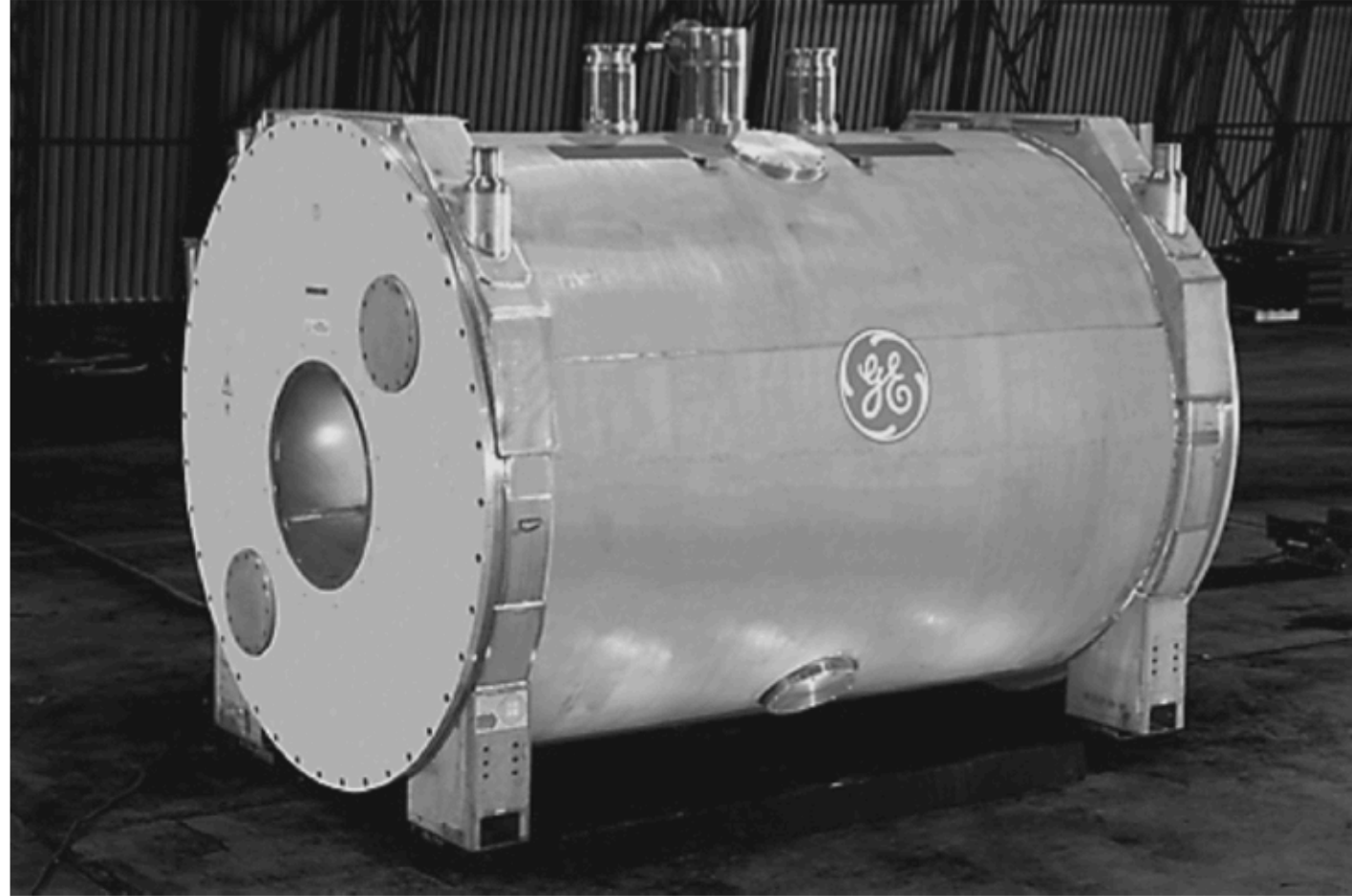


Fig. 10. GE 9.4 T MRI magnet before shipment.

TABLE II
PARAMETERS OF GE 9.4 T MRI MAGNET

Central Field B_0 (T)	9.4
B_{peak}/B_0	1.024
Uniformity at 40cm DSV, peak-to-peak	5 ppm
Stored energy (MJ)	140
Conductor length (km)	540
Conductor weight (ton)	30
Magnet weight (ton)	45
Magnet length (m)	3.1
Room shielding weight (ton)	520

Magnetic Weber Bar

Domcke, SARE, Rodd (2024)

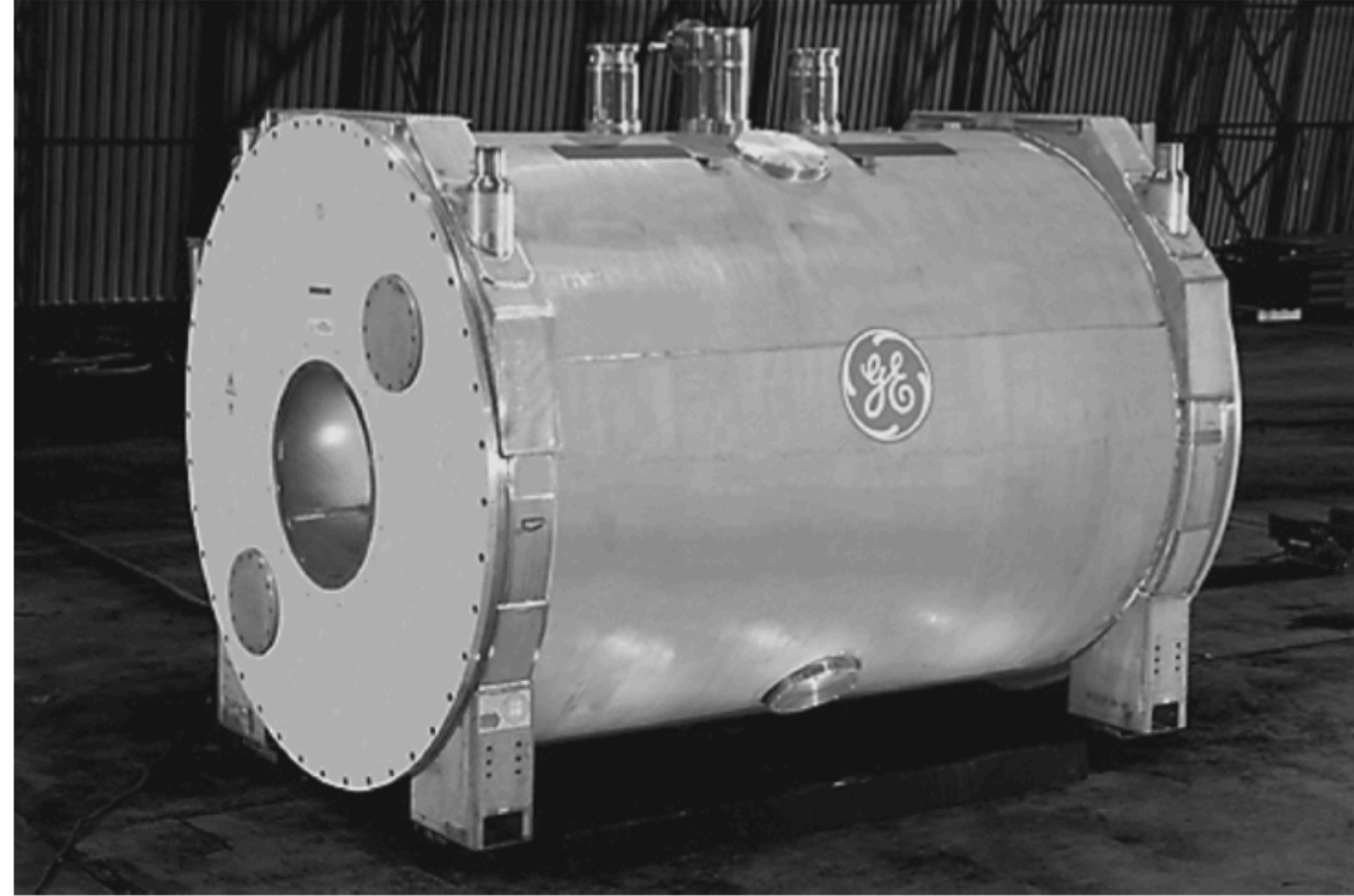


Fig. 10. GE 9.4 T MRI magnet before shipment.

140 MJ stored energy $\leftrightarrow S_h^{1/2} \sim 10^{-21} \text{ Hz}^{-1/2}$
(up to transfer function)

Operates in the regime $\omega_1 \gg \omega_g \gg \omega_m$

TABLE II
PARAMETERS OF GE 9.4 T MRI MAGNET

Central Field B_0 (T)	9.4
B_{peak}/B_0	1.024
Uniformity at 40cm DSV, peak-to-peak	5 ppm
Stored energy (MJ)	140
Conductor length (km)	540
Conductor weight (ton)	30
Magnet weight (ton)	45
Magnet length (m)	3.1
Room shielding weight (ton)	520

Magnetic Weber Bar

Domcke, SARE, Rodd (2024)

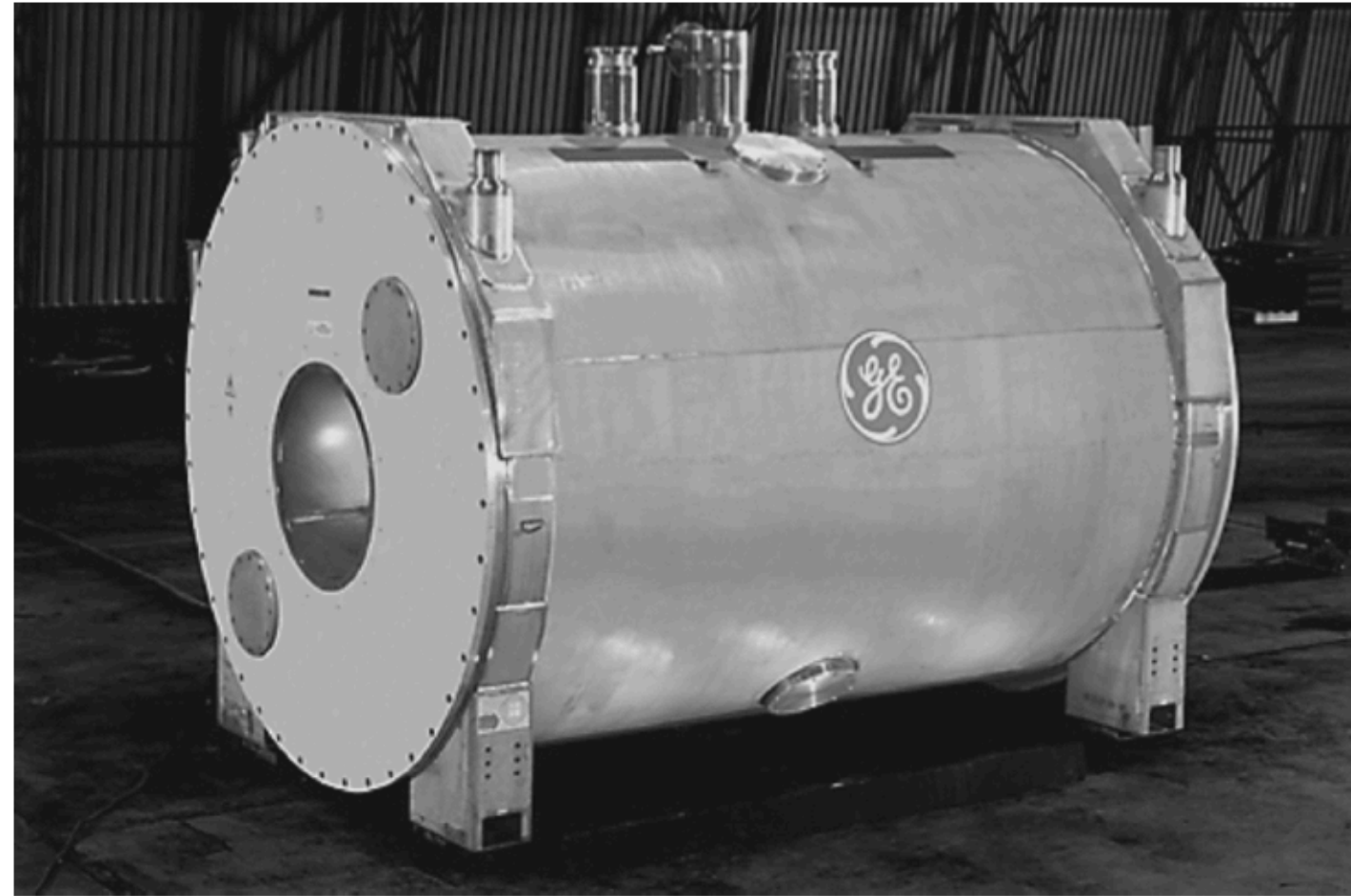


Fig. 10. GE 9.4 T MRI magnet before shipment.

TABLE II
PARAMETERS OF GE 9.4 T MRI MAGNET

Central Field B_0 (T)	9.4
B_{peak}/B_0	1.024
Uniformity at 40cm DSV, peak-to-peak	5 ppm
Stored energy (MJ)	140
Conductor length (km)	540
Conductor weight (ton)	30
Magnet weight (ton)	45
Magnet length (m)	3.1
Room shielding weight (ton)	520

140 MJ stored energy $\leftrightarrow S_h^{1/2} \sim 10^{-21} \text{ Hz}^{-1/2}$
(up to transfer function)

Operates in the regime $\omega_1 \gg \omega_g \gg \omega_m$

$$\mathcal{T}_{\text{mech}}^2(\omega) = \frac{\omega_g^4 \omega_1^4}{\left((\omega_1^2 - \omega^2)^2 + \frac{\omega^2 \omega_1^2}{Q^2} \right) \left((\omega_m^2 - \omega_g^2)^2 + \frac{\omega_g^2 \omega_m^2}{Q_m^2} \right)}$$

Expect $\mathcal{T} \sim 1$

Magnetic Weber Bar

Domcke, SARE, Rodd (2024)

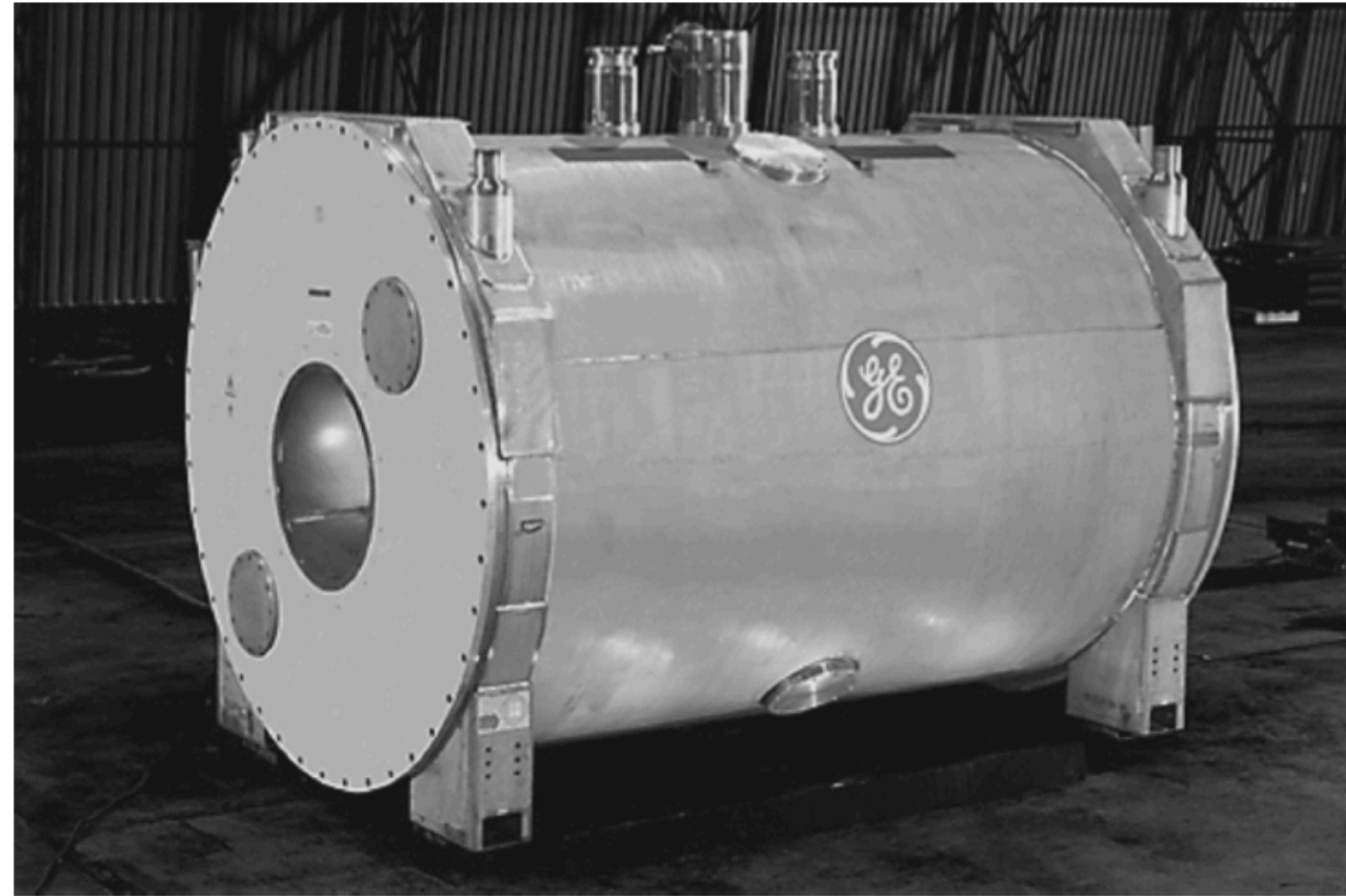
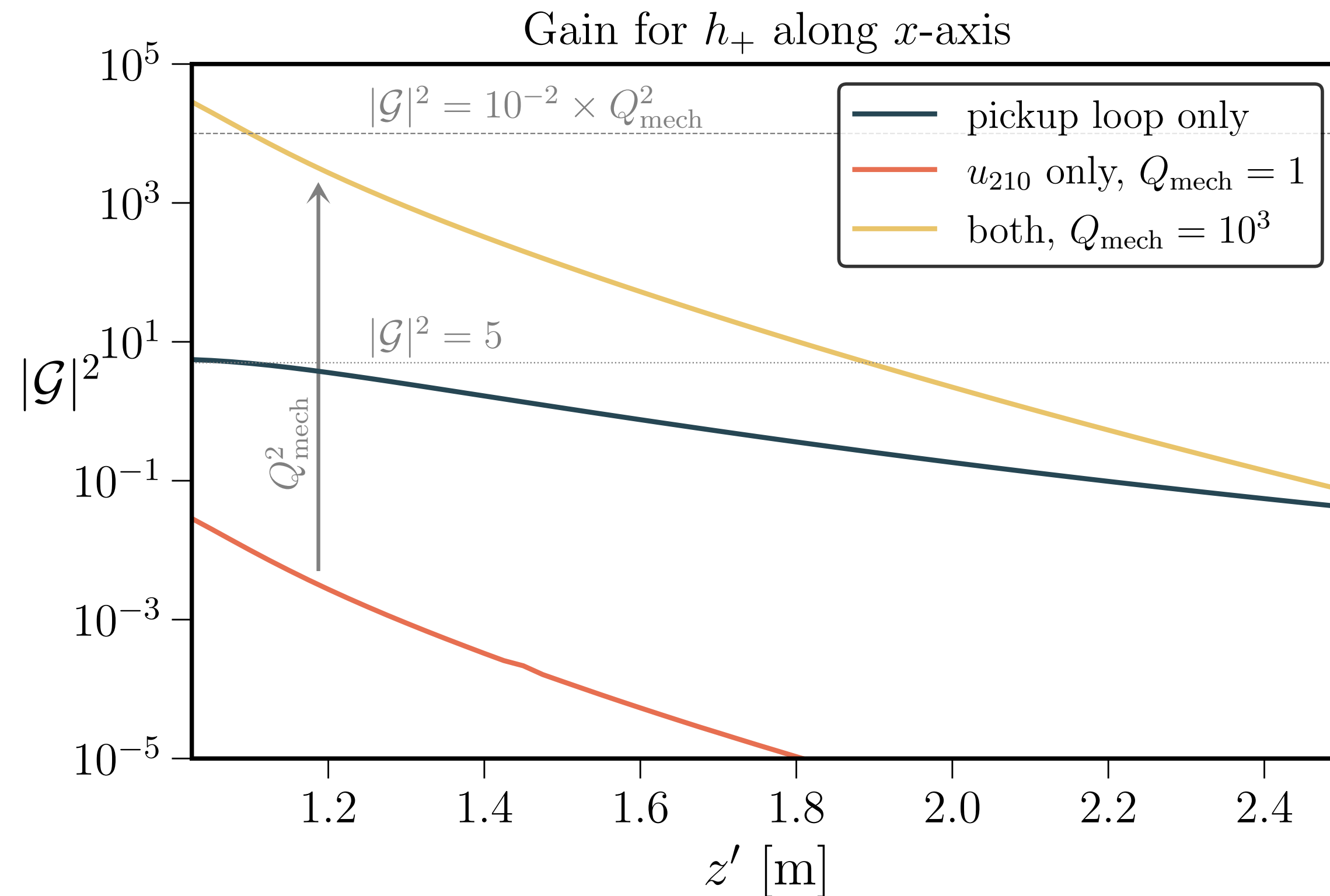


Fig. 10. GE 9.4 T MRI magnet before shipment.

TABLE II
PARAMETERS OF GE 9.4 T MRI MAGNET

Central Field B_0 (T)	9.4
B_{peak}/B_0	1.024
Uniformity at 40cm DSV, peak-to-peak	5 ppm
Stored energy (MJ)	140
Conductor length (km)	540
Conductor weight (ton)	30
Magnet weight (ton)	45
Magnet length (m)	3.1
Room shielding weight (ton)	520

Heuristics confirmed in detailed calculation...



Magnetic Weber Bar

Domcke, SARE, Rodd (2024)

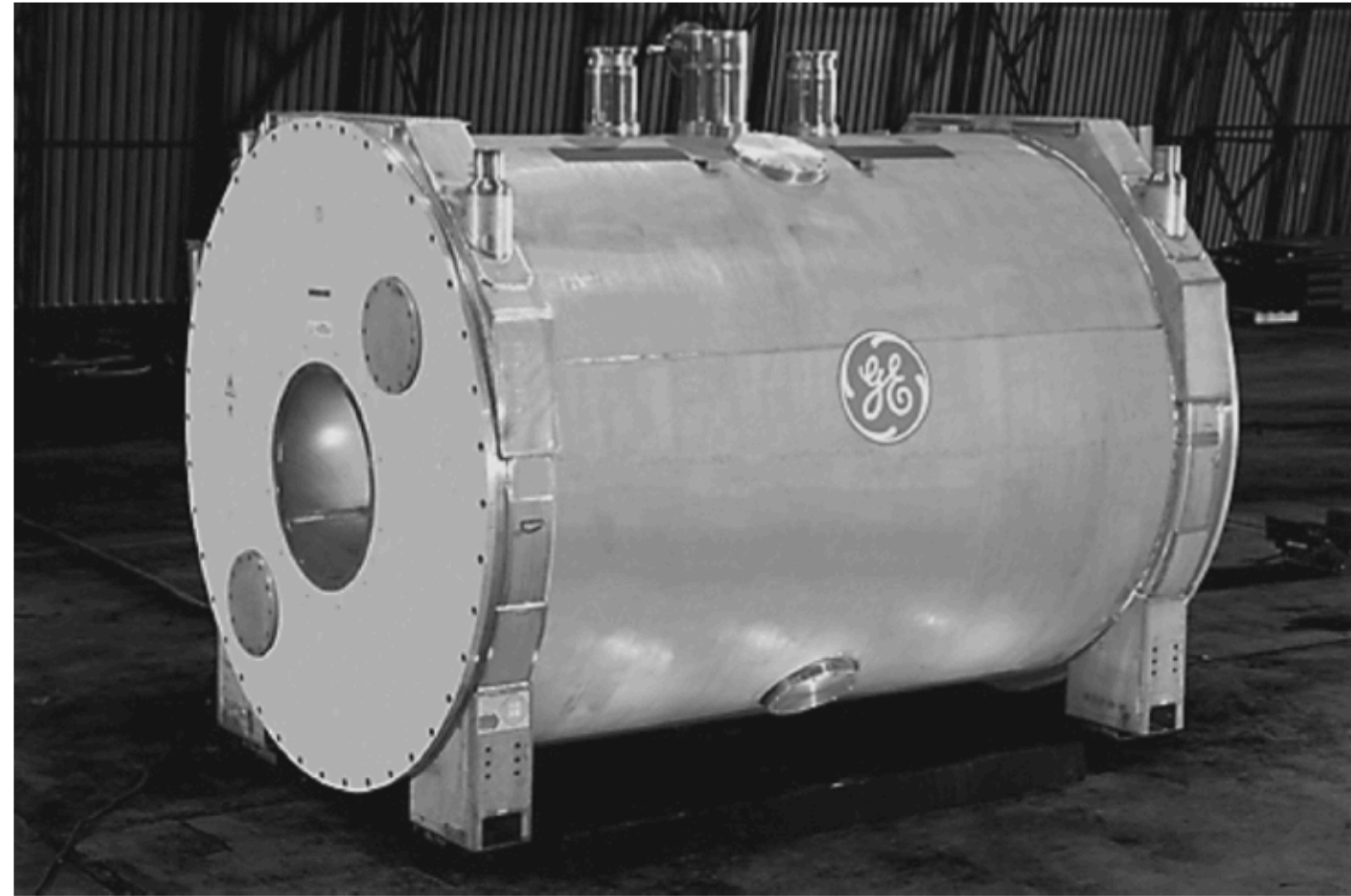
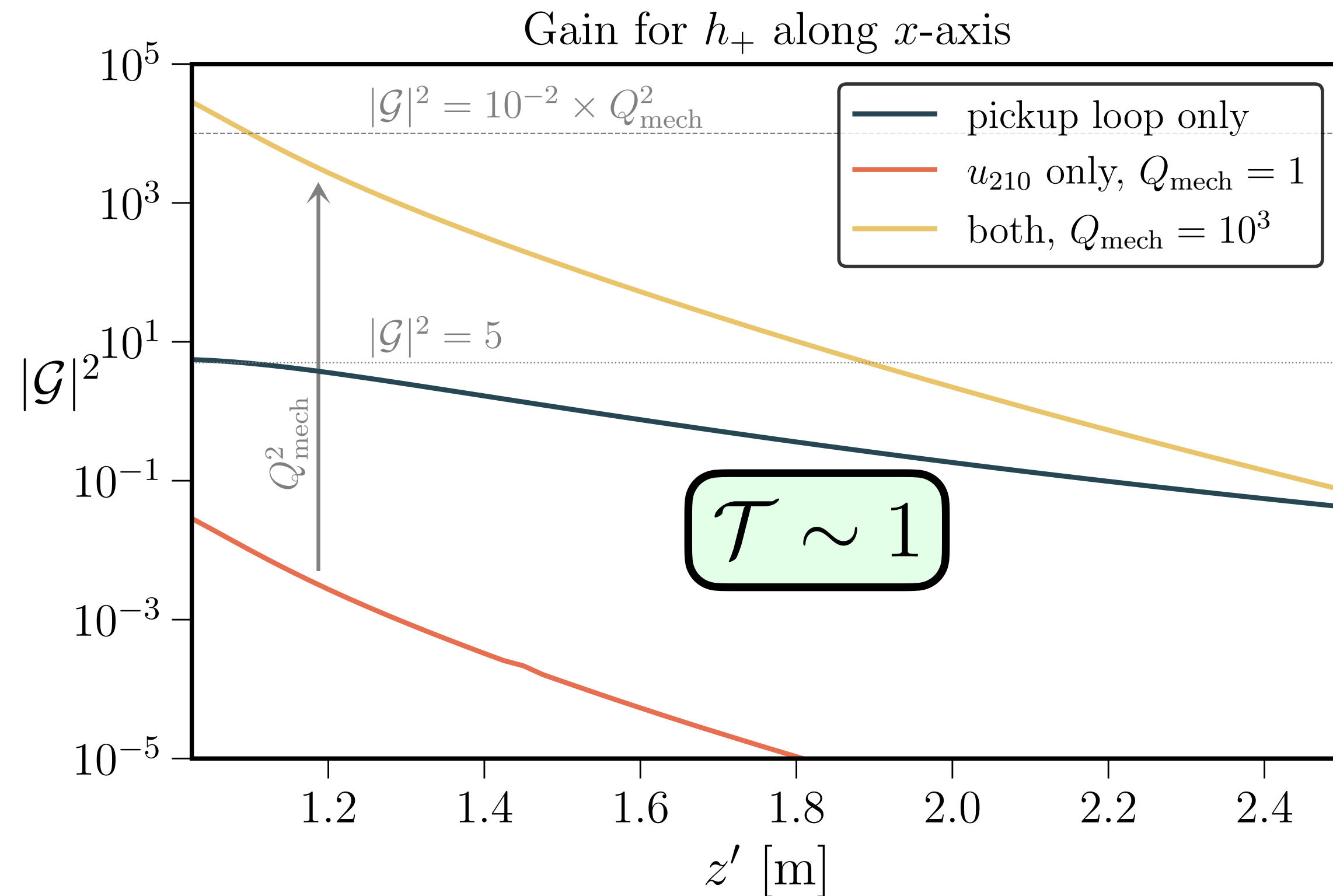


Fig. 10. GE 9.4 T MRI magnet before shipment.

TABLE II
PARAMETERS OF GE 9.4 T MRI MAGNET

Central Field B_0 (T)	9.4
B_{peak}/B_0	1.024
Uniformity at 40cm DSV, peak-to-peak	5 ppm
Stored energy (MJ)	140
Conductor length (km)	540
Conductor weight (ton)	30
Magnet weight (ton)	45
Magnet length (m)	3.1
Room shielding weight (ton)	520

Heuristics confirmed in detailed calculation...



Magnetic Weber Bar

Domcke, SARE, Rodd (2024)

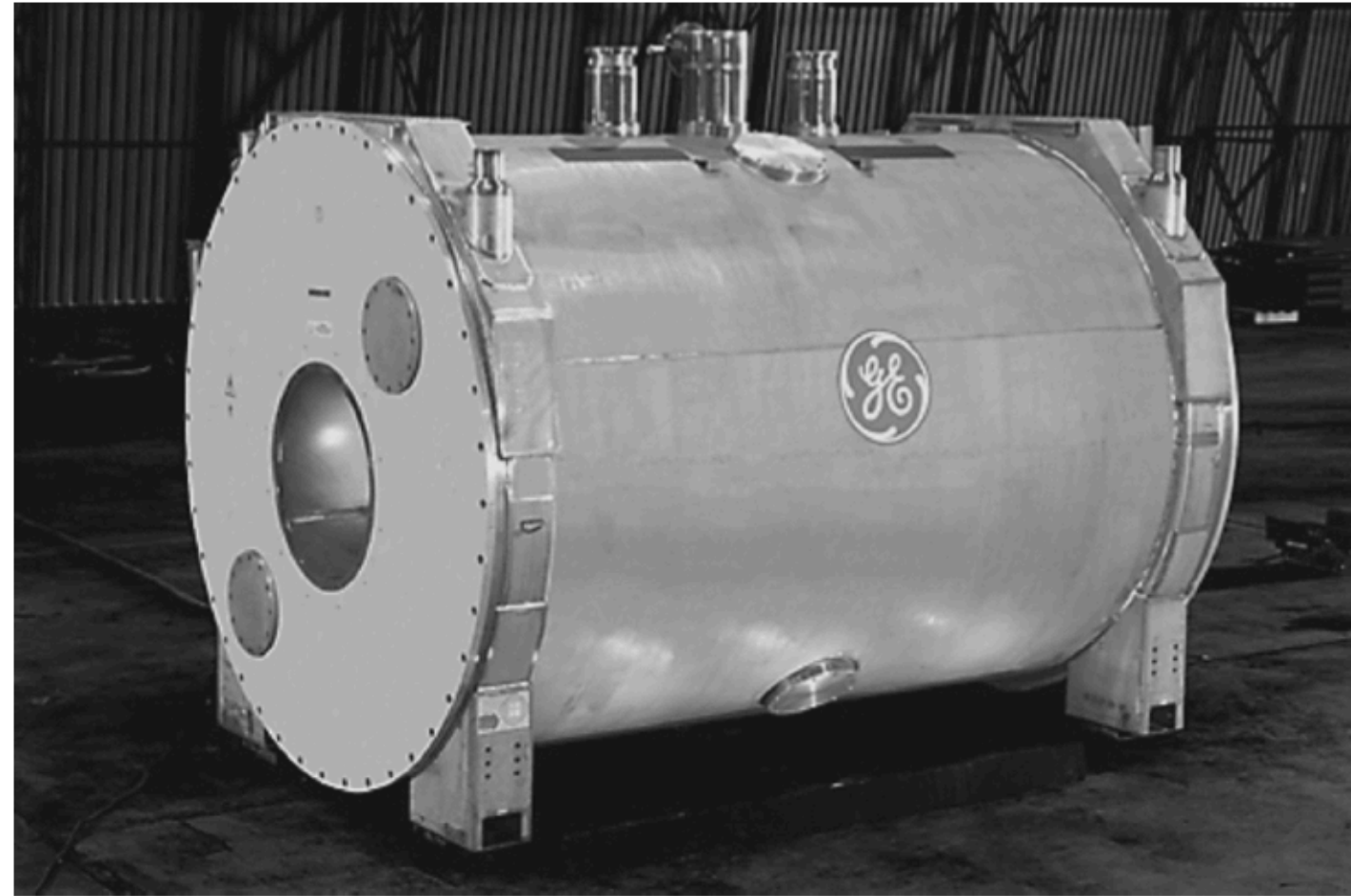
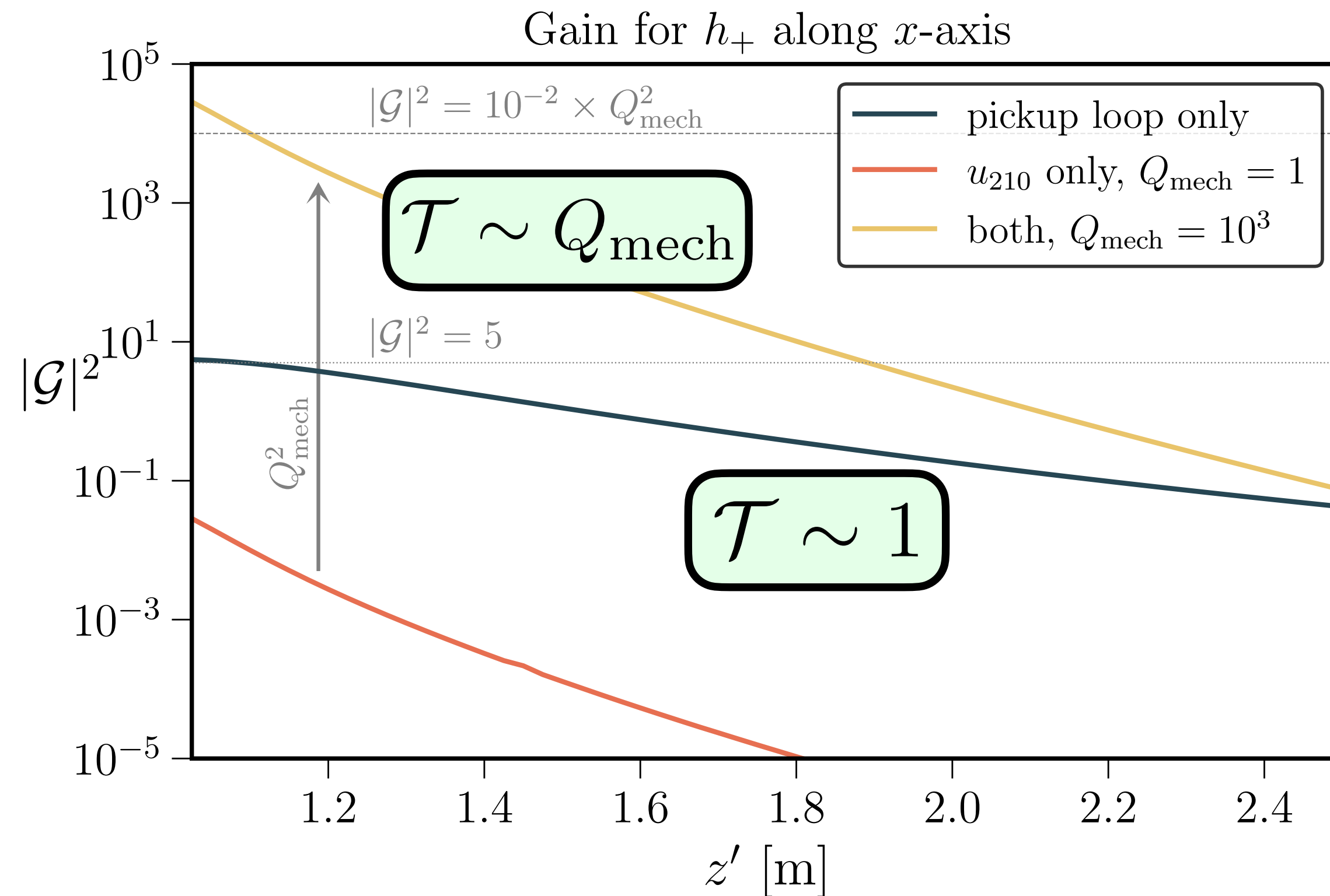


Fig. 10. GE 9.4 T MRI magnet before shipment.

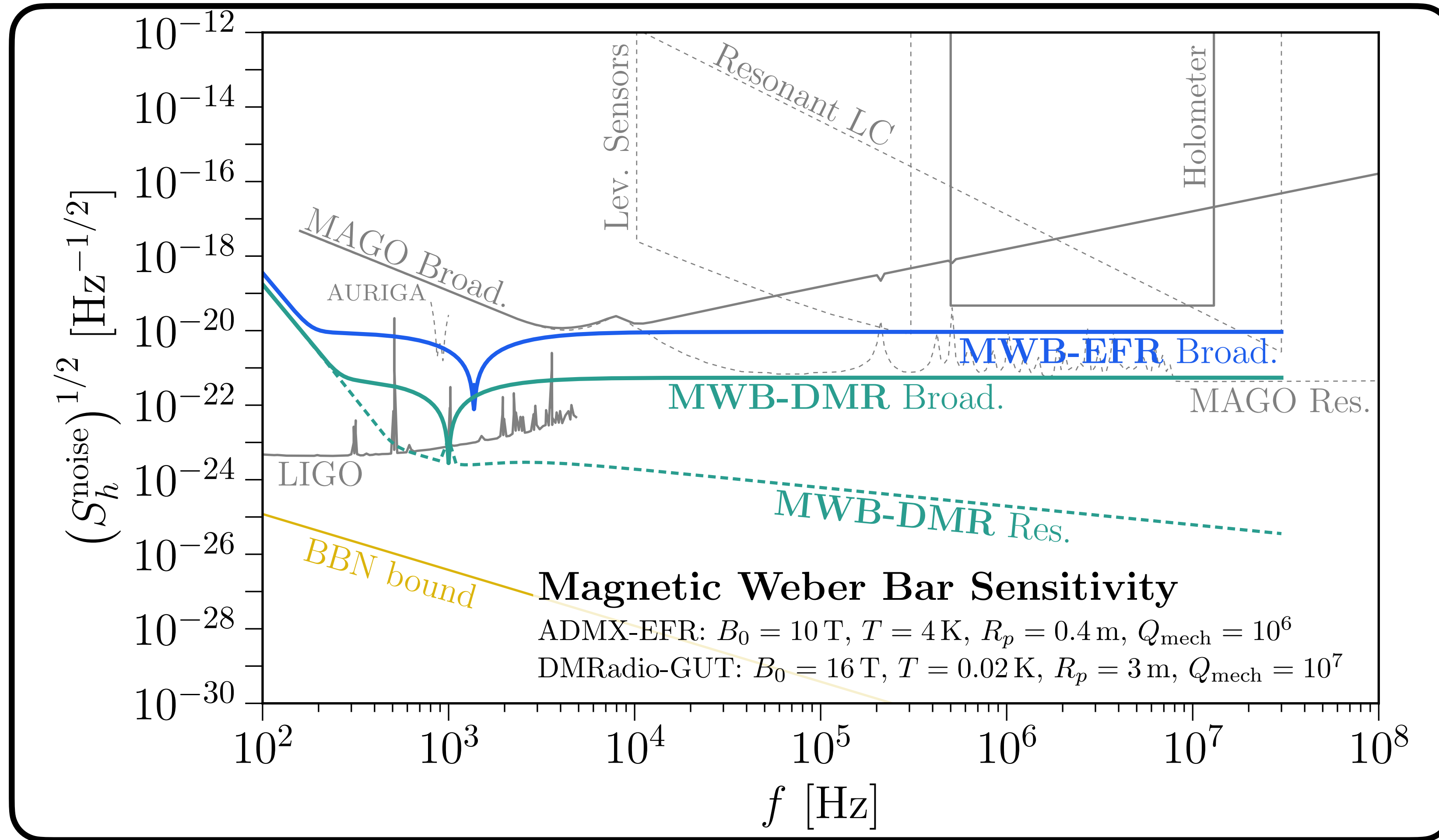
TABLE II
PARAMETERS OF GE 9.4 T MRI MAGNET

Central Field B_0 (T)	9.4
B_{peak}/B_0	1.024
Uniformity at 40cm DSV, peak-to-peak	5 ppm
Stored energy (MJ)	140
Conductor length (km)	540
Conductor weight (ton)	30
Magnet weight (ton)	45
Magnet length (m)	3.1
Room shielding weight (ton)	520

Heuristics confirmed in detailed calculation...

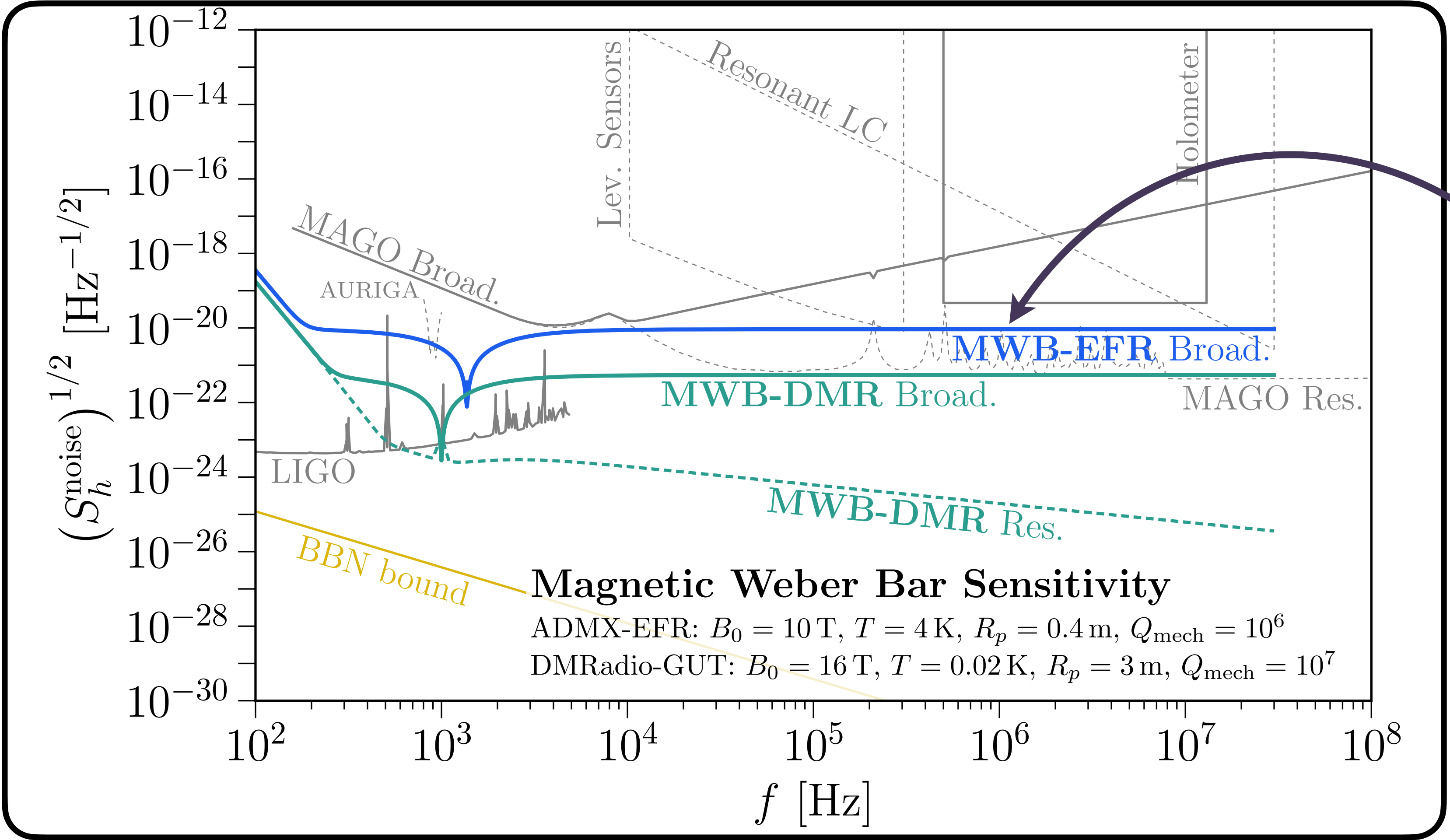


Magnetic Weber Bar



Domcke, SARE, Rodd (2024)

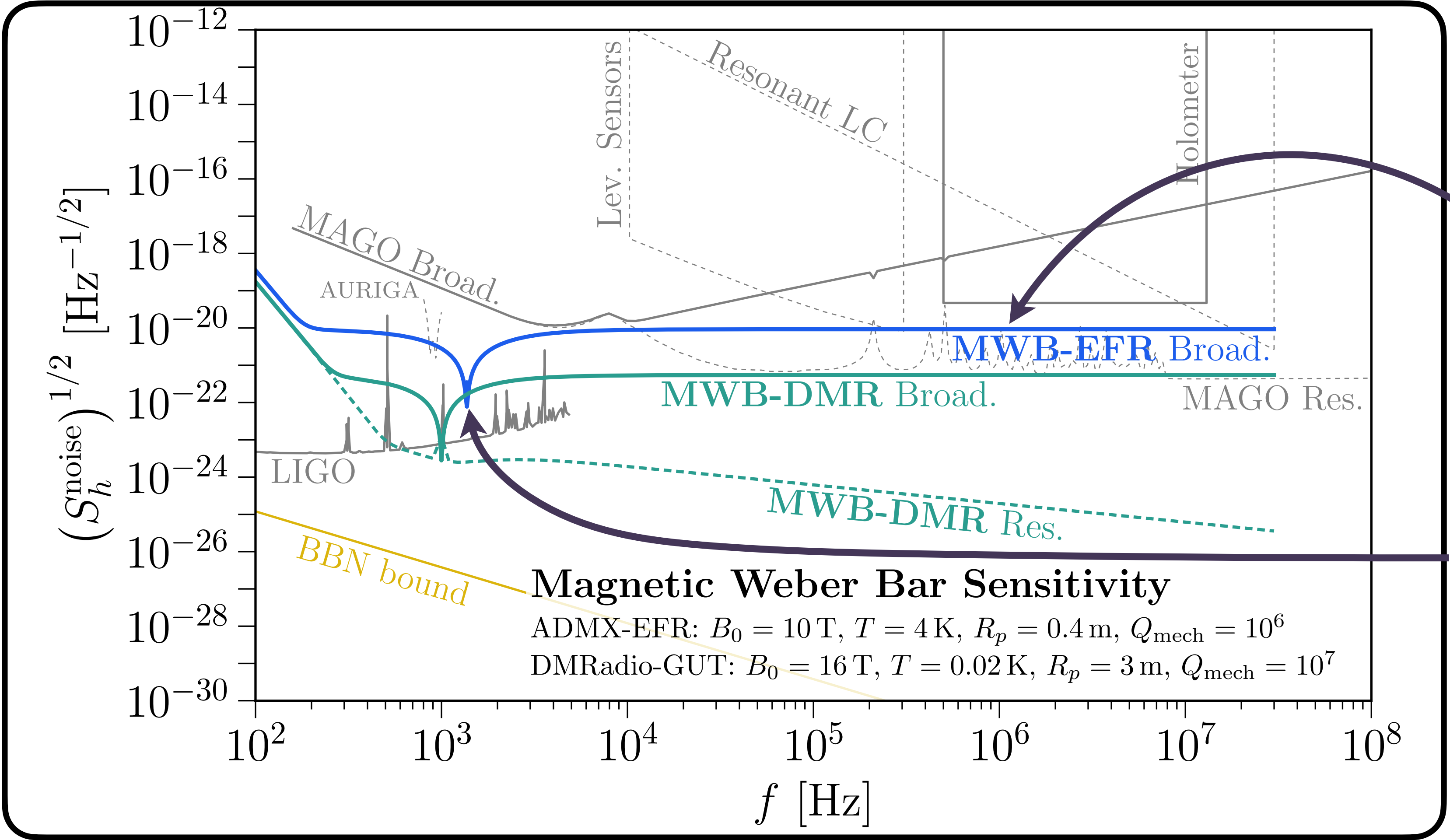
Magnetic Weber Bar



Intuition confirmed, with small penalty from noise

Domcke, SARE, Rodd (2024)

Magnetic Weber Bar



Intuition confirmed, with small penalty from noise

Enhancement from mechanical resonance transfer function

Domcke, SARE, Rodd (2024)

Conclusions

Identify regime of GW by hierarchy with respect to size of detector:

- Resonant regime: $\omega_g \sim 1/L \gg c_s/L$ — use PDF and account for current & boundary changes

e.g. axion cavity experiments

Berlin, Blas, D'Agnolo, SARE, Harnik, Kahn, Schutte-Engel (2021)

- High-frequency regime: $\omega_g \gg 1/L \gg c_s/L$ — use TT gauge

e.g. MADMAX

Domcke, Ellis, Kopp (2024)

- Low-frequency regime: $1/L \gg \omega_g$ — use PDF and account for current & boundary changes

Domcke, Garcia-Cely, Rodd (2022)

Domcke, Garcia-Cely, Lee, Rodd (2023)

Domcke, Ellis, Rodd (2024)

e.g. Magneto-quasistatic experiments

e.g. Heterodyne experiments

Berlin, Blas, D'Agnolo, SARE, Harnik, Kahn, Schutte-Engel, Wentzel (2023)